

https://dspace.org/

Investigating the effects of engine flue gas on dielectric strength of air gaps

Msimango, Nkosinathi

2018

https://hdl.handle.net/10539/26739

Msimango, Nkosinathi (2018) Investigating the effects of engine flue gas on dielectric strength of air gaps, University of the Witwatersrand, Johannesburg, https://hdl.handle.net/10539/26739

Downloaded from a DSpace repository. https://dspace.org/

University of the Witwatersrand

MSc(Eng) Dissertation

Investigating the effects of engine flue gas on dielectric strength of air gaps

Author:

Nkosinathi Msimango

Supervisors:

Prof. C. Nyamupangendengu

Dr. N. West

A dissertation submitted to the Faculty of Engineering and the Built Environment, University of the Witwatersrand, in fulfilment of the requirements for the degree of Master of Science in Engineering



April 5, 2018

Declaration of Authorship

I, Nkosinathi Msimango, declare that this thesis titled, "Investigating the effects of engine flue gas on dielectric strength of air gaps" and the work presented in it are my own. I confirm that:

- This work was done wholly or mainly while in candidature for a research degree at the University of the Witwatersrand.
- Where any part of this thesis has previously been submitted for a degree or any other qualification at this University or any other institution, this has been clearly stated.
- Where I have consulted the published work of others, this is always clearly attributed.
- Where I have quoted from the work of others, the source is always given. With the exception of such quotations, this thesis is entirely my own work.
- I have acknowledged all main sources of help.
- Where the thesis is based on work done by myself jointly with others, I have made clear exactly what was done by others and what I have contributed myself.

Signed:

_____

Date:

_____

Abstract

South African diesel locomotives travel under electrified railway lines that use the IEC 60913:2013 clearances. It has been identified that the IEC standard does not cater for the diesel locomotive exhaust pollution in the air gap clearance design, and this may have unknown electrical implications. This research aims therefore to investigate the effects of engine flue on the dielectric strength of the air gaps and contribute to the knowledge needed to safely operate diesel locomotives under the railway high voltage catenary system. The research is executed through computer simulations and laboratory experiments. The Wits High Voltage laboratory is used for air breakdown tests in normal air and in engine flue polluted air conditions. Breakdown simulations are implemented in MATLAB^{TM} using a fluid gas discharge model to represent the discharge process taking into account gas composition through Townsend coefficients. Experiments have shown that there is a linear relationship between breakdown voltage and gap sizes for the tested range of 1 cm to 30 cm. It is observed that for gap sizes less than 25 cm, the DC voltage breakdown strength of air is enhanced by the presence of engine flue gas by a maximum of 26 %. Beyond 25 cm the flue gas reduces the breakdown strength of air by as much as 21 % in petrol flue and by 36 % in diesel flue. The enhancement is attributed to the increased flue humidity and the corona stabilization effect. For the gap sizes greater than 25 cm the corona mechanism is different, thus the humidity and corona stabilization cease to be influential. Lightning impulses were used to observe the extent of the corona stabilization, tests showed a similar trend to that of DC voltage but most importantly, the difference between flue and normal air breakdown voltages was less than that of DC voltage results by 8 %. This is attributed to the decrease in corona stabilization effect due to the reduced space charge in impulse tests. The simulations predicted the actual breakdown voltages observed in the experiments and it showed the same trends for gap sizes less than 25 cm for DC voltages. The research concluded that the presence of engine flue enhances the dielectric strength of air for the gap size range 3 cm to 25 cm under the tested environmental conditions. This is due to the increased humidity of the flue. No differences were observed for 1 cm and 2 cm.

Acknowledgements

The author would like to thank Eskom for their support of the High Voltage Engineering Research Group through the Tertiary Education Support Programme (TESP). They would also like to thank the Department of Trade and Industry (DTI) for THRIP funding and to thank the National Research Foundation (NRF) for direct funding of the research group. Appreciations are also extended to the Passenger Rail Agency of South Africa (PRASA) for funding this research and to the SAIEE for the SAIEE/ISH2009 scholarship to present this work at ISH 2017. Lastly, the authors would also like to thank Mr Sfiso, Mr Mark and Mr Muzi from the Wits HV and Gemnin Labs for their guidance and assistance on building the test chamber.

Contents

Declaration of Authorship i

Abstract ii

Acknowledgements iii

1 Introduction 1
- 1.1 Problem Statement . . . 3
- 1.2 Research Question . . . 3
- 1.3 Research Aims and Objectives . . . 3

2 Background 5
- 2.1 The South African Railway System . . . 5
- 2.2 Engine Exhaust Flue Gases . . . 8
- 2.3 Effects Of Atmospheric Conditions . . . 10
  - 2.3.1 Pressure . . . 10
  - 2.3.2 Wind Movement . . . 11
  - 2.3.3 Temperature . . . 12
  - 2.3.4 Humiditiy . . . 12
  - 2.3.5 Contamination . . . 14

3 Gas Discharge Theory 15
- 3.1 Electrical Breakdown Phenomena In Gases . . . 15
  - 3.1.1 Ionization . . . 15
  - 3.1.2 Avalanche Formation and Corona . . . 16
  - 3.1.3 Streamer Formation and Arc Formation . . . 17

4 Experimental Tests and Results 19
- 4.1 Common Breakdown Experimental Methods . . . 19
- 4.2 DC Breakdown Experiment . . . 23
  - 4.2.1 Experimental Setup . . . 23
  - 4.2.2 The Test Procedure . . . 27
- 4.3 DC Experiment Results and Discussion . . . 27
  - 4.3.1 Test Calibration . . . 29
  - 4.3.2 Rod Plane Breakdown . . . 31
  - 4.3.3 Pre-Breakdown Corona . . . 33
    - Corona Inception . . . 34
    - Why Corona Inception is Independent of Gap Size and Environment . . . 35

Pre-Breakdown Corona Magnitude and Pulsation 37
Observed Corona Stabilization 40
4.4 Impulse Experiment Setup and Procedure 43
4.4.1 Experimental Setup 44
The Test Procedure 44
4.5 Impulse Experiment Results and Discussion 46
Impulse Breakdown 46

5 Discharge Modelling and Simulations 51
5.1 Modelling of Gas Discharge Phenomena 51
5.1.1 Flux Corrected Transport Algorithm 52
Drift-Diffusion Model 54
Molecular Distribution and Cross Sections 55
Transport and Townsend Coefficients 59
Photoionisation 62
Electric Field 62
Circuit Current 63
Boundary Conditions 63
Accuracy, Stability and Noise 64
5.2 Breakdown Simulation and Results 64
5.2.1 Simulation Procedure 64
5.2.2 Simulation Results 66
Positive Corona 68

6 Conclusion and Recommendations 77
6.1 Conclusions 77
6.1.1 DC and Impulse Experiments 77
6.1.2 Simulations 78
6.2 Recommendations for future work 79

A ISH 2017 Paper 86

B SAUPEC 2017 Paper 93

List of Figures

1.1 Illustration of RCS clearances and locomotive 2

3.1 Schematic of the formation of corona due to localised avalanches. . . . 17
3.2 Schematic of streamer channel and corona at the head, developing into a leader. 18

4.1 FEM simulation of a wire-plane geometry and it's field distribution within 2 cm of the gap from HV wire to plane. 20
4.2 FEM simulation of a point-plane geometry and it's decaying field distribution within 0.4 cm of the gap from the HV eletrode. 21
4.3 FEM simulation of a rod-plane geometry and it's decaying field distribution within 0.4 cm of the gap from the HV eletrode. 22
4.4 Experimental setup: testing DC breakdown of engine flue inside a brick chamber. 24
4.5 DE88E0 Catappilar diesel electric generator with 70 kW output. 24
4.6 Test gap geometries, (a) Sphere-Sphere and (b) Rod-Plane 25
4.7 Image of the laboratory experiment setup with the petrol engine source. 25
4.8 Image of the laboratory DC generator connection to water resistor that connects to the HV rod. 26
4.9 Experiment flow chart, the tested gap sizes are increased in 10 mm increments to 300 mm 28
4.10 Sphere-Sphere breakdown calibration results compared to published data. 29
4.11 Breakdown voltage curves for the rod-plane tests in air, petrol and diesel flue. 31
4.12 Effective ionisation coefficient for air and flue 36
4.13 Pre-breakdown corona magnitude in air and in engine flue gas. 37
4.14 Comparison of pre-breakdown corona activity in air and flue at 4 cm and at 23 cm. CT output shown as voltage. 38
4.15 Illustration of electric field collapse due to corona space charge. 39
4.16 Illustration of points used to compute pulsation % 40
4.17 Corona stabilization with increasing gap size. 42
4.18 Impulse test setup 44
4.19 Image of the laboratory experiment setup for impulse tests 45
4.20 Laboratory generated standard 1.2/50 μs lightning impulse waveform . 46
4.21 Experimental impulse U50 breakdown characterstics for flue and air . . 47
4.22 Weighted Mean Percentage Increase from air to flue experimental results in impulse tests and DC tests. 49

5.1 Flux Corrected Transport algorithm flow chart [18] 53
5.2 Maxwell-Boltzmann's distribution for number of particles with enough energy to react at temperature T. adapted from [18] 56
5.3 O_2 Collisional Cross Sections for the various possible reactions depending on the energy of the electrons colliding with the molecule. 57
5.4 N_2 Collisional Cross Sections for the various possible reactions depending on the energy of the electrons colliding with the molecule. 58
5.5 CO_2 and H_2O Collisional Cross Sections for the various possible reactions depending on the energy of the electrons colliding with the molecules. 59
5.6 A comparison of transport parameters and townsend's coefficients for air and diesel flue gas compositions. 61
5.7 Simulation flow chart, the simulated gap sizes are increased in 1 cm steps to 30 cm and the result is a plot of the breakdown characteristic. 65
5.8 Simulation Results: breakdown characteristics of air and flue under standard conditions. 67
5.9 Current pulse in air (top) and in flue (bottom) for a 1 cm gap size. . . 68
5.10 Space charge in air (top) and in flue (bottom) for a 1 cm gap size. . . . 69
5.11 Electric field in air (top) and in flue (bottom) for a 1 cm gap size. . . . 70
5.12 Current pulse in air (top) and in flue (bottom) for a 3 cm gap size (the cross over). 71
5.13 Space charge in air (top) and in flue (bottom) for a 3 cm gap size (the cross over). 72
5.14 Electric field in air (top) and in flue (bottom) for a 3 cm gap size (the cross over). 73
5.15 Current profile during breakdown of a 200 mm gap in air 74
5.16 Space charge (top) and electric field (bottom) profile during breakdown of a 20 cm gap in air 75

List of Tables

2.1 Types of locomotives and the voltages they operate under [5]. 6
2.2 Heights of diesel locomotives in South Africa [5]. 7
2.3 Summary of reduced clearance for minimum contact wire height and condition of locomotive subjected to clearance [5]. 8
2.4 Comparison of typical flue gas composition in a diesel engine exhaust and gas composition of normal air. 8
2.5 Locomotive Diesel Emissions Standard by the UIC 10

4.1 Chamber air conditions for the calibration tests 30
4.2 Chamber air conditions for the Rod-Plane tests 31
4.3 Chamber air conditions for the Rod-Plane impulse tests 46

5.1 Model Boundary Conditions 63
5.2 Input Parameters for Positive breakdown Simulations in Air and in Flue 66

List of Abbreviations

RCS	**R**ailway **C**atenary **S**ystem
IEC	**I**nternational **E**lectrotechnical **C**ommission
DC	**D**irect **C**urrent
LI	**L**ightning **I**mpulse
CT	**C**urrent **T**ransformer
UIC	International Union of Railways
ESI	**E**lectrical **S**afety **I**nstruction

For my late grandmother & mother

Chapter 1

Introduction

Since the inception of railway catenary systems (RCS) in South Africa, British standards have always been used for guidance on technical requirements such as the determination of electrical clearances. Defined as the air gap between the locomotive electric supply lines and the ground and the top of an electric locomotive [1]. As the economy grows, there is increased reliance on locomotives to transport passengers and bulk goods. Unfortunately, there are many regions in the country where there are unelectrified railway systems and this entails the use of diesel powered locomotives. Consequently therefore the South African railway systems are operated with a fleet comprising of both electric and diesel powered locomotives.

The diesel locomotives often have to make use of the electrified RCS for various reasons and the exhaust outlets located on top of the locomotive release flue gases directly to the electrical cables causing contamination of the electrical air gap. From a high voltage perspective, pollution of the air and high voltage equipment may compromise the integrity of the dielectric strength of the air and equipment of the RCS [2]. Figure 1.1 is an illustration of an RCS showing various clearances, where the reduced clearance is of interest in this study. The South African railway operators are concerned that the criteria for determining the air clearances may have not taken into account flue contamination of the air. Thus the above stated possible knowledge deficiency was the basis of the present research. The approach would be to conduct a more comprehensive fundamental study on air breakdown mechanisms. The objective therefore

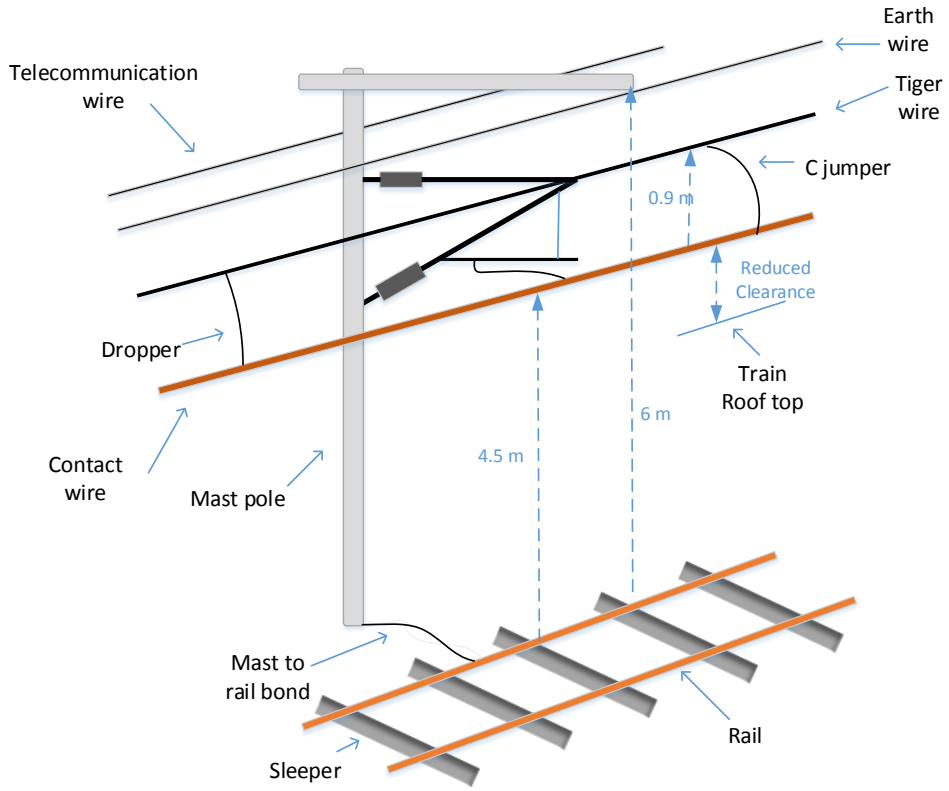

FIGURE 1.1: Illustration of RCS clearances and locomotive

would be not to evaluate the adequacy of the railway catenary system's clearences but to provide knowledge for use by the designers in developing appropriate technologies. The generated knowledge would be generic and therefore applicable in similar scenarios where there exists flue contaminated air in close promixity of high voltage lines. The scope of this research will be limited to air gaps only, more work could be done on equipment such as RCS insulators. In the case of RCS, the flue affects the air gap that would have been set to meet minimum international standards and this may lead to catastrophic accidences causing damage to equipment and injurying passengers. It may become a major problem more so when the locomotives pass under a bridge or a tunnel because the clearances under these structures are already set at their minimum mostly due to costs [3], and more so the flue gases cannot easily escape the tunnel which might have unknown electrical safety implications.

1.1 Problem Statement

Currently the standard used to design electric railway systems in South Africa is the IEC 60913:2013 international standard [4] that unfortunately does not cater for diesel flue gas pollution of the RCS. The omission is presumably because the case of diesel locomotives travelling under electrified railway lines is unique to the country. This poses a unique problem as there is no knowledge of how the flue gases interact with electric systems and how they can possibly be a risk to people and equipment due to electric breakdown. It is therefore important to understand how combustion engine flue gases affect the electrical breakdown characteristics of air in order to generate knowledge for mitigating this problem.

1.2 Research Question

The problem outlined above leads to the research question:
How does engine flue gas affect the dielectric strength of air gaps in the context of railway overhead catenary systems?

1.3 Research Aims and Objectives

The aim of this study is to experimentally determine how pollution caused by flue gases from locomotive engines affect the dielectric strength of RCS air clearances. The study is conducted through:

1. High voltage physical experiments comparing breakdown voltages of an air gap under normal air conditions and under flue polluted air conditions.
2. Computer simulations to comfirm and develop the theory explaining the voltage breakdown mechanisms of an air gap under normal air conditions and flue polluted air conditions.

This dissertation is structured as follows:

- **Chapter 2** gives the background and related work for the research.
- **Chapter 3** delves into the chemistry and physics of gas discharge phenomena in air.
- **Chapter 4** explains the laboratory experimental setup, validation and corresponding procedure with the results and analysis.
- **Chapter 5** details the mathematical modeling for the computer gas breakdown simulations and gives the corresponding results and analysis.
- **Chapter 6** gives the research conclusion and recommendations for possible future work.

Chapter 2

Background

There exists limited literature directly addressing the effects of engine flue pollution on breakdown voltage levels of air or any equipment. An experimental study conducted in 1985 by Lambeth and Nguyen [3] showed that the introduction of diesel and gasoline flue gases in a rod-plane gap length greater than 25 cm resulted in a 20 % reduction in the AC breakdown voltage of such a gap at a temperature of 20 ^oC. This decrease was observed with both petrol and diesel flue gases when compared to other pollution experiments which included water droplets, wheat flour and salt fog pollution. These results may suggest that the chemical compositions of the flue gases are the major contributors to these results since this is the only difference between the tested pollution types. All the experiments were conducted under the same pressure and temperature. The following sections give a brief overview of the South African railway systems and reviews relevant literature on how the presence of engine flue gas might affect the processes involved in gas discharge phenomena.

2.1 The South African Railway System

The South African railway system operates it's fleet on three lines with different voltages. There are locomotives that operate only under DC, AC or dual AC-DC voltage and there are also diesel locomotives along with dual DC-Diesel mode locomotives. The system consists of a 3 kV DC line, a 25 kV AC line, and a 50 kV AC line to operate the various locomotives. A summary of the South African fleet of locomotives

is given in Table 2.1 along with the conditions under which these locomotives can be found traveling under DC traction.

TABLE 2.1: Types of locomotives and the voltages they operate under [5].

Locomotive Type	**Locomotive Class**	**Operating Condition for 3 kV DC**
Single Voltage 3 kV DC	6E1,8E, 10E, 10E1,10E2,18E	Operate or hauled dead
Single Voltage 25 kV AC	7E,7E1,7E2,7E3,11E	Hauled dead
Single Voltage 50 kV AC	9E, 15E	Hauled dead
Dual Voltage 3 kV DC & 25 kV AC	14E, 14E1, 19E	Operate or Hauled dead
Dual Mode 3 kV DC & Diesel	38 Class	Operate or Hauled dead or diesel mode

As can be seen from the summary, the only case where a diesel locomotive travels under an electrified line is when the dual mode 3 kV DC-Diesel locomotive operates in the diesel mode. The AC systems are only used by the 25 kV AC and 50 kV AC locomotives and sometimes the AC-DC dual locomotives. The study is therefore only concerned with the scenario where the diesel locomotive is operated under the 3 kV DC traction as it is the practical case and the interest therefore would be air gap breakdown under normal operational DC voltages.

The presence of the diesel flue in the reduced electrical clearance (the distance between the catenary system's contact wire and the top of the locomotive) is of interest in this study. In the case of the South African electrified traction system, the air clearances are normally specified as the distance between rail and the contact wire. This allows ease of locomotive classification by it's height also known as the vehicle gauge height. The Transnet Electrical Safety Instructions (ESI) [5] specify that the absolute minimum contact wire height with reference to the rail level is 4240 mm on a DC line. The reduced electrical clearance can then be inferred from this and the

original "as built" height of diesel locomotives as given in Table 2.2. The minimum reduced electrical clearance is therefore calculated to be 110 mm as dictated by the height of the class 38 dual 3 kV DC-Diesel locomotive. The shortest locomotive (class 36-000) will leave a reduced electrical clearance of 366 mm. The clearance range in this work is therefore chosen to be from 0 mm to 300 mm in order to cover the range of clearances arising from the various diesel locomotives. The tests below 110 mm and voltages above 3 kV will be conducted for generic knowledge generation purposes that will help develop a more holistic understanding of breakdown characteristics of diesel flue polluted air.

TABLE 2.2: Heights of diesel locomotives in South Africa [5].

Locomotive Class	**Maximum vertical distance between top of rail and upper surface of roof metal structure**	**Clearance**
33-200	3 943 mm	297 mm
34-000	3 962 mm	278 mm
35-000	3 874 mm	366 mm
36-000	3 924 mm	316 mm
37-000	3 924 mm	316 mm
38 (Dual 3 kV DC/Diesel)	4 130 mm	110 mm

The absolute minimum clearances for all the South African locomotive types are summarised in Table 2.3 for completeness.

The contact wire delivers the power to the locomotive, it is made of a solid copper conductor with grooves at the top for the dropper and c-jumper clamps to hold it from the tiger wire. The contact wire has a cross-section of 107 mm^2 for the 25 kV AC system and a 161 mm^2 cross-section for the 3 kV DC and 50 kV AC systems. The following section explores the characteristics of flue contamination and how it may interact with the high voltage environment near the contact wire and into the reduced electrical clearance.

TABLE 2.3: Summary of reduced clearance for minimum contact wire height and condition of locomotive subjected to clearance [5].

Locomotive type	**Contact wire height**	**Clearance**	**Limiting condition**
Single voltage 3 kV DC	4 240 mm	100 mm	Class 8E hauled dead
Dual voltage 3 kV DC/25 kV AC	4 240 mm	120 mm	Class 14E/19E hauled dead
Dual mode 3 kV DC/Diesel	4 240 mm	110 mm	Diesel mode or hauled dead
Diesel	4 240 mm	$>$ 100 mm	All classes hauled or powered
Single voltage 25 kV AC	4 300 mm	100 mm	Hauled dead with pantographs
Single voltage 25 kV AC	4 240 mm	120 mm	Hauled dead with no pantographs
Singled voltage 50 kV AC	4 240 mm	340 mm	Hauled dead with pantographs

2.2 Engine Exhaust Flue Gases

A major by-product of the engine combustion process is heat and the other byproducts are water vapour, carbon dioxide and nitrogen, which according to Majewski [7], their volumetric concentrations are usually in the ranges stipulated in Table 2.4.

TABLE 2.4: Comparison of typical flue gas composition in a diesel engine exhaust and gas composition of normal air.

Gas Molecule	**Flue Volumentric % Range**	**Air Volumetric %**	**Typical Flue Volumetric %**
CO_2	2 - 12	-	12
H_2O	2 -12	-	11
O_2	3 - 17	22	9
N_2	92 - 59	78	67

In Table 2.4 the typical volumetric concentrations of engine exhaust flue gases are compared to that of normal air. It can be seen that the presence of flue in the air decreases the amount of oxygen and nitrogen molecules while increasing the amount of water vapour and carbon dioxide molecules. The gas composition in an engine

exhaust varies depending on the quality of the engine's combustion process. As such a range is also specified for the volumetric concentration of molecules in flue.
In the experimental and simulation investigations therefore, the worst case scenario would need to be considered. Among these gases, there are additional pollutants that come from various non-ideal combustion processes. The pollutants are hydrocarbons (HC), carbon monoxide (CO), nitrous oxides (NO_x) and particulate matter (PM_{10}, PM_{25} for particulate diameters of 10 and 25 microns respectively). The combined volumetric concentration has been experimentally found to be approximately 0.1 % [7]. Due to the small amounts of these pollutants, Jasskelainen [8] argues that the particulates can be ignored and the diesel exhaust gas properties may be approximated to that of air. He further states that this method brings errors and requires results to be corrected for the increased vapour, carbon dioxide and decreased oxygen. In that regard these changes in oxygen, nitrogen, vapour and carbon dioxide constituencies can be regarded important for this study's accuracy of findings.

The international union of railways (UIC) sets the standards for the maximum diesel emissions of diesel locomotives [9]. These are specifically for particulate matter due to their effects on human health. The restrictions are tabulated in Table 2.5 for different diesel locomotive engines grouped according to the period of manufacture as per Directive 97/68/EC (as amended by 2004/26/EC). Most of South Africa's locomotives fall within the UIC stage III group; these specified emissions are not used in the simulations of this research due to their small combined volumetric concentrations being less than 0.1 % as stated above. These characteristics affect the atmospheric conditions which in turn may affect the breakdown strength of an air gap. The next section discusses how the atmospheric conditions that are likely to be affected by engine flue can individually affect the dielectric strength of air.

TABLE 2.5: Locomotive Diesel Emissions Standard by the UIC

Stage	Power P_N Cylinder displ.	NO_x g/kWh	HC g/kWh	CO g/kWh	PM g/kWh	Date
	$130 \leq P_N \leq 560kW$	4.0	4.0	3.5	0.2	2007
IIIA	$560 < P_N \leq 2000kW$	6.0	0.5	3.5	0.2	2009
	$P_N > 2000kW, V_{h,z} > 5l$	7.4	0.4	3.5	0.2	2009
IIIB	$P_N > 130kW$	4.0	4.0	3.5	0.025	2012

2.3 Effects Of Atmospheric Conditions

Locomotive diesel flue has a number of chemical properties as mentioned above, and the gas temperatures are normally in the order of 200 ^oC [10]. The high temperature is in combination with the increased vapour, caborn dioxide, decreased oxygen and possibly the particulate matter. Such atmospheric conditions have been both postulated theoritically and experimentally to have an effect on the dielectric strength of air. Below is a discussion of the effects of the environmental factors that are likely to be affected by the engine flue.

2.3.1 Pressure

Atmospheric air pressure is a function of altitude and a number of studies have conducted experiments showing that a decrease in gas pressure (increase in altitude) results in a decrease in the breakdown voltage of an air gap [11, 12, 13, 14, 15, 16]. The process of breakdown requires an avalanche of electrons to propagate from one end of an air gap to the other and as such, the electrons need energy to sustain this movement. The avalanche is caused by electron collisions with molecules and a mean free path exists between the colliding electrons and molecules; the distance of this mean free path allows the electron to gain kinetic energy as it moves [2]. In a low pressure gas, the electrons and molecules are relatively loosely packed and the mean free paths are increased, which results in electrons gaining more energy and being able to eject other electrons through collisions and sustaining the avalanche [17]. In

the case of this study, the locomotive's diesel flue is directed to the open atmosphere and thus it is assumed that the diesel flue has very little effect on the atmospheric pressure in the air gap clearance. However the altitude of the site of the tests relative to the sea level atmospheric pressure needs to be taken into account.

2.3.2 Wind Movement

The pressure is further affected by the movement of the exhaust draft, in which accelerating molecules due to the wind speed might have an impact on the mean free path of the collisions of electrons and molecules. Experiements conducted by Mahatho *et al* [20] on the effect of wind with a velocity of 3.6 $m.s^{-1}$ on the sparkover voltage of a rod-plane air gap showed that wind reduced the sparkover voltage by 10 kV for small air gaps (5 cm) but this difference became smaller with the increase of the air gap length where at 8 cm it was 5 kV. This result was observed for a positive polarity voltage, where no effects were apparent on a negative polarity voltage. According to experiments conducted by Swanson [18] on the effect of wind on the repeatition rate of corona, it was observed that airflow with a velocity of 2.5 $m.s^{-1}$ affected the repeation rates by removing space charge from the air gap. It is noted that the direction of the wind and the wind speed played a critical role on the affected space charge and consequently the effect on onset streamers. Swanson's experiments showed that the space charge moves with the direction of the wind and the amount of the dispersed space charge increased with wind speed [18, 19]. It was found that the wind speed affected the repeatition rate of the discharge pulses but did not affect the discharge mechanism itself as the measured average peak current under both airflow and no airflow conditions remained the same. This indicates that the movement of the exhaust draft might influence the dielectric strength of the air gap by removing space charge. The extent of the effects of the exhaust draft in this study will likely depend on the velocity and direction of the draft.

2.3.3 Temperature

Allen, Lam and Greaves [21, 22] performed tests to determine the effect of elevated temperatures on breakdown of non-uniform fields. It was found that the breakdown voltage of a rod-plane air gap exponentially decreased with increased temperature. From their test results, it is found that temperature reduces the breakdown voltage more in gaps longer than 20 cm and not so much in gaps shorter than 10 cm when testing under the temperature range 21 ^oC to 148 ^oC [21]. This result agrees with other publications that investigated the effect of temperature on the dielectric strength of air. Cowen *et al* [23] investigated the cause of transmission line flashovers under sugar cane plantation fires in South Africa and found that the main cause was the increased temperature and that the ash particles and smoke density had little effects. Aleksandrov and Bazelyan [24] used a 1.5D simulation to show the effects of temperature and density on properties of a long positive streamer in air. A 1.5D simulation is a term used for simulations showing 1 dimensional movement in time for an applied force. The calculated results showed that temperature had a more pronounced effect than density. Where the temperature decreased the rate of dissociative electron-ion recombination, allowing more free electrons to exist. Experimental measurements performed by Alexandrov *et al* [25] showed that the channel's plasma conductivity increased by a factor of 100 with increasing temperature in the range 17 ^oC to 700 ^oC. It is therefore expected that the increased temperature of the engine flue degrades the dielectric strength of the air gap. Experimental studies should therefore take temperature changes into account.

2.3.4 Humiditiy

Humidity is a measurement of the presence of water molecules in the atmosphere [2]. One of the byproducts in diesel flue is water molecules. The effect of water particles on streamer breakdown can be explained in terms of charge dynamics in the streamer air breakdown channel. The processes of electron loss and generation in the streamer

channel are not as well understood as the electron-impact processes at the streamer head. It is believed that the loss of electrons in the channel in air is dominated by the three-body attachment process in equation 2.1 [26]:

$$e + O_2 + M \rightarrow O_2^- + M, \qquad k = k(E/N, T, M) \tag{2.1}$$

Where $M = O_2$ in dry air and $M = O_2$ & H_2O in humid air and k is the reaction rate which is a function of reduced electric field E/N, gas temperature T and M. The loss of electrons through the dissociative recombination with simple molecular ions (O_2^+ ,N_2^+) is given by:

$$e + AB^+ \rightarrow A + B \tag{2.2}$$

These simple models may fail in describing a number of the observations in the kinetic processes in the channel. As such, Aleksandrov *et al* [6, 24] have used simulations to study the properties of a long streamer in air by taking into account a detailed kinetic model with decreased model dimensionality. According to their simulations, an increase in humidity leads to an increase in the voltage required to breakdown a gap. It is found that this is due to the process represented in equation 2.1 being dominant in the channel since the rate of processes 2.1 with $M = H_2O$ is ten times greater than with $M = O_2$. This is also due to the decrease of electron detachment from negative ions due to clustering negative ions or quenching of the metastable states of O_2 in collisions with H_2O. The overall result agrees with the results of Lambeth and Nguyen's experiments [3] which tested breakdown under clean fog created by steam and by salt steam. In the context of the present work, an interesting fact about engine exhaust flue is that it has both increased temperature and humidity. Therefore, since temperature and humidity have opposing effects, it means that the dominant parameter will determine the overall result of breakdown in engine flue.

2.3.5 Contamination

The particulates in diesel emissions can be regarded as pollution since according to Kuffel [2], pollution is the presence of foreign particles in an air gap or insulator. In this case, the foreign particles are particulate matter classified in into two groups, PM_{10} and PM_{25} for particulates with sizes upto 10 μm and upto 25 μm in diameter respectively. It has been theoretically shown that the presence of conducting particles in an electric field distorts this electric field by creating localised regions of enhanced electric field and hence reduce the strength of air [2]. Tests conducted by Loft *et al* in [31] on the effects of 0.2 mm and 0.63 mm diameter sand particles on air gap breakdown showed that the presence of sand particles decreased the dielectric strength of air and more so when the particles were charged. Furthermore, the increased size of the particles also further decreased the breakdown voltage. This is in agreement with investigations conducted by Naidoo and Swift [32] on large particle initiated breakdown of air gaps of transmission lines. They tested particles with sizes ranging from 1 mm to 50 mm. Wheat flour and coal dust pollution was used by Lambeth [3] and there was little difference between the two but the breakdown voltage showed a slight decrease from dry normal conditions.

The effects recorded in the studies above are for large particles as compared to the ones expected from the flue gas in this study, and the changes observed are small. As such, in the context of this study, it is expected that the particulates have minimal effects due to their small sizes (μm) and concentrations being less than 0.1 %. The next chapter delves into the theory that is needed to represent these environmental conditions in the numerical modeling of the gas discharge process.

Chapter 3

Gas Discharge Theory

Gas discharge is characterised by the many possible ionization processes involving electrons, molecules and ions in a gaseous system. It is important to understand the basics of gas discharges and how various molecules interact with electrons in order to model the gas discharge process and comment on any effects of flue gas on the dielectric strength of air. This chapter presents an overview of the gas ionisation and discharge process. The details of this process are further revealed in the discussion and analyses of the research results.

3.1 Electrical Breakdown Phenomena In Gases

The process of electrical breakdown involves a number of important stages that have been covered in literature and are still being explored as authors come up with new theories of the possible processes and conditions involved in breakdowns [27, 28]. It is generally accepted that these stages occur sequencially as described in the subsections below.

3.1.1 Ionization

The fundamental process in gas discharge mechanisms is the ionization stage, in which molecules in a gaseous system lose electrons [2]. The molecules may lose electrons through various means; which include collision with electrons and ions, photoionization, thermionic ionization. These reactions are represented by equations 3.1 to 3.3,

and they can occur due to an electron-molecule collision where the electron has enough energy to eject electrons from the molecule. Free electrons (termed seed electrons) may exist in the gaseous system due to natural processes and thus can initiate this process of ionization. When there exists a photon from natural processes with enough energy, the energy is absorbed by a molecule and an electron is ejected. Thermionic ionization occurs due to heat energy ejecting an electron from a molecule.

$$e + A \rightarrow A^{+} + 2e \tag{3.1}$$

$$photon + A \rightarrow A^{+} + e \tag{3.2}$$

$$heat + A \rightarrow A^{+} + e \tag{3.3}$$

Other sources of electrons include cathode emissions but the most dominant sources are collisional and photoionization [2]. The growth of these freed electrons leads to breakdown as described in the following sections.

3.1.2 Avalanche Formation and Corona

The electrons generated from the ionization process move through the gap in the direction determined by the electric field polarity. They collide with other molecules and release more electrons as described in the ionization stage. The number of electrons increases exponentially forming an avalanche as each freed electron releases more electrons, this growth is defined by equation 3.4 [2].

$$N = N_0 e^{\int (\alpha - \eta) d} \tag{3.4}$$

Where N is the resulting total number of avalanche electrons in a gap distance d created by a seed electron. N_0 is the number of seed electrons, α is Townsend's first ionization coefficient, describing the number of electrons created per unit length. η is the Townsend's attachement coeffiecient describing the number of electrons attached to molecules per unit length. The growth process of the avalanche electrons is known

as "Townsend's Discharge" [2]. The avalanche of free electrons will form localised conducting plasmas known as corona near the high voltage rod [29] as shown in Figure 3.1 for a positive high voltage rod.

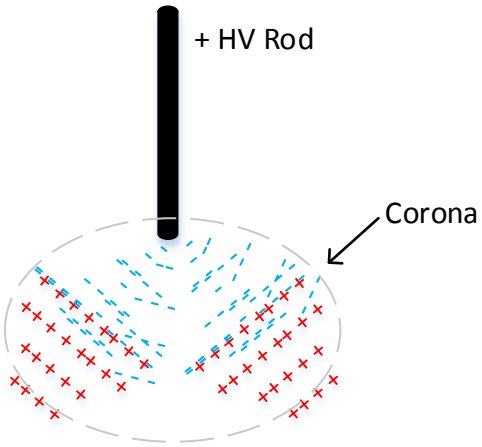

FIGURE 3.1: Schematic of the formation of corona due to localised avalanches.

3.1.3 Streamer Formation and Arc Formation

The plasma begins growing into a streamer depending on the magnitude of the applied voltage, the gap geometry, and the environmental conditions. During this process, the streamer avalanche groups itself into two zones, known as the head and the channel (tail) of the streamer. The streamer head consists of corona as shown in Figure 3.2. Furthermore, the tail and the head are not mutually exclusive, the corona activity (ionization, excitation and dissociation of molecules) happening in the streamer head's high electric field provide the channel with charged particles. These particles, molecules and atoms can enable the streamer to self-sustain and bridge the gap with a leader. The "Streamer Breakdown Criterion" [2] maintains that for a streamer to initiate and self-propagate through the gap, the number of avalanche electrons in the head must reach a critical value as defined by equation 3.5.

$$N = N_0 e^{\int (\alpha - \eta) d} \geq 10^8 \tag{3.5}$$

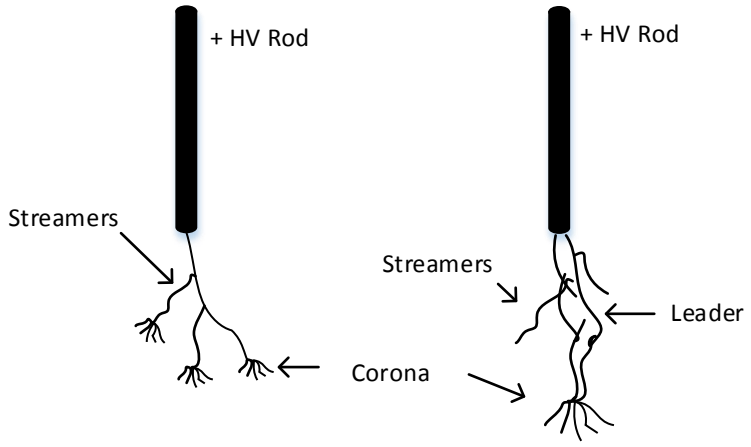

FIGURE 3.2: Schematic of streamer channel and corona at the head, developing into a leader.

The propagation of the streamer to the anode distorts the electric field due to the development of an opposing electric field arising from the space charge distribution. The electric potential in the streamer head which affects the electron-impact processes that results in the streamer breakdown criterion being met or not [6] is then changed by the distorted electric field. It has been found that for the streamer to propagate, the critical electric field near the streamer head must be about 2.5 kV/mm in small gaps. As such, the space charge modified electric field at the streamer head then dictates whether the streamer will continue propagating to the anode depending on the magnitude of this modified electric field. If the field meets the critical value, the streamer is self-sustained and continues the propagation and bridges the gap, at which point an arc may form. Since electrons are the main players in these phenomena, the gases involved have a major impact as various gas molecules have different properties that influence the ease of attaching or detaching electrons from them [2] which is why it is crucial to consider gas composition when dealing with engine flue.

The next two chapters detail the experimental tests and simulations to observe how engine flue affects the breakdown charateristics of air. The theory described above is the fundamental knowledge from which the discussion and analysis is derived to interpret the results.

Chapter 4

Experimental Tests and Results

This chapter gives the details of the experimental tests conducted to investigate the effects of engine flue on the dielectric strength of air gaps. High voltage breakdown tests were conducted in a laboratory using DC voltages, then impulse voltages were used to verify some of the effects uncovered from the DC tests. For both DC and impulse voltage tests, a gap in normal clean air and a gap in flue polluted air is used and the test results are analysed and compared. The investigation is conducted for a petrol and a diesel engine.

4.1 Common Breakdown Experimental Methods

The common methods of performing breakdown experiments are to choose a gap geometry that approximates the setup being studied. It is preferable to choose a worst case gap geometry that is applicable to the study. Studies concerned with electrical breakdown use a rod-plane gap geometry to perform breakdown tests. This is because the rod-plane gap geometry has been shown experimentally and mathematically to represent a worse case scenario and most importantly, many real world setups approximate to a rod-plane geometry [2]. In the case of a RCS-locomotive geometry, the setup is a wire-plane gap geometry with the reduced electrical clearance as the gap. While a horizontal rod-plane (or wire-plane) geometry is appropriate for the RCS-locomotive setup as was used in [3], it can be simplified to a rod-plane geometry by considering the cross-sectional view of a locomotive under a RCS, which is

just a point-plane setup that then can be approximated by a rod-plane setup. The finite element modeling (FEM) simulations in the figures below illustrates how this is possible, the same arbitrary voltage of 120 kV is applied in all models. Figure 4.1 shows the electric field distribution of a horizontal line-plane geometry which gives a uniform distribution and thus cannot be used to model and test for a worst case scenario in this study.

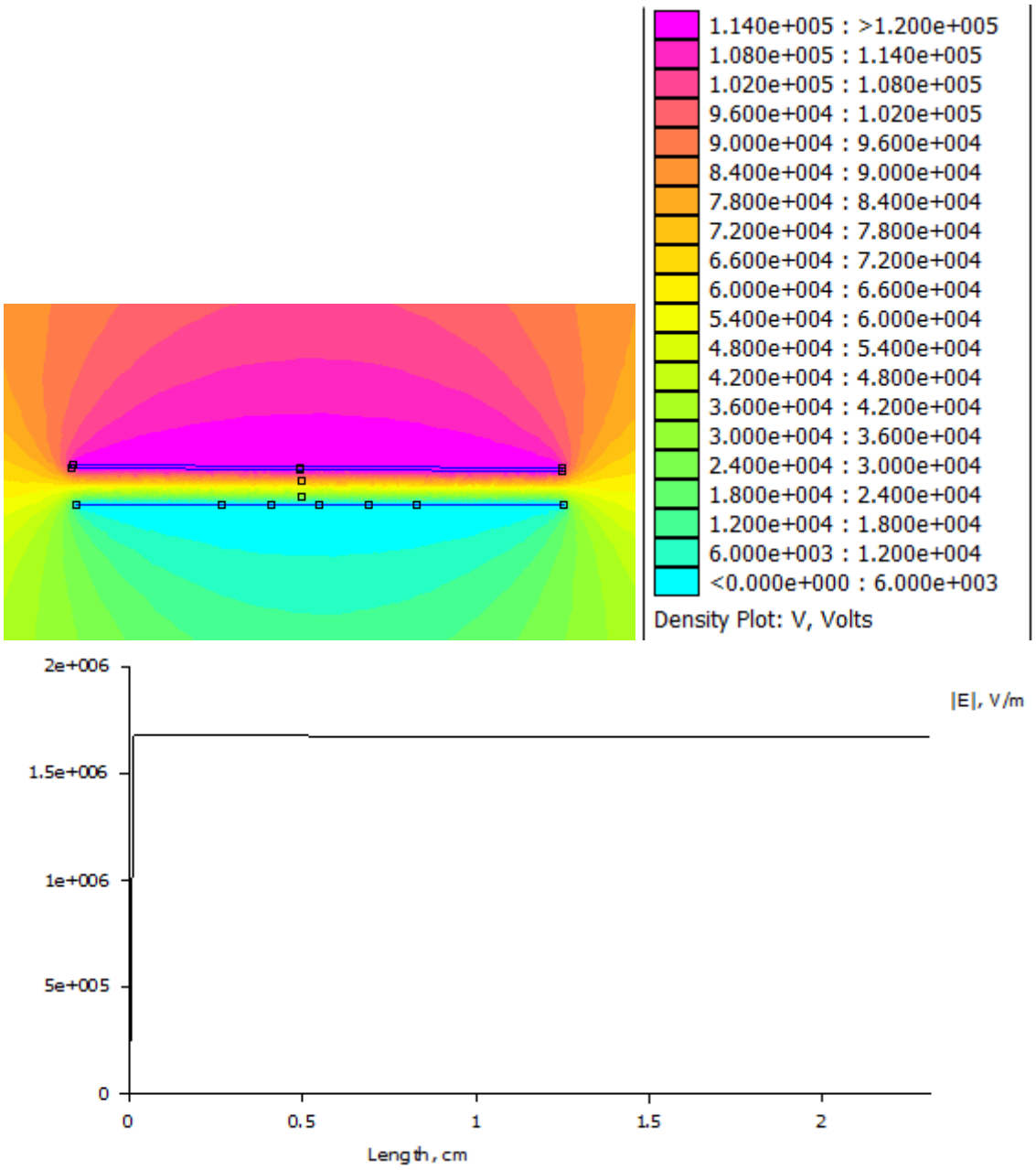

FIGURE 4.1: FEM simulation of a wire-plane geometry and it's field distribution within 2 cm of the gap from HV wire to plane.

Considering a cross-sectional view of this geometry shows a point-plane (or small disc-plane) setup, the FEM simulation and field can be seen in Figure 4.2 and the corresponding field distribution is a decaying exponential function outside the point conductor.

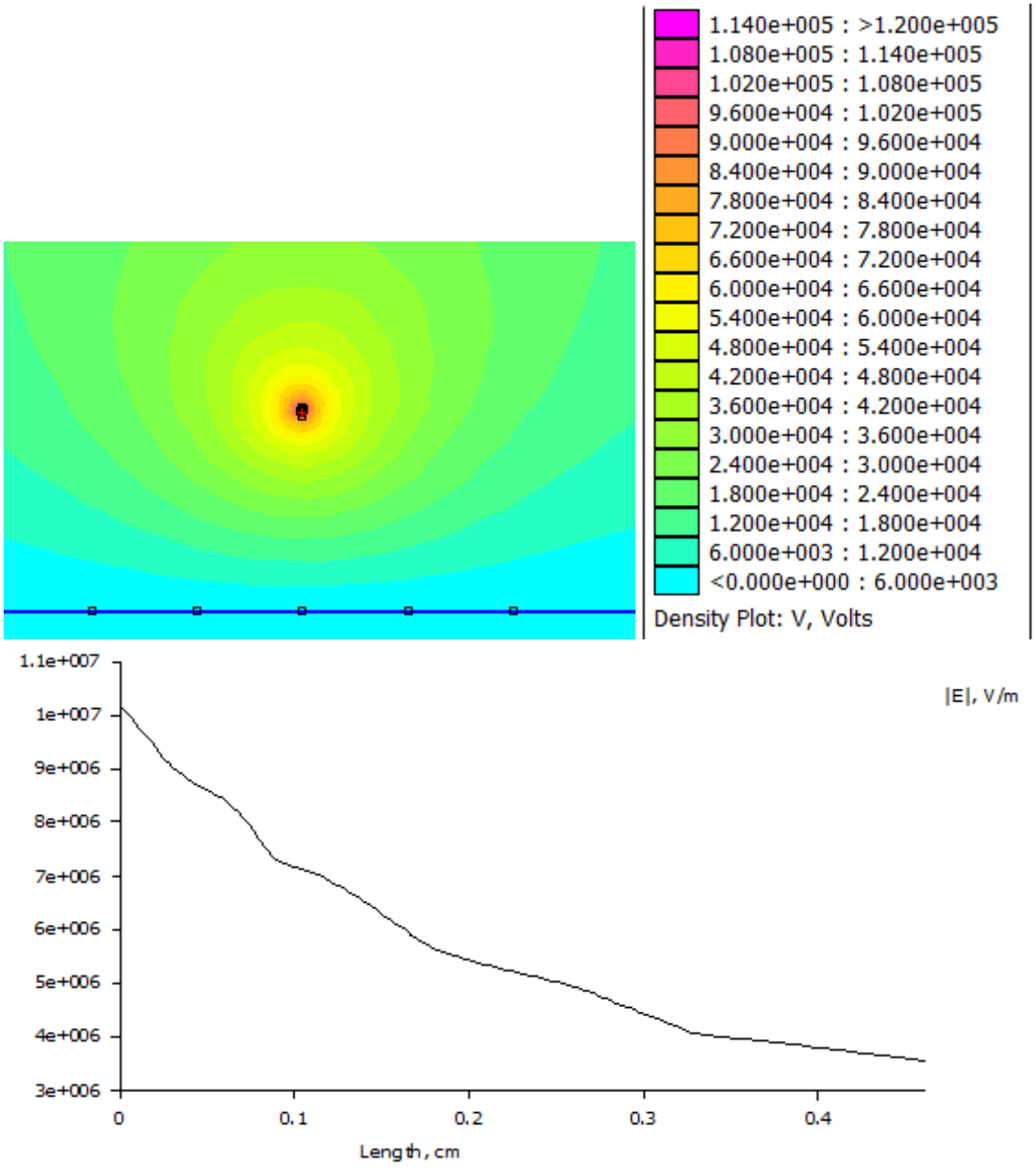

FIGURE 4.2: FEM simulation of a point-plane geometry and it's decaying field distribution within 0.4 cm of the gap from the HV eletrode.

A rod-plane geometry is shown in Figure 4.3 from which it is can be seen that the field distribution approximates to that of the point-plane geometry with a possible

difference of 2 kV to 3 kV. The rod-plane setup allows ease of scaling down the RCS-locomotive setup to a laboratory setup since one can easily construct a rod-plane setup and introduce engine flue in the air gap. The drawback is that the amount of flue and concentration in the laboratory setup would not be the same as that of an actual locomotive.

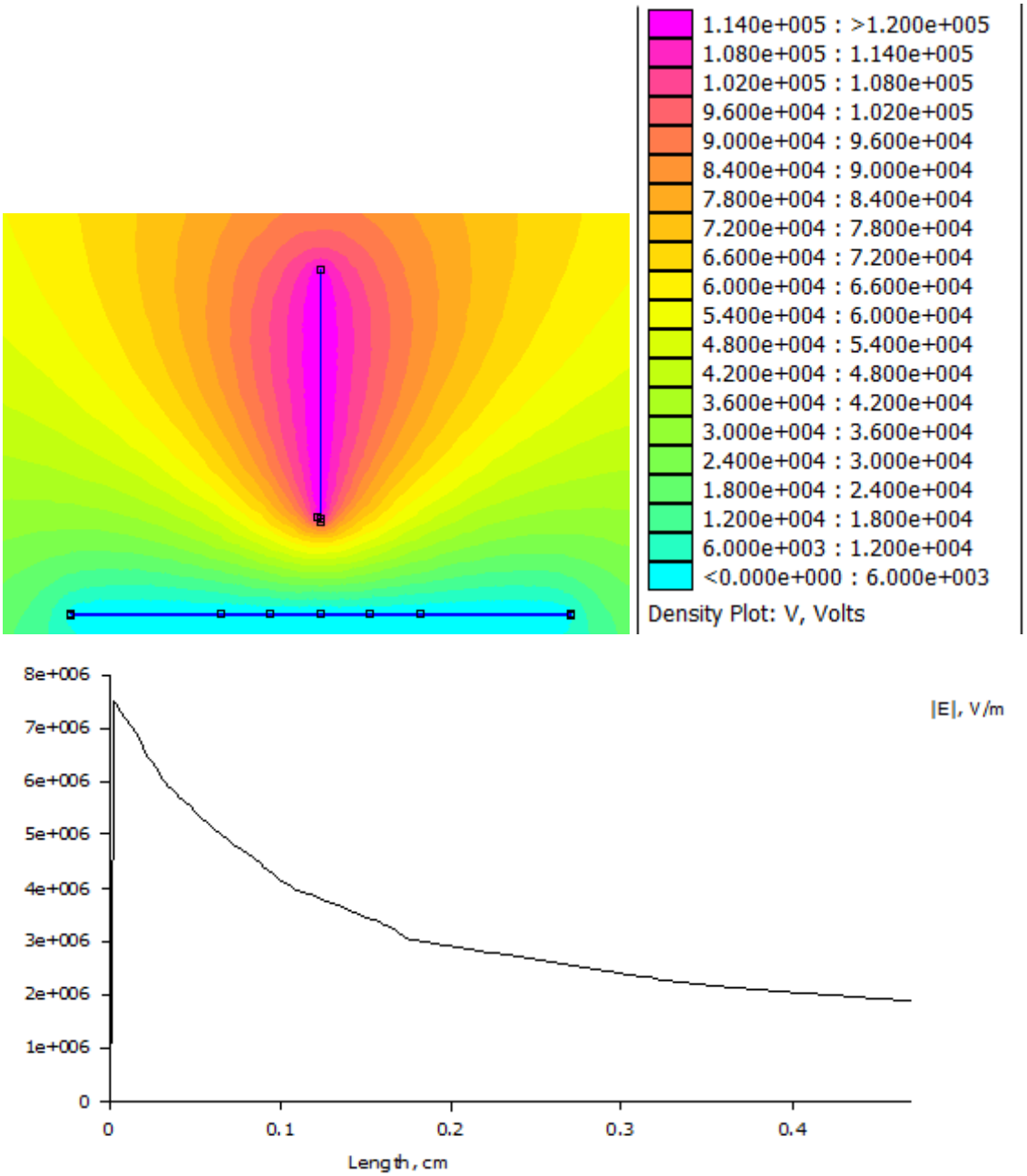

FIGURE 4.3: FEM simulation of a rod-plane geometry and it's decaying field distribution within 0.4 cm of the gap from the HV eletrode.

The common measuring instruments in high voltage tests are oscilloscopes and potential dividers or high voltage probes. Apart from measuring the breakdown voltages in the experiments, pre-breakdown corona is often of particular interest in literature. This is because it is known that corona has an effect on the breakdown voltages observed. Thus measuring pre-breakdown corona enables a more detailed analysis of how the breakdown characteristic is governed by charge dynamics. The tests conducted in this study are for diesel flue and petrol flue to contrast the two and for normal air conditions.

4.2 DC Breakdown Experiment

The DC voltage experiment is conducted in a laboratory setup as described in this section. The tests are conducted only for DC because the case when diesel locomotives travel under electrified lines is only under 3 kV DC lines. The polarity of the DC voltages in the railway system is positive, thus the experiments are conducted with positive DC voltage. Voltage magnitudes higher than 3 kV DC are used in the tests to get an understanding of the breakdown dynamics of engine flue for the tested gap range in the high voltage laboratory at the Witwatersrand University at an altitude of 1740 m above sea level.

4.2.1 Experimental Setup

The DC voltage experimental setup is shown schematically in Figure 4.4. It is composed of a 300 kV DC Cockroft-Walton high voltage generator, a partially top open gas chamber made of bricks representing a case where a locomotive travels under a tunnel and exhaust flue cannot easily escape. The engine flue sources are a petrol electric generator and a 70.4 kW caterpillar (model DE88E0) diesel electric generator shown in Figure 4.5. Data acquisition is accomplished through a data logger system that is composed of a high frequency current transformer (HFCT) that connects the air breakdown leakage current to a PicoLog 1012 data logger with a 1% accuracy [30].

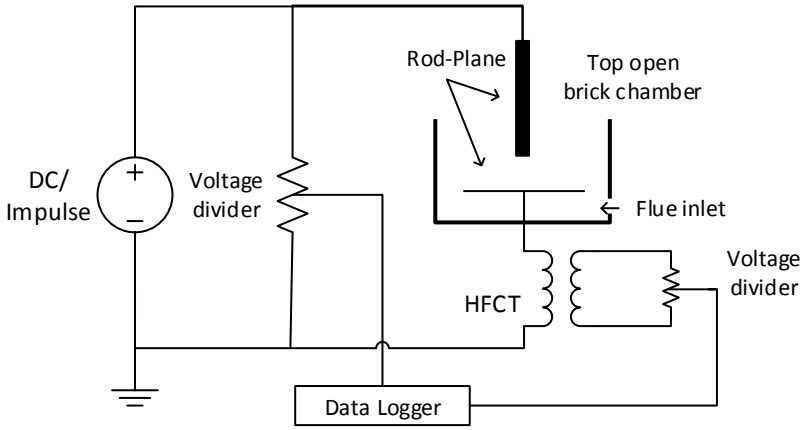

FIGURE 4.4: Experimental setup: testing DC breakdown of engine flue inside a brick chamber.

The applied voltage is also measured through the data logger which connects to a personal computer to continuously store the logged data. The meassured gap leakage current data during the tests represents corona activity as it is due to the movement of the space charge in the air gap. High voltage 1000:1 and 2000:1 potential dividers and a set 20 A fuses are used to connect the applied voltage and leakage current CT to the data logger for protection.



FIGURE 4.5: DE88E0 Catappilar diesel electric generator with 70 kW output.

Two electrode configurations are used as shown in Figure 4.6; (a) sphere-sphere and (b) rod-plane.The sphere-sphere gap has been well studied and the breakdown voltage corrected to standard conditions of various gap sizes can be easily calculated or read out from graphs [2]. Thus the sphere-sphere gap is suitable to be used as a calibration setup.

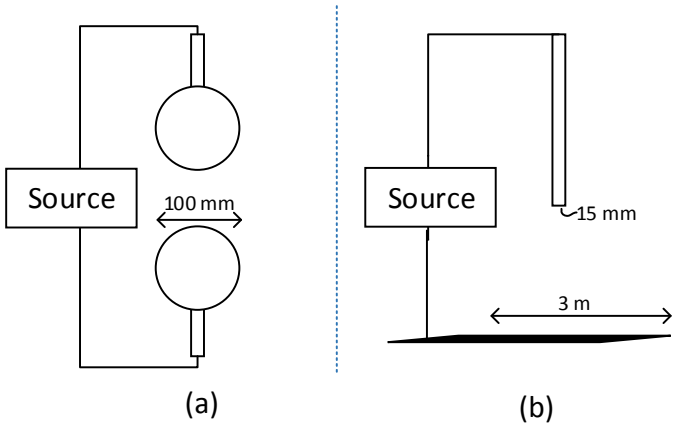

FIGURE 4.6: Test gap geometries, (a) Sphere-Sphere and (b) Rod-Plane

Breakdown tests are conducted on a sphere-sphere setup placed inside a chamber for the calibration. The vertical rod-plane geometry has been shown above to approximate the geometry presented by a locomotive and overhead line system.

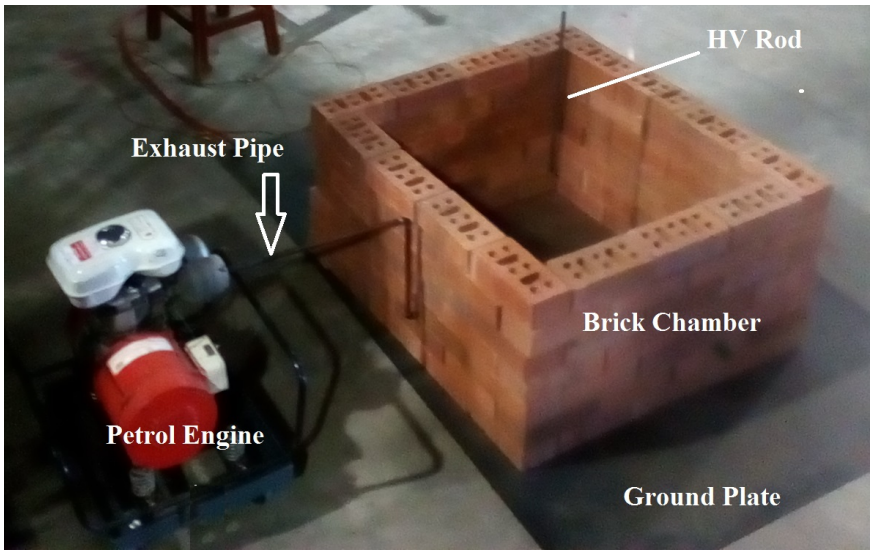

FIGURE 4.7: Image of the laboratory experiment setup with the petrol engine source.

The diameters of the spheres are 100 mm each, chosen such that their curvature is large enough and does not represent a point-to-point gap geometry. The copper rod electrode with a flat-bottom diameter of 15 mm emulates the railway copper contact wire of 16 mm in diameter, it has an edge radius of 1 mm and the ground plane is 3m-by-3m. Figure 4.7 and Figure 4.8 are images of the laboratory setup showing the components of the experiment setup.



FIGURE 4.8: Image of the laboratory DC generator connection to water resistor that connects to the HV rod.

The diesel electric generator is not in these images as it is placed outside the laboratory. The square chamber is 60 cm in width, calculated by taking into account that

the DC generator can give a maximum of 300 kV, which would breakdown to the wall of the chamber if it was 12 cm closer to the rod, implying that the chamber width must be at least 24 cm (twice the the minimum distance to the rod since it is a square chamber).

4.2.2 The Test Procedure

The breakdown tests are performed in accordance with the SANS 60060-1:2011 testing techniques [33]. Figure 4.9 gives the experimental flow chart based on this testing technique. Gap sizes from 10 mm to 300 mm are tested in 10 mm increments for breakdown in both normal air conditions and in engine flue gas conditions. The gap size range of 10 mm to 300 mm is chosen such that the absolute minimum reduced clearance of 110 mm in a RCS as mentioned in the background is within the test range. The 300 mm is to accommodate the clearance of the shorter locomotives that create a reduced clearance of 366 mm. For each electrode geometry, a gap size of 10 mm is fixed, then the applied voltage is increased at a rate of 1 kV/sec until the gap breaks down as detected through the data acquisition system. The input source voltage and the leakage current are measured and logged through the data logger throughout this process. The air gap is given 5 minutes to de-ionise and disperse the formed space charge then the process is repeated 10 times before the gap size is increased by 10 mm. This process is repeated until a gap size of 300 mm is reached. The temperature, pressure and humidity measurements are done once for every gap size once the flue source generator has been running for 10 minutes to allow steady flow of the flue and get the steady state measurement of the chamber atmospheric conditions.

4.3 DC Experiment Results and Discussion

This section gives the results from the DC tests in normal air conditions and in engine flue polluted air conditions. The experiment calibration results are compared to published data. The test results from the two environmental conditions are compared

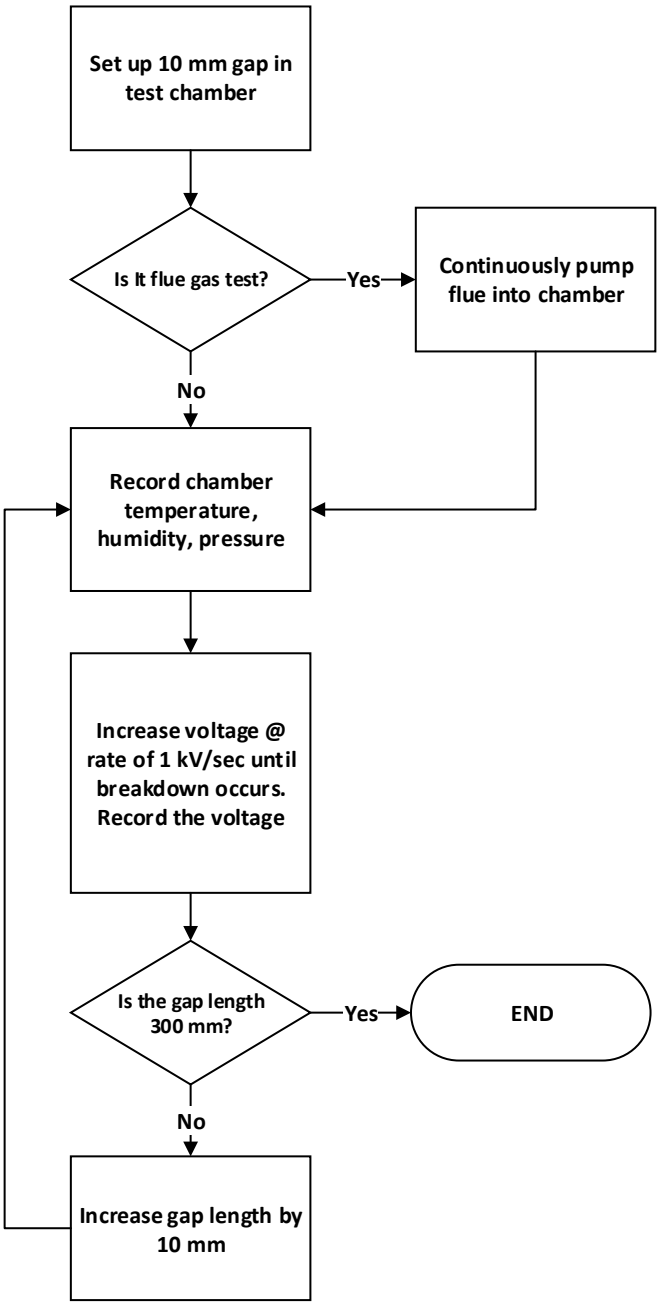

FIGURE 4.9: Experiment flow chart, the tested gap sizes are increased in 10 mm increments to 300 mm

and contrasted. An analysis and discussion based on the observed differences or similarities thereof are given in this section. The results are given as breakdown voltages against gap distances, furthermore, the pre-breakdown corona is measured and analysed to further understand the phenomena governing the differences in breakdown

mechanisms between the air and flue environmental conditions.

4.3.1 Test Calibration

Figure 4.10 shows the breakdown voltage as a function of gap size for the sphere-sphere gap electrode geometry in air. The experimental results are compared to the data published by Kuffel [2] for the gap size range of interest in this work; 10 mm to 300 mm. It can be seen that the two data sets practically overlap, with a maximum percentage difference of 3 % which shows the correctness of the test setup calibration.

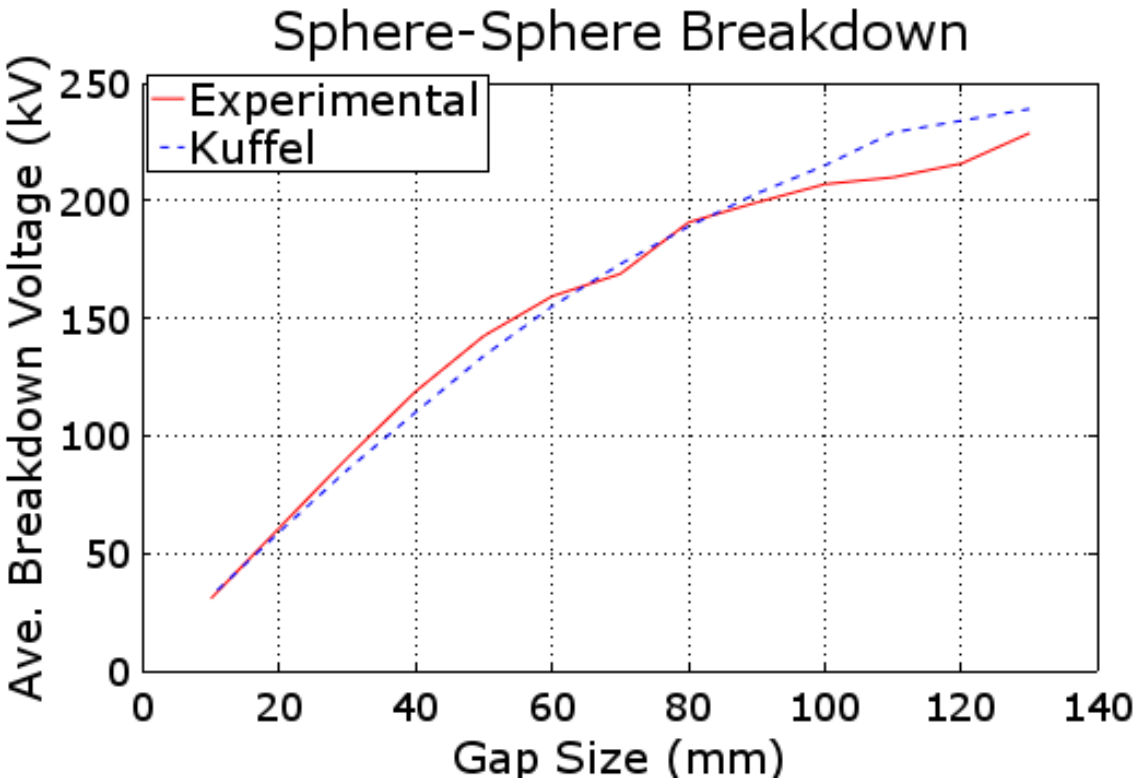

FIGURE 4.10: Sphere-Sphere breakdown calibration results compared to published data.

The data was corrected to standard atmoshperic conditions using the SANS60060-1:2011 standard. The measured environmental conditions for the test calibration are given in Table 4.1. The fact that the corrected data replicates the published data shows that the correction is valid. Based on this, the validity of the remainder of the tests and measurements for the rod-plane electrode geometry can be trusted to

represent accurate measurements since the only difference to the calibration setup would be the gap geometry in the tests.

TABLE 4.1: Chamber air conditions for the calibration tests

Parameter	Sphere-Sphere
Temperature $[^oC]$	21
Pressure $[mBar]$	833.7
Relative Humidity [%]	35.2

The data has been corrected for pressure, temperature and humidity according to the SANS 60060-1:2011 standard [33]. Stating that if the tests were performed in standard atmospheric conditions defined as the pressure p_0 being 1013 mbar, temperature t_0 at 20 ^oC and humidity h_0 being 11 g/m^3 the breakdown voltage U_0 would have been observed to be given by equation 4.1.

$$U_0 = U/K_t \tag{4.1}$$

Where U is the measured voltage, and the correction factors k_1 for air density correction and k_2 for humidity correction are embeded in K_t as:

$$K_t = k_1 k_2 \tag{4.2}$$

And the air density correction factor is given by:

$$k_1 = \delta^m \tag{4.3}$$

Where m is an exponent dependent on gap geometry and assumed to be 1 in this study. The relative air density is:

$$\delta = \frac{p}{p_0} \times \frac{273 + t_0}{273 + t} \tag{4.4}$$

And the humidity correction factor is given by:

$$k_2 = \left(1 + 0.014\,(h/\delta - 11) - 0.00022\,(h/\delta - 11)^2\right)^w \tag{4.5}$$

4.3.2 Rod Plane Breakdown

The average chamber conditions for the rod-plane tests in both air and flue are presented in Table 4.2. An increase of approximately 105% and 76.6% in the chamber temperature and humidity is recorded, while the pressure remained almost constant.

TABLE 4.2: Chamber air conditions for the Rod-Plane tests

Parameter	Normal Air	Petrol Flue	Diesel Flue
Temperature $[^oC]$	23.4	48	35
Pressure $[mBar]$	832.8	833.5	838
Relative Humidity [%]	36.8	65	62

The test results are plotted in Figure 4.11, each data point is an average of 10 breakdowns per gap size. The plots shown are for normal air and for flue polluted air conditions where the tested gap size range is from 10 mm to 300 mm. Gap sizes beyond 300 mm could not be tested due to the limitations of the used DC generator.

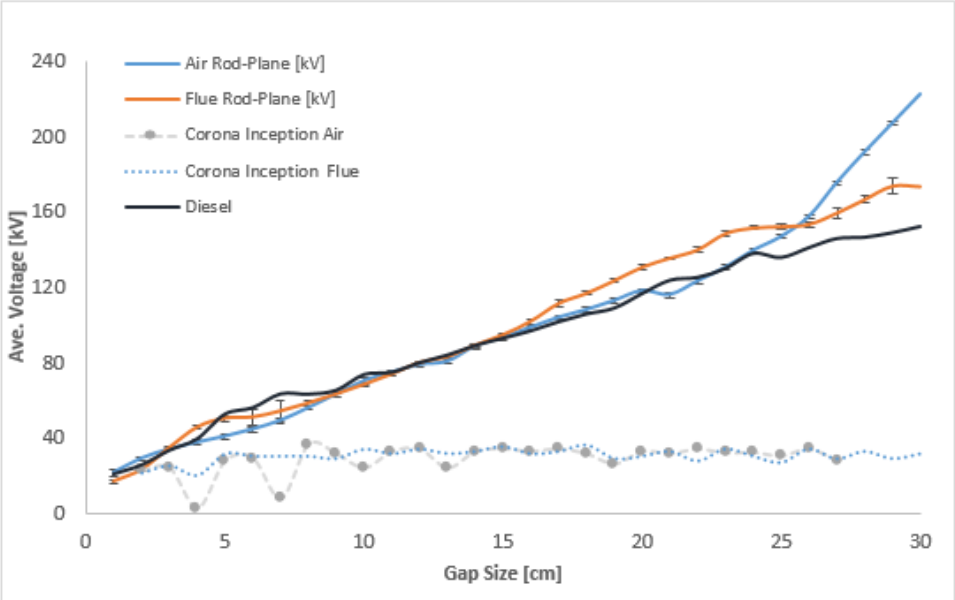

FIGURE 4.11: Breakdown voltage curves for the rod-plane tests in air, petrol and diesel flue.

As expected, the breakdown voltages are much less than that of the sphere-sphere tests. This is due to the high magnitude and non-uniformity of the electric field distribution in the rod-plane gap geometry compared to that of the sphere-sphere geometry. The results have not been corrected to standard atmospheric conditions as the main focus is to understand the practical impact of the atmospheric conditions created by the engine flue. Atmospheric correction of HV breakdown results is normally performed to get a view of how the tested gap or equipment would behave under a different atmosphere. In the case of this study, the environmental conditions created by the engine flue are of interest and thus no corrections are needed since the results already depict the scenario of interest. The general trend is as expected, the breakdown voltage increases almost linearly with increasing gap size. The results show that the breakdown voltages in petrol flue conditions are marginally higher than that of normal air conditions in the range of 30 mm to 250 mm. While diesel flue breakdown results overlap with the air breakdown results for this range.

The introduction of engine flue pollution compromises the breakdown strength of the air outside this range; where the major compromise is seen at the gap sizes bigger than 250 mm for petrol flue and for sizes bigger than 240 mm for diesel flue. The maximum recorded increase in breakdown voltage is 26 % occuring at the 50 mm to 70 mm gap sizes while the maximum decrease in breakdown voltage is 21 % at 300 mm for petrol flue and 36 % at 300 mm for diesel flue. Interestingly, a decrease has also been reported by Lambeth [3] on AC tests for cooled flue and different rod dimensions. These results show that in a real world scenario where the voltage is 3 kV and the minimum clearance of 110 mm, the gap would not breakdown in both normal air and in flue polluted conditions provided that the flue temperature averages at 35 ^oC to 50 ^oC. It can be seen from Figure 4.11 that 70 kV to 80 kV is required to breakdown the 110 mm air gap.

In order to explain these observations, gas dynamics and corona needed to be investigated as it is known that pre-breakdown corona mechanisms determine the breakdown voltages and the behaviour of the streamers. The manner in which pre-breakdown corona affects breakdown phenomena in gases is described below and an analysis of the corona results is then given.

4.3.3 Pre-Breakdown Corona

In non-uniform gap geometries, many forms of discharges are often observed prior to complete breakdown of the gap. The various discharges are caused by the electron-impact processes occuring within the region of high electric field stress. The pre-breakdown discharges are called corona and they often affect the level of voltage at which complete breakdown is observed [2]. The electron dynamic processes such as ionisation and attachment occur near the high voltage electrode, the region in which the reactions are dominant is known as the active region. In the presence of an applied voltage, free electrons will accelerate and collide with molecules, freeing more electrons and creating negative and positive ions in the process.

This process creates a plasma of charge, in which the electrons are attracted to the positive electrode, positive ions slowly drift towards the ground electrode and faint streamers of discharge known as corona discharges are formed. The level at which the corona discharges begin is termed corona inception and the inception voltage depends on the gas pressure, electric field, gap geometry and gas types. The discharge streamers formed may propagate through the gap only if the applied voltage is high enough to allow the electric field in the streamer head to be greater than the minimum field E_c being about 2.5 kV/mm [2]. At this point the ionisation processes in the streamer head are able to self propagate and bridge the gap.

Often the corona reaches a steady state before it transforms into self sustained streamers, this state is observed by a luminious glow at the high voltage electrode and can be seen to be purple in positive voltage electrodes, this mode of corona is called glow corona. The type of breakdown that occurs is also affected by whether the corona mode is glow or just streamer corona [2, 45]. The positive glow has many positive ions that suppress the electric field needed for sustained streamers, therefore more voltage is needed to breakdown the gap, or alternatively, the gap size may be decreased in the presence of the glow in order for spark breakdown to occur [2, 43, 45]. Below is a discussion of the observed corona and how it may be affecting the breakdown voltage characteristics of the experiments in this study. The corona measurements shown are for petrol flue, the measurements for diesel flue are similar as was seen from the breakdown results.

Corona Inception

Corona inception is defined as the onset of the discharge activity and the voltage at which the discharge activity is first observed is known as the inception voltage [2]. Corona activity has been measured using a current transformer that measures the leakage current due to the discharge in the gap. The corona activity is reported in volts rather than amperes as the output of the CT is volts and the study is more interested in the behaviour rather than the actual magnitudes of the corona currents. The inception voltages for the DC tests are shown in Figure 4.11, and interestingly the observed inception voltages do not change with increasing gap sizes. For both air and flue conditions, the inception voltages average at 30 kV. This invariance of the inception voltage was also reported by Hassan in [43] who experimentally studied corona and breakdown in small gaps with a needle-plane gap geometry. It can be seen that for gap sizes less than 50 mm, corona inception is very close to breakdown voltage. In the present work, no corona was observed for 10 mm and 20 mm as there was no measured pre-breakdown activity; this is attributed to the fact that at these gap sizes, the 15 mm diameter of the flat-bottom rod was bigger than the gap size

and so created a quasi-parallel plate gap geometry with a uniform field where corona may not exist before gap breakdown.

Why Corona Inception is Independent of Gap Size and Environment

To understand why the observed corona inception voltages are independent of the gap sizes and type of environment, focus is on the critical region also known as the active region. For corona to occur, the threshold for inception in the critical region is governed by the streamer criterion, stating that the number of electrons in the avalanche head must be greater than the critical minimum value of N_{crit} described by equation 4.6 [2, 46]:

$$exp\left[\int_{\delta z}(\alpha-\eta)dz\right] > N_{crit} \tag{4.6}$$

It is evident from equation 4.6 that the important parameter is the effective ionisation $(\alpha-\eta)$, as such, the effective ionisation was computed for air and flue and is shown in Figure 4.12. The effective ionisation $(\alpha-\eta)$ is computed by taking into account the gas molecular compositions of air and that of diesel flue given in Table 2.4 using the the Bolsig method described in [39]. They are calculated for a generalised volume with gas neutral particle density N, the output coefficients are then given with respect to a reduced electric field E/N with units of Townsend (Td) where:

$$1 \quad Td = 10^{-17} \quad V.cm^2 \tag{4.7}$$

It can be seen from Figure 4.12 that the effective ionisation of air is higher than that of flue, with the trend being linear for the most part of the electric field range. More importantly, for explaining why corona is independent of gap size, two electric field ranges are identified in Figure 4.12. These are for electric fields less than 200 Td and greater than 200 Td; where the effective ionisation coefficients for both air and flue are equal for fields less than 200 Td. For fields greater than 200 Td, the two

coefficients differ, with air having a greater effective ionization coefficient.

According to equation 4.6, if the effective ionisation $\alpha - \eta$ is the same for two different gaseous systems and the critical region δz kept constant, then N_{crit} will be reached at the same voltage for the different gaseous systems. In the case of the air and flue systems, Figure 4.12 shows that the effective ionizations of these gases are equal for electric fields below 200 Td. As such, the corona inception voltage would be the same for these gases if the critical field is below 200 Td. Since the experimental measurements showed that the inception voltages for the gases are the same, it follows that for air and flue in this study, corona inception occurs in the critical region δz when the electric field is approaching 200 Td, an exact value cannot be determined at this point.

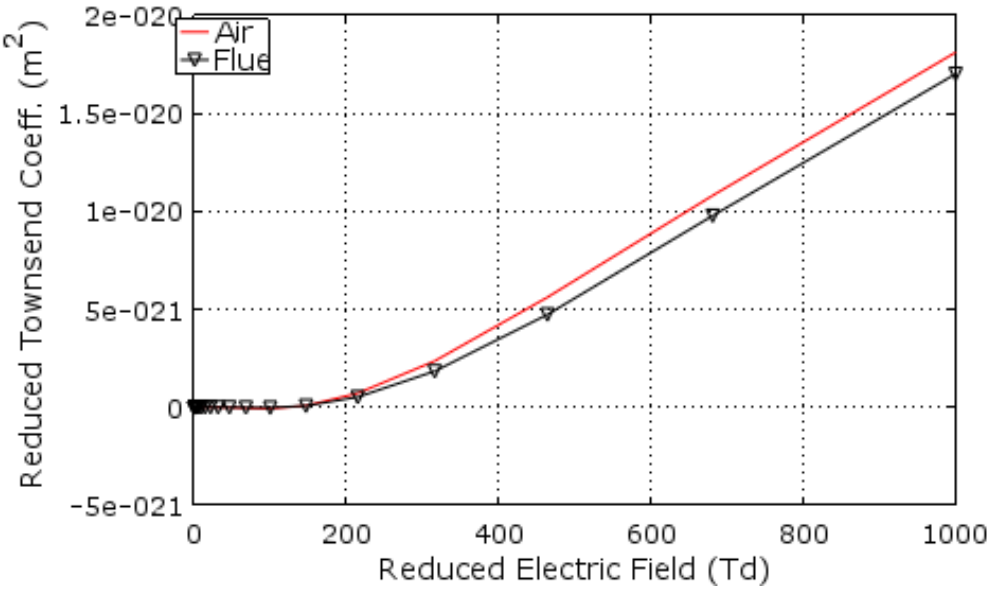

FIGURE 4.12: Effective ionisation coefficient for air and flue

For the specific gap geometry in this study, it is found that this electric field of 200 Td corresponds to an applied voltage of 30 kV, the measured inception voltage. Additionally, the size of the critical region is speculated to be 10 mm to 20 mm. This is because at these gap sizes, no corona inception was observed prior to breakdown, meaning that the corona inception voltage was the breakdown voltage observed to be in the range 20 kV to 30 kV. The corona inception is independent of the gap size

because inception happens in the critical region, which in this study was deduced to be 10 mm to 20 mm and thus because all the gap sizes were greater then this critical region, the applied voltage exceeded the inception voltage of 30 kV, consequently satisfying the inception voltage criteria.

Pre-Breakdown Corona Magnitude and Pulsation

The corona voltage magnitude before breakdown is shown in Figure 4.13 where it is evident that the magnitude of the corona breakdown is much higher in flue than in air. This is consistent with the breakdown voltages reported above, but most importantly, it is noted that the difference between air and flue pre-breakdown corona magnitude increases with increasing gap size. This shows a direct relationship between pre-breakdown corona magnitude and breakdown voltage. The corona magnitude is defined as the peak of the corona waveform in Figure 4.14 captured before breakdown.

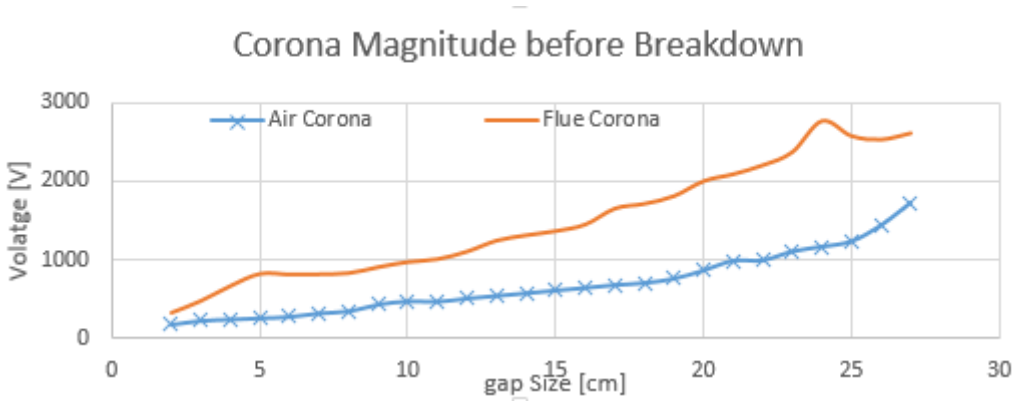

FIGURE 4.13: Pre-breakdown corona magnitude in air and in engine flue gas.

The corona pulsation activity was recorded for both air and flue conditions, Figure 4.14 shows the recorded corona waveforms for a 4 cm gap and a 23 cm. The pulsations represent corona activity and are present in all four waveforms, but it is noted that the pulsations in flue are more pronounced and significantly higher in magnitude than that in air.

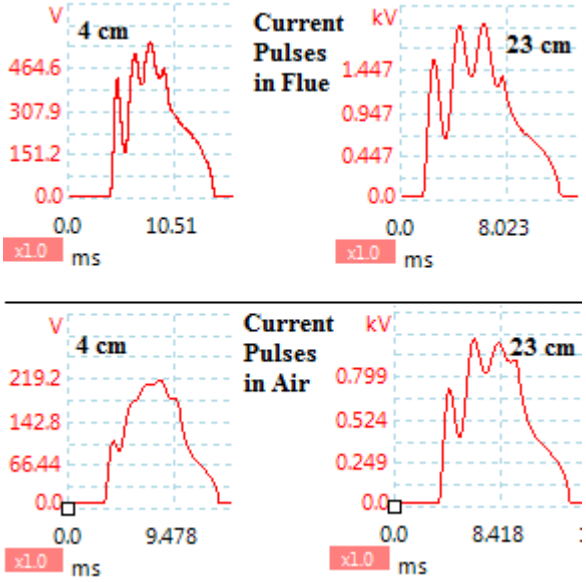

FIGURE 4.14: Comparison of pre-breakdown corona activity in air and flue at 4 cm and at 23 cm. CT output shown as voltage.

Two major observations are noted. The first one being that the pulsations in air are not as pronounced as in flue. In flue, the pulses are clearly visible while this is not the case for air. This implies that the pre-breakdown corona activity in flue is more intense than that in air. The magnitude of the pulses was measured from each pulse's origin on top (peak-to-peak) of the ripple waveform of the DC generator, where it was found that the peak-to-peak corona voltages in flue are 95 % higher than that of air at 40 mm. With this consistancy showing a 94 % difference in peak-to-peak corona voltage of flue compared to that of air at 230 mm. This result is as expected because of the observed higher breakdown voltages in flue shown in Figure 4.11.

To explain the reason for these corona behavioural differences, one needs to look at what really happens that forms corona pulsations and how flue gas might then affect this. It is known that in positive corona, particularly in the onset streamer mode of corona, the pulsation in Figure 4.14 is due to the collapse and rejuvenation of the electric field during ionisation. The sketch shown in Figure 4.15 illustrates how the electric field is collapsed due to the corona space charge; as the laplacian electric field is increased, a number of ionisation processes occur near the anode.

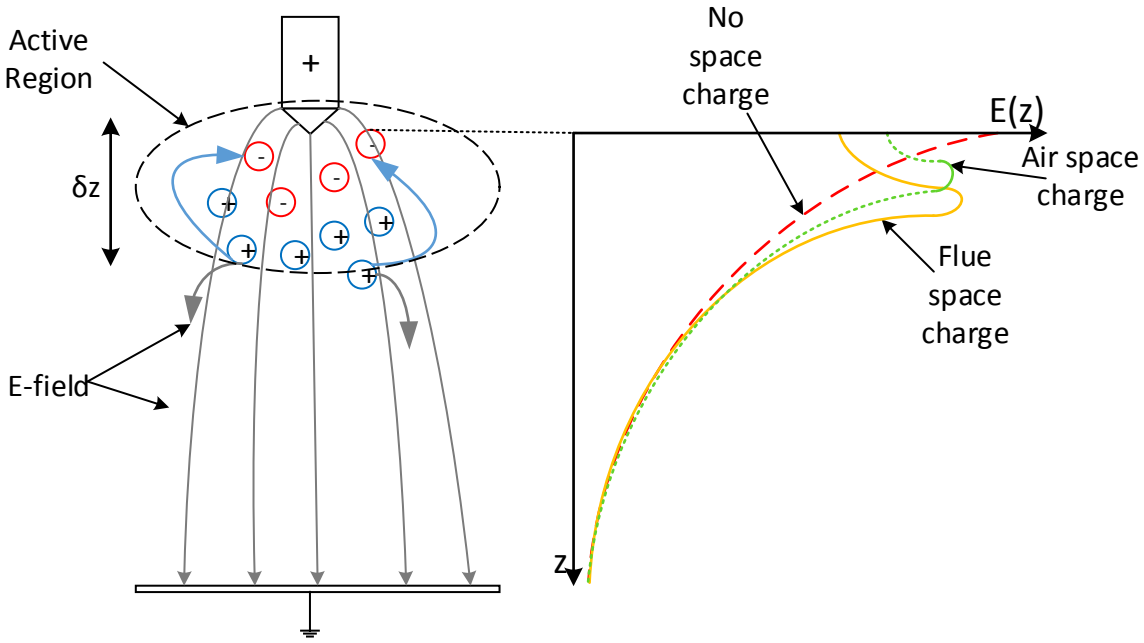

FIGURE 4.15: Illustration of electric field collapse due to corona space charge.

These processes include electrons being absorbed into the anode and electrons being absorbed by electronegative molecules to form negative ions leaving a positive space charge around the anode. The positive ions are attracted to the ground electrode but move much slower than electrons due to their size and low mobility. As a result, the positive space charge then shields the anode by forming a local space charge cloud before moving away from the anode [47]. Consequently, the electric field inside the discharge area is decreased by the opposing electric field formed by the positive space charge distribution. The space charge distribution results in the electric field being enhanced a distance away from the anode, which may then allow self-sustained ionisation irrupting at this distance. If the resultant electric field is less than the critical minimum electric field E_c in δz then self-sustained ionisation is supressed.

This results in the ceasation of the electron avalanches and the developing streamers may extinguish. The space charge cloud is then removed by the applied voltage and the laplacian electric field is restored, allowing the avalanche electrons to regenerate

and this process repeats itself for as long as the applied voltage does not provide enough E-field strength for sustained ionisation. At this point, if the streamers are unable to finally propagate out of the active region, the pulsations will not stop. When the breakdown finally happens, it is said that the breakdown is corona stabilized. This corona phenomena inhibits breakdown of the air gap, hence the phenomenon is called corona stabilization [2, 43].

Observed Corona Stabilization

Corona stabilization is a specific phenomena in which during partial discharge, a cloud of positive ions (also referred to as space charge) forms around the tip of the positive electrode due to a slow rising voltage [44]. The positive ion cloud decreases the electric field strength near the electrode, which results in breakdown occuring at a higher voltage. Consequently, corona stabilization then also results in the corona taking longer to transition from streamer mode to glow then breakdown. In this work, the author defines corona stabilization by quantifying the magnitude "X" of the corona pulses as a percentage increase of where the pulse occurs at "Y" as shown in Figure 4.16.

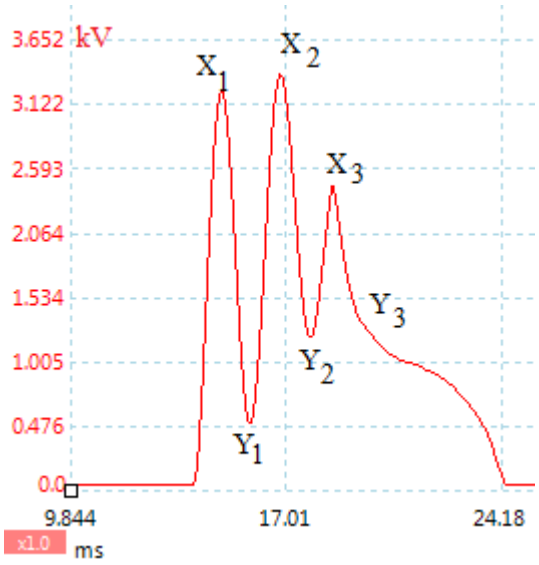

FIGURE 4.16: Illustration of points used to compute pulsation %

The pulsation % is defined by equation 4.8. Which calculates the average pulsation % for a gap size, the average is for the number of pulses n that occur on a corona waveform which were observed as 2 pulses for air and 3 pulses for flue in the tests.

$$pulsation\% = \sum_{i}^{n} \frac{X_i - Y_i}{n \times Y_i} \times 100\% \tag{4.8}$$

From Figure 4.14, it is evident that the corona stabilization phenomenon is more prevalent in flue than in air. In the case of this study, the major difference between flue and air is the gas composition of the flue gas system. In which water molecules and carbon dioxide are introduced into the oxygen and nitrogen gas system. Furthermore, it has been found that in small air gaps, the three-body attachement process given in equation 2.1 dominates the gas dynamics during ioninzation in air which results in the loss of electrons [26]. Hence due to the increased humidity of the flue gas, the processes by which possible electrons get depleted near the anode to form negative ions are increased. This means that more positive ions are left over to form the space charge cloud around the anode, and as such, corona stabilization is enhanced in flue which lead to the higher breakdown voltages observed in flue comapared to air. This explains why the calculated Townsend effective ionisation coefficient for flue is low; the rapid attachment of electrons leaves behind the positive space charge which in turn enhances the corona stabilization effect. The curves plotted in Figure 4.17 show the characterisation of the corona stabilization effect through equation 4.8, which shows that the percentage increase of the pulse magnitudes for air and flue both increased with increasing gap size.

The corona stabilization is generally higher in flue, which confirms that indeed breakdown voltage is governed by corona mechanisms. Most interestingly, as the gap size is increased, the corona stabilization increased in both gas systems, but increased 20 % more in air than that in flue. Furthermore, It can be seen that after 250 mm the rate of this increase in air becomes even higher while that of flue continues in the slow

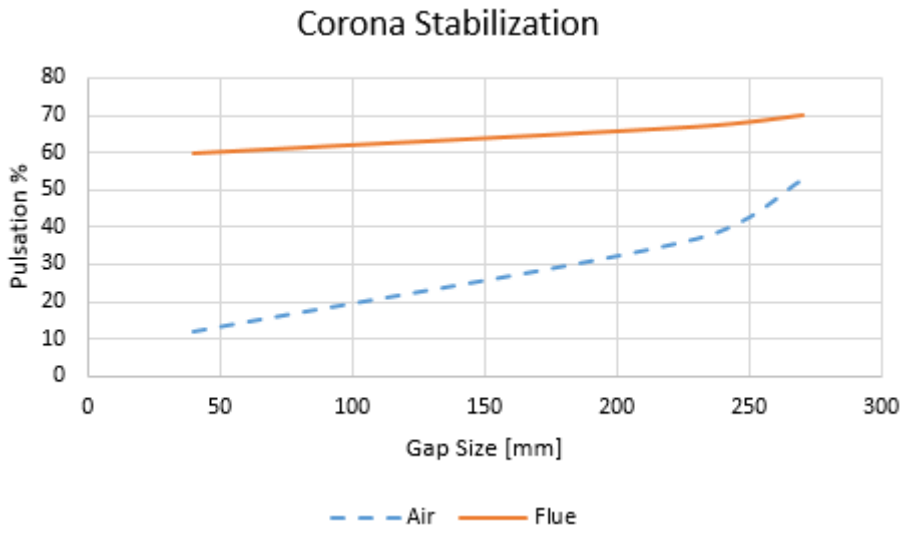

FIGURE 4.17: Corona stabilization with increasing gap size.

steady increase. This change also reflects on the breakdown voltages at the cross over point, where breakdown in air becomes higher than in flue. It is thought that above 250 mm, the breakdown mechanism in air is different due to the change in the corona mechanism while that in flue does not change. It seems as though the enhanced corona stabilization in flue prevents the change of corona mechanism and hence no change in breakdown mechanism as observed in air, this consequently allows the flue gas to maintain the steady rate of increase in breakdown voltage. It is speculated that the change of breakdown mechanism in flue may happen at bigger gap sizes than the tested range, that the enhanced corona stabilization shifts the point at which the change must occur.

The characteristics of the engine flue included the airflow of exhaust draft which it was stated in the background section that this might affect the breakdown in flue. The engine flue was introduced inside the chamber from the bottom and the measured airflow velocity was 2.5 $cm.s^{-1}$ upwards which is quite slow when compared to the velocities mentioned in the background section. Thus it is concluded that the flue velocity was too small to remove any space charge and have any considerable influence on the corona. Furthermore, Swanson [18] identified that airflow speed affects

the repeatition rate of corona pulses; which was calculated to be 0.6 $pulses.ms^{-1}$ and 0.55 $pulses.ms^{-1}$ in flue and air respectively. This small difference in repeatiton rates confirms that the measured airflow speed of 2.5 $cm.s^{-1}$ could not affect the corona and thus the effect of humidity and corona stabilization is thought to be the major contributor to the observed corona and breakdown characteristics of flue when compared to that of air.

To verify the effects of space charge and humidity on corona stabilization that increased the breakdown voltages of flue, impulse tests were conducted as presented in the following section. Where the aim is to observe any changes in the breakdown voltages in flue since the space charge in impulse voltages is reduced due to the short time available for charge formation.

4.4 Impulse Experiment Setup and Procedure

The impulse experiment setup and procedure is detailed in this section. The parameter of interest is the difference between the breakdown voltages of air and flue polluted air. As mentioned above, the effects of space charge on corona stabilisation is said to be the main factor in the observed differences on the breakdown voltages of flue and air. The space charge is affected by the increased humidity of the flue and results in increased corona stabilisation. This resulted in increased breakdown voltage levels of flue when compared to that of air. As such, the impulse tests are performed to verify the effect of the flue humidity on corona stabilisation. Impulse voltages force breakdowns without allowing enough time for space charge to build up, this characteristic is suitable for observing how the humidity which is postulated to act on the space charge will affect the breakdown in a low space charge environment. This is beacuse the absence of the space charge should then allow the flue and air breakdown levels to be almost the same if the proposed effects of humidity on stabilisation are true.

4.4.1 Experimental Setup

The impulse experiment setup is shown in Figure 4.18; the only difference between the impulse and the DC experiment setup is the type of source and the data acquisition system. A five stage Marx generator is used in this experiment, with the wave shaping output resistor and capacitor selected for a standard 1.2/50 μs standard lightning impulse. In this setup, no corona measurements are made, instead an oscilloscope is used to record the lightning impulse waveform through a potential divider circuit as the data acquisition system.

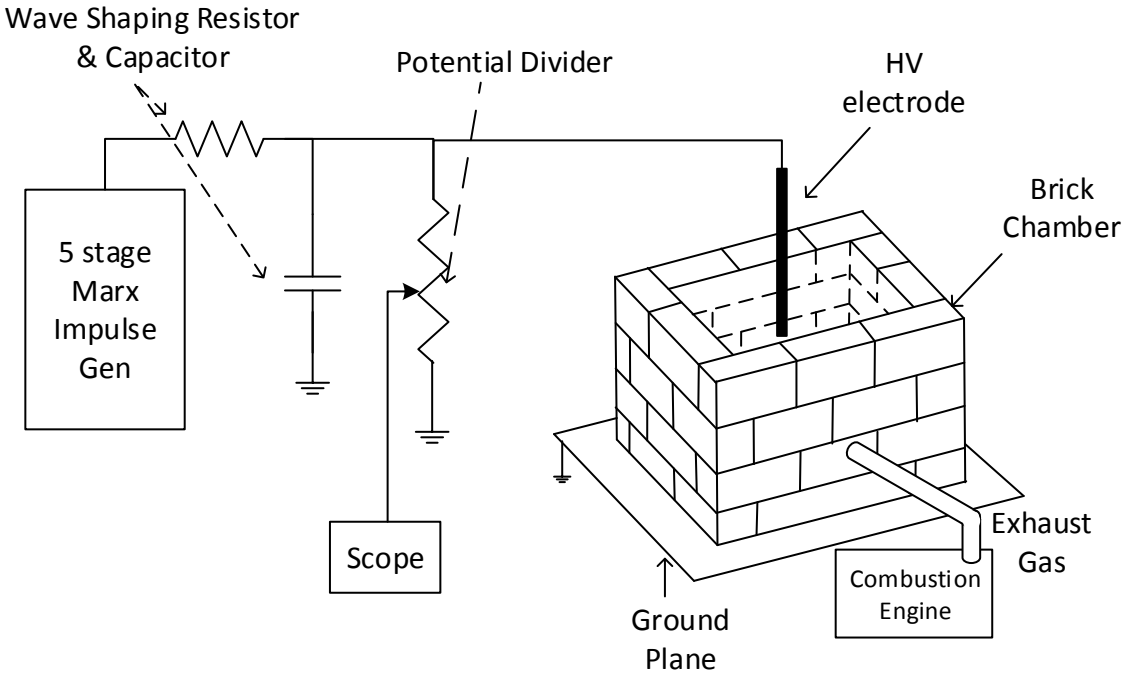

FIGURE 4.18: Impulse test setup

Only a rod-plane gap geometry is tested under impulse conditions and Figure 4.19 shows the images of the laboratory setup. The chamber image is the same as the one in the DC setup.

The Test Procedure

The impulse tests are conducted for the gap range of 10 mm to 300 mm in both air and in flue conditions. The experiment is conducted in accordance to the IEC 60060

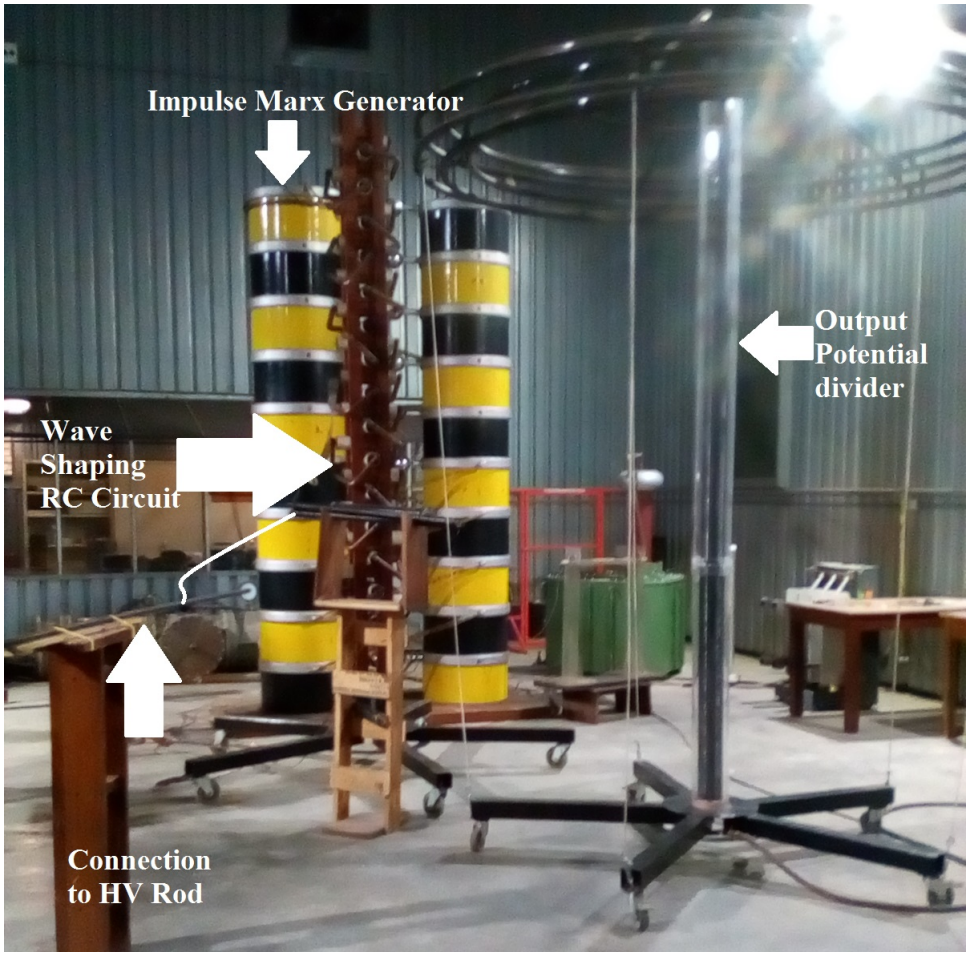

FIGURE 4.19: Image of the laboratory experiment setup for impulse tests

U_{50} impulse test procedure. The gap sizes are increased in steps of 10 mm and for each gap size, a U_{50} impulse test is performed with 20 breakdowns.

After performing the U_{50} test for each gap size, the voltage at which there is a 50 % probability that the gap might breakdown is then calculated by taking the average of the recorded 20 breakdown and withstand voltages through equation 4.9 per gap.

$$U_{50} = \frac{1}{20} \sum_{i}^{20} V_i \tag{4.9}$$

Where V_i is the recorded breakdown or withstand voltage.

4.5 Impulse Experiment Results and Discussion

This section gives the impulse experiment results for both air and flue conditions. The U_{50} results are given and discussed, furthermore, they are contrasted with the DC results in order to check the extent of the effect of space charge on the corona stabilization discussed in the DC results section. Figure 4.20 shows the 1.2/50 μs standard lightning impulse waveform used in the experiments, generated in the HV laboratory. Table 4.3 gives the average chamber environmental conditions for the impulse tests.

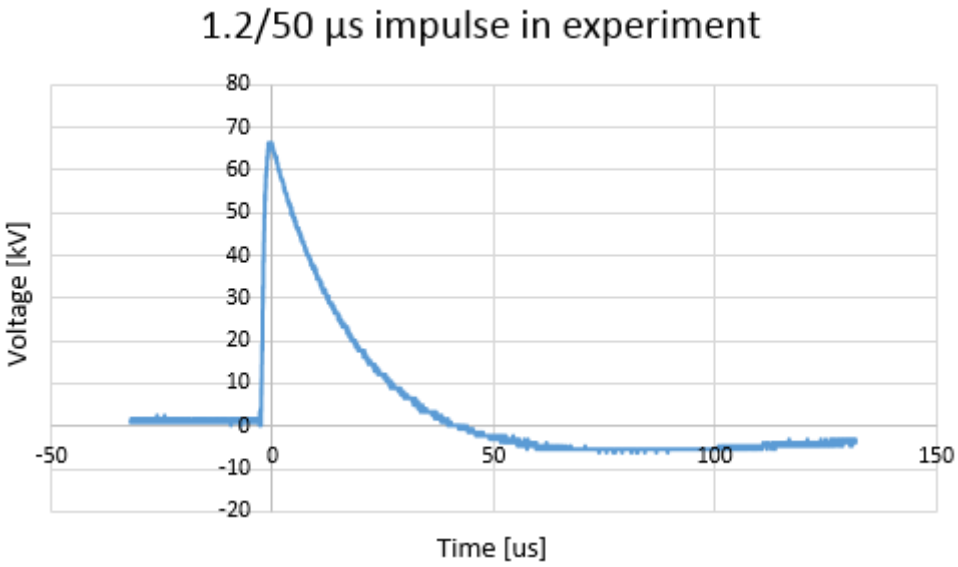

FIGURE 4.20: Laboratory generated standard 1.2/50 μs lightning impulse waveform

TABLE 4.3: Chamber air conditions for the Rod-Plane impulse tests

Parameter	Normal Air	Petrol Flue	Diesel Flue
Temperature [^oC]	24	47	19
Pressure [$mBar$]	833	834	836
Relative Humidity [%]	36	64	62

Impulse Breakdown

The U_{50} impulse voltages with increasing gap size for flue and air are shown in Figure 4.21. As expected, the U_{50} voltages are higher than that of DC breakdown voltages,

this is because in impulse test, the impulse waveform is applied for a very short period of time which results in more voltage needed to breakdown the gap. The electron avalanche formation then needs to happen within the rise and fall time of the applied impulse waveform. The overall time needed to realise an impulse breakdown is known as the lag time t. It is composed of the statistical time lag t_s, which is the time lapse between the application of an impulse voltage and the occurance of a seed electron to initiate discharge. Then the time lapse after the initiation to breakdown is known as the formative time lag t_f [2]. Furthermore, it is known that the statistical time lag and formative time lag depend on the pre-ionisation and discharge mechanism respectively.

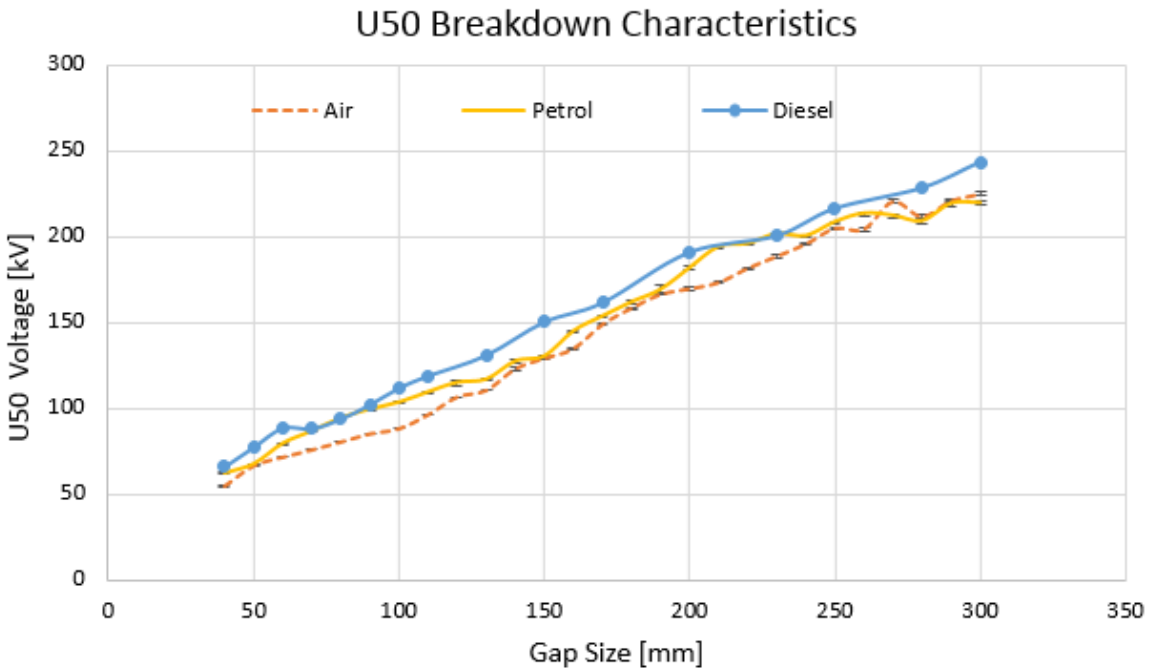

FIGURE 4.21: Experimental impulse U50 breakdown characterstics for flue and air

The overall trend is still linear and the presence of flue has similar effects as in the DC tests where it can be seen that the impulse breakdown voltages in flue are slightly higher than in air. This shows that breakdown processes in gases in both cases of impulse and DC are essentially a function of the effective ionisation coefficient, since in both cases of impulse and DC tests the breakdown in flue is higher than in air. These results confirm the correctness of the Bolsig+ calculated effective ionisation

coefficients in Figure 4.12 found to be smaller in flue gas than in air. Interestingly, no cross over points where observed at 30 mm and at 250 mm as was the case with DC tests. Instead, the breakdown voltage of air after 250 mm is seen to fluctuate around the breakdown voltages of the petrol flue curve rather than crossing it. The breakdown voltage curve of diesel flue is however marginally higher than that of both petrol and air. The average difference is calculated to be 18 kV when compared to air. This difference is attributed to the decreased temperature of 19 ^oC during the diesel impulse tests as given in Table 4.3. It is thought that humidity played no major role in this increased breakdown curve because the humidity of the petrol and the diesel tests were similar, as a result it can be expected that if the temperatures were also similar the curves would overlap more closely than the current result.

The impulse experiment is used to test if the decrease in pre-breakdown space charge would affect the corona stabilization effect that was enhanced by the flue humidity in DC. Visually, it is difficult to tell from Figure 4.21 if the deviation of the flue breakdown voltages from that of air have changed in impulse conditions compared to DC. As such, the weighted mean percentage increase (WMPI) between the DC and impulse results is used to compute any differences between these two cases, the WMPI is given by equation 4.10.

$$WMPI = \frac{U_{air}}{\sum_{i=1}^{k} U_{air_i}} \left(\left| \frac{U_{air} - U_{flue}}{U_{air}} \right| \times 100\% \right) \tag{4.10}$$

The WMPI is used to highlight the relavancy of the differences between the two curves while ensuring that the points where there is no difference do not void the differences observed, which is the case with simply taking an average difference accross the data. Figure 4.22 compares the WMPI of DC breakdown voltages against that of impulse U_{50} voltages. It is found that the use of LI decreases the WMPI between air and petrol flue; in DC tests, the calculated WMPI between air and flue is 10.3 % while it is found to only be 6.55 % in impluse tests. Furthermore, the maximum percentage

increase observed in impulse tests is 11.8 % occuring at 210 mm for petrol and 12.4 % for diesel occuring at 200 mm, which is lower than the maximum percentage increase of 26.39 % observed at 50 mm for petrol and 36 % for diesel at 300 mm in the DC tests. The decrease in the WMPI when using impulse voltages shows that space charge has influence in the gap breakdown voltage under DC voltage and therefore the concept of corona stabilization is more applicable to DC. This is consistent with Bhutt's [44] argument that stabilization occurs when a slow rising applied voltage is used, whereby a DC voltage can also be clasified as a slow rising voltage during breakdown testing.

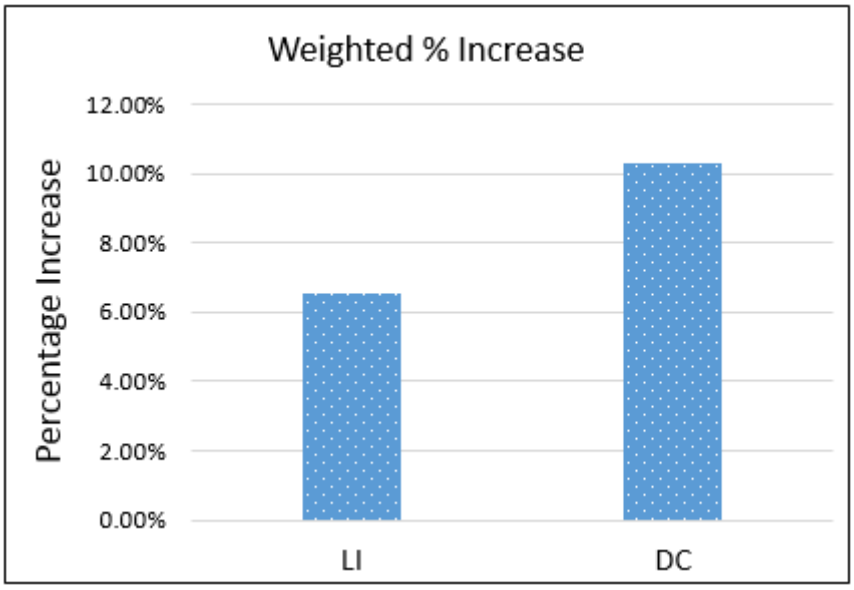

FIGURE 4.22: Weighted Mean Percentage Increase from air to flue experimental results in impulse tests and DC tests.

The diminished difference in breakdown voltages between air and flue under impulse voltages show that the recorded high humidity in the flue had minimal effects on the breakdown voltages due to the lack of space charge. The theory that the humidity acted through the space charge to enhance corona stabilization by absorbing electrons in the DC tests can be said to have been verified by the decrease in the WMPI between air and flue impulse breakdowns voltages.

This chapter presented the laboratory experimental component of the research. It was broken into two main experiments, which are DC breakdown experiments and impulse breakdown experiments. The setups and procedures of both experiments were in accordance with IEC standards. Results from the DC tests showed that the breakdown voltages in flue conditions are higher than those in normal air conditions for gap sizes less than 250 mm. The flue contamination compromised the air strength for gap sizes greater than 250 mm.

Upon analysing the results, it was found that the increased humidity of the flue caused an enhancement of the corona stabilization effect by increasing electron attachment, which then lead to an increase in the dielectric strength of air. The stabilization effect is mainly a property of the space charge, and therefore, impulse tests were conducted to evaluate the extent of how the flue affects the space charge. The results of the impulse tests also showed that flue increased the dielectric strength of the air but these effects decreased in the impulse tests. The decrease confirmed that the impact of space charge on corona stabilization had been affected by the high humidity in the flue gas. In the next chapter, the mathematical model and simulations for gas discharge are presented, where the main aim is to provide a way to verify experimental data, more so when comparing different gas systems.

Chapter 5

Discharge Modelling and Simulations

The gas discharge mathematical modelling and computer simulations are presented in this chapter. The simulations are primarily used to validate the DC experimental results by running the mathematical model in MATLAB^{TM}. A fluid dynamic model is adopted from literature and used to model the gas species as fluid under the influence of an electric field. The simulation results are given for both air and flue conditions while the shortfalls of the model are highlighted.

5.1 Modelling of Gas Discharge Phenomena

Gas discharge can be modeled as the movement of charged particles originating from the gas molecular constituents. The charged particles are primarily accelerated by an applied electric field. Among the various methods for modelling gas discharge are those using the kinetic model of gases, where the kinetic energy of the particles is from the applied electric field. This model has some limitations and thus a fluid dynamic model is often used to model gas discharge.

The most used fluid dynamics model is the flux corrected transport algorithm by Boris and Book [34] and later proposed by Morrow to be used to numerically describe the flow of charged gas particles in air [35]. The model has been used by Morrow and Lowke to succesfully describe streamer development and propagation in standard air conditions [36]. They found that a streamer created by a 20 kV DC source did

not brigde the 5 cm rod-plane gap tested, the streamer only travelled 3.5 cm which is expected as 20 kV is expected to breakdown only a 1 cm gap. In the model, the motion of charge is described by drift-diffusion equations and influenced by the chemical characteristics of the gas molecules in the electric field environment. Kim *et al* [37] also managed to use fluid equations in COMSOL Multiphysics to investigate and estimate the breakdown voltage of air under standard conditions. Swanson [18] used this model in investigating the role of singlet oxygen on corona in air and in a similar manner this model can be used to investigate the effects of the diesel flue gases on streamer breakdown. The model in itself is not new, Swanson combined it with a number of other developed models to represent phenomena such as photo-ionization and electric field effect. The unique aspect in this study is how it is used to understand the effects of the engine flue gas composition on breakdown strength; a phenomenon which has not been explored.

5.1.1 Flux Corrected Transport Algorithm

In order to accurately model real physical gas dynamics, Boris [34] developed a method of solving contuinity equations where the results are out of bounds due to cases of shocks and steep gradients of flows. The method is known as flux corrected transport (FCT) algorithm of solving continuity equations. This concept has two major stages, where in the first stage (called the transport), the fluid is transported from one point in space to another through a said time. In the second stage, called antidifusion stage, errors introduced in the first stage by fluid shocks and steep flow gradients at the bounds of the interested space are corrected.

Figure 5.1 is a flow diagram of the flux corrected transport algorithm, where positive and negative ions along with electrons are considered to be plasma. A seed plasma is introduced in the gap, then based on the applied voltage, the Laplacian electric field is determined and combined with the Poissonian electric field to compute the net electric

field. Swamp parameters such as Townsend, diffusion and mobility coefficients that represent the specific gas system being studied are fed into space-time drift-diffusion equations that transport the plasma ions and electrons through the gap. Furthermore, an external current due to the resulting charge movement is determined and fed back into the algorithm as a voltage drop in the next iterations. The various components that make up the algorithm are discussed in the next sections.

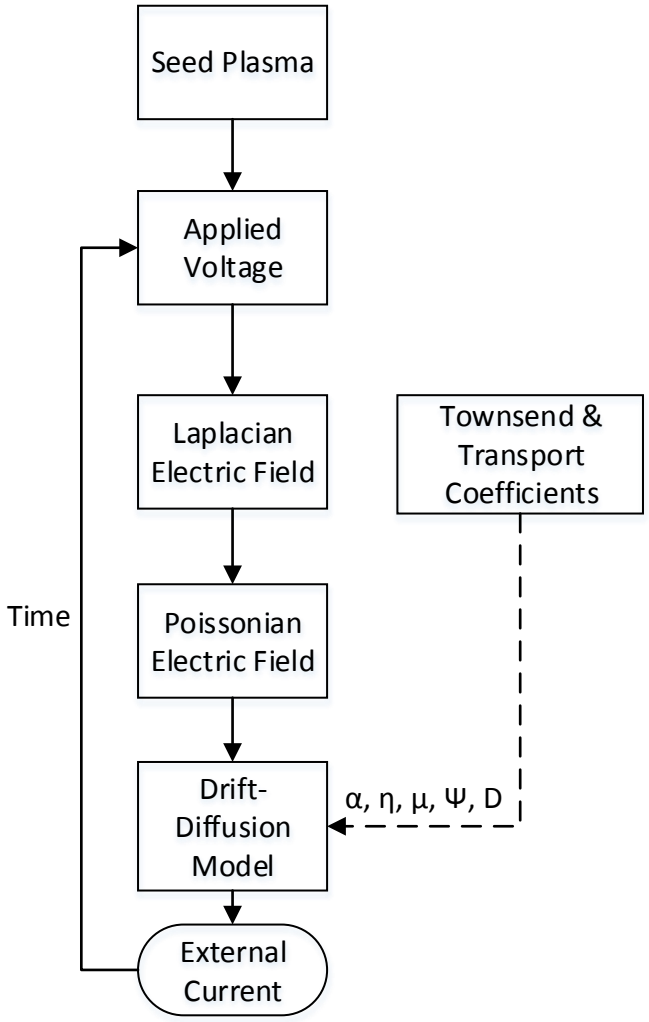

FIGURE 5.1: Flux Corrected Transport algorithm flow chart [18]

Drift-Diffusion Model

The transport algorithm performs its main function by employing drift-diffusion equations for electrons and ions, moving them through the gap like fluid. The coupled drift-diffusion equations in one dimension are given as equations 5.1, 5.2 and 5.3 [18, 34, 35, 36]:

$$\frac{\partial N_e}{\partial t} = S + N_e\alpha\,|\overrightarrow{v}_e| - N_e\eta\,|\overrightarrow{v}_e| - N_eN_p\beta - \frac{\partial\,(N_e\,\overrightarrow{v}_e)}{\partial z} + \frac{\partial}{\partial z}\left(D_e\frac{\partial^2 N_e}{\partial z^2}\right) \tag{5.1}$$

$$\frac{\partial N_p}{\partial t} = S + N_e\alpha\,|\overrightarrow{v}_e| - N_nN_p\beta - N_eN_p\beta - \frac{\partial\,(N_p\,\overrightarrow{v}_p)}{\partial z} + \frac{\partial}{\partial z}\left(D_p\frac{\partial^2 N_p}{\partial z^2}\right) \tag{5.2}$$

$$\frac{\partial N_n}{\partial t} = N_e\eta\,|\overrightarrow{v}_e| - N_nN_p\beta - \frac{\partial\,(N_n\,\overrightarrow{v}_n)}{\partial z} + \frac{\partial}{\partial z}\left(D_n\frac{\partial^2 N_n}{\partial z^2}\right) \tag{5.3}$$

Where:

$$_x = \text{Electrons } e, \text{negative ions } n \text{ and positive ions } p$$

$$N_x = \text{Number density for electrons and ions } [cm^{-3}]$$

$$\overrightarrow{v}_x = \text{Electron and ion velocities } [cm.s^{-1}]$$

$$\alpha, \eta = \text{Ionisation and attachment coefficients } [cm^{-1}]$$

$$S = \text{Photoionisation term } [cm^{-3}.s^{-1}]$$

$$\beta = \text{Recombination coefficient } [cm^{3}.s^{-1}]$$

$$D_x = \text{Diffusion coefficient } [cm^{2}.s^{-1}]$$

The equations give the change of particle density in time at a certain position in the air gap space. For example, by looking at equation 5.1, the major transport components

affecting the electron density N_e are photo-ionization S, Townsend first ionization α that generates electrons based on their velocity v_e influenced by the applied electric field, while η depletes electrons through attachemnt processes. β is the recombination coefficient governing the recombination of electrons N_e with positive ions N_p. Lastly, the last two terms describe how electrons move out of the said point in space with mobility v_e and how electrons diffuse into the said point in space through D_e.
It is apparent that the gas transport and Townsend coefficients which form part of the swam parameters need to be determined before hand in order to apply the drift-diffusion equations that will transport the charge plasma, therefore the following sections details how these are calculated.

Molecular Distribution and Cross Sections

Before delving into how the swamp parameters are calculated, one needs to understand the molecular interactions of the gas constituents. The swamp parameters are a function of electric field but the final result largely depends on the many types of electron-molecule collision reactions that could occur in the gas volume. The reactions are based on a probabilistic distribution phenomena related to the energy of an electron and the collisional cross sections for various types of reactions [18].

Molecular Distribution

One of the main aspects of electron-molecule reactions is the availability of molecules in a said volume and how their molecular energy is distributed. This is because for every possible reaction, there needs to be an electron with minimum electron kinectic energy such that the reaction results in the ejection of electrons in the air gap. Equation 5.4 describes the distribution of molecular velocities resulting from the random collisions [2] and how it varies with increasing gas temperature.

$$f(v) = \left(\frac{m}{2\pi k_B T}\right)^{\frac{1}{2}} exp\left(-\frac{mv_i^2}{2k_B T}\right) \tag{5.4}$$

Where:

$$f(v) = \text{Probability density}$$

$$k_B = \text{Boltzmann's constant}$$

$$m = \text{Mass of particle}[g]$$

$$T = \text{Temperature}[K]$$

$$v_i = \text{Velocity of particle}[m.s^{-1}]$$

And it can be seen from Figure 5.2 that the increase in gas temperature results in an increased probability that a higher number of molecules will have increased kinetic energy. This in turn implies that more electrons and ions will be freed during collisions due to the sufficient kinetic energies and hence affect the discharge process.

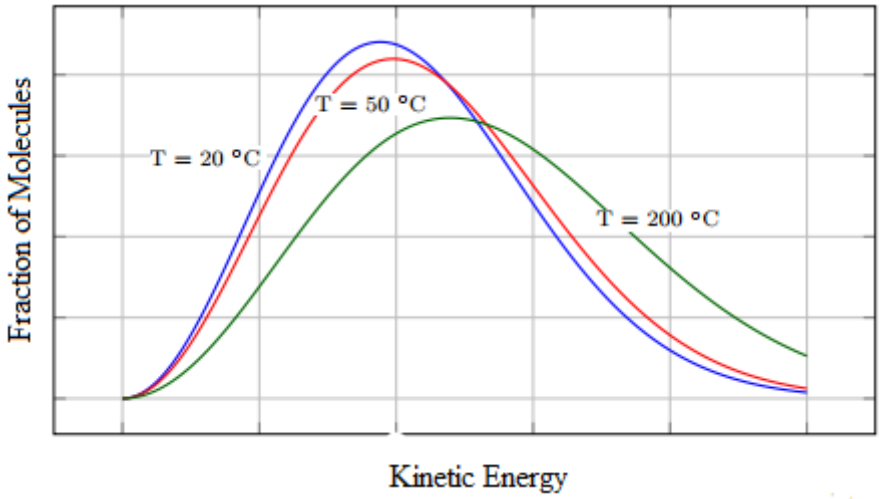

FIGURE 5.2: Maxwell-Boltzmann's distribution for number of particles with enough energy to react at temperature T. adapted from [18]

Collisional Cross-Sections

A collisional cross section is the effective area around a gas particle that another particle's center needs to be within in order to realise a collision [18]. Particles have different cross sections for various possible reactions which affect the particle's mobility, diffusion and the overal gaseous system's ionization coefficient. The collisional cross sections for the gas molecules constituting normal air and engine flue are given

and interpreted in this section. The cross-sections are based on the data published in the LXcat database [38, 40]. The collisional cross sections for oxygen, nitrogen, carbon dioxide and water are shown in Figures 5.3, 5.4 and Figure 5.5 respectively. In these figures, the cross sections are calculated for collisions between the gas molecules and an electron with energy eV. These graphs give the possible collisional reaction if the electrons with energy eV collide with the said molecule. Figure 5.3 and Figure 5.4 would represent air composition, while flue composition would have all the molecules from Figures 5.3, 5.4 and 5.5.

Cross sections for air: As expected, it can be seen from Figure 5.4 that nitrogen has a wide range of excitation reactions which absorb energy and prevent gas discharges, making it a good insulating medium. Furthermore, momentum (effective) reaction is most likely to occur across all energy ranges for all the molecules which does not contribute to any of the factors affecting discharge. Ionization in nitrogen is seen to only be possible in the upper ranges of electron energies with only one possible ionization reaction. Oxygen has a number of excited states in the lower energy regions, and two electron attachment reactions are possible in the energy ranges of 10 eV to 100 eV.

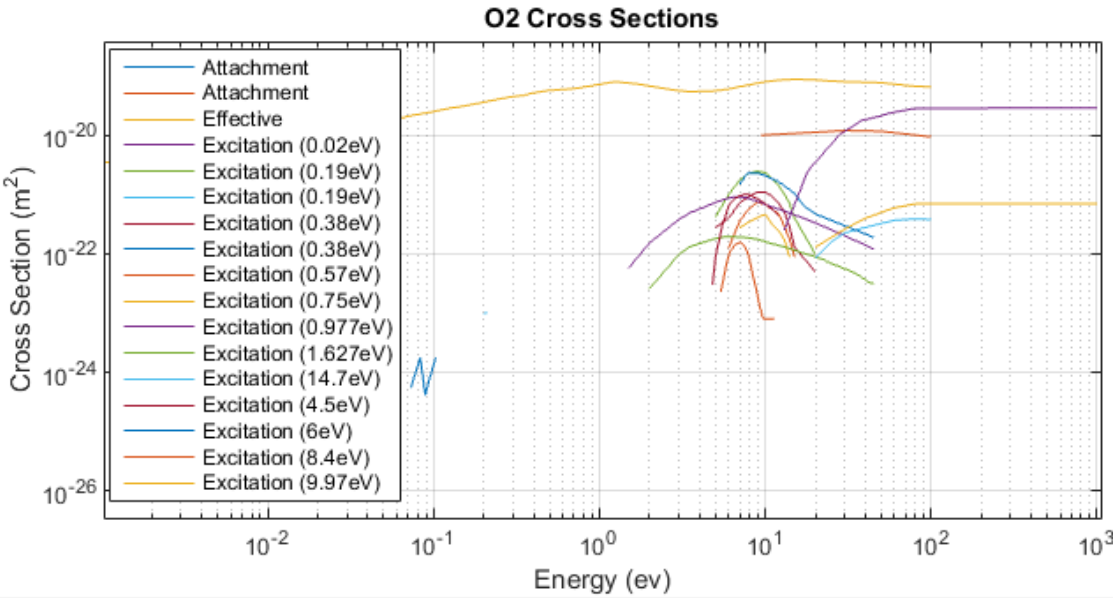

FIGURE 5.3: O_2 Collisional Cross Sections for the various possible reactions depending on the energy of the electrons colliding with the molecule.

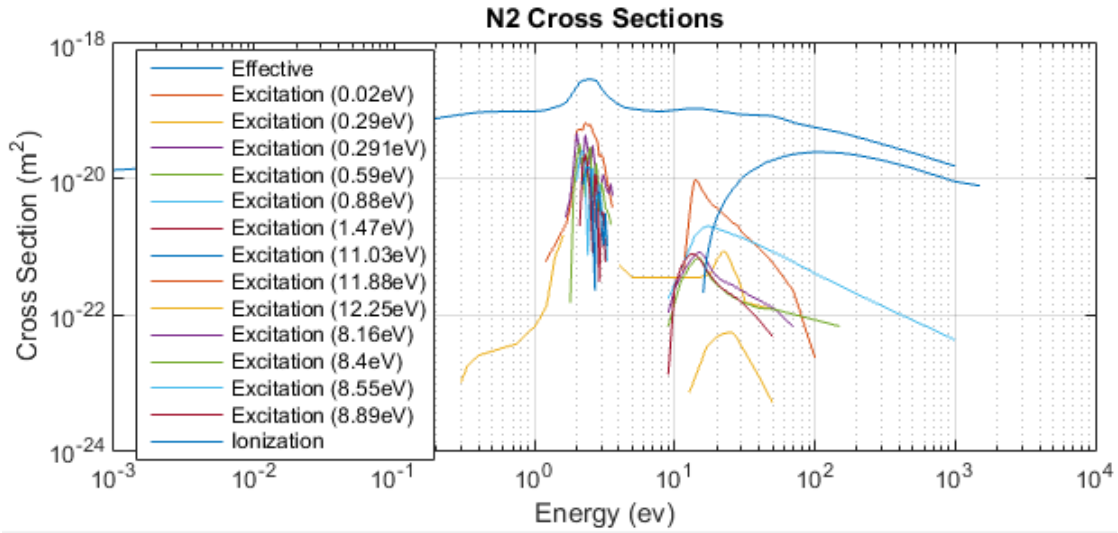

FIGURE 5.4: N_2 Collisional Cross Sections for the various possible reactions depending on the energy of the electrons colliding with the molecule.

Cross sections for Flue: Figure 5.5 is the additional molecules that flue introduces in air. The oxygen and nitrogen characteristics in air also apply here, but in reduced concentrations. It is seen that water molecules have the most attachment reactions and they are possible within a small range of energies before 10 eV. For both carbon dioxide and water molecules, the excitation states span a wide range of energies but with only one possible ionization reaction occuring at higher energies. In general, it is seen that ionization is favoured at higher energies but there's only one possible reaction for all the molecules, and attachment is seen across three molecules with the most in H_2O. In engine flue, this implies that compared to air, ionization may be counteracted by the increased attachment posibilities. These collisional cross-sections along with Maxwell's molecular distribution are used in computing the Townsend and transport coefficients for flue and air in the following section.

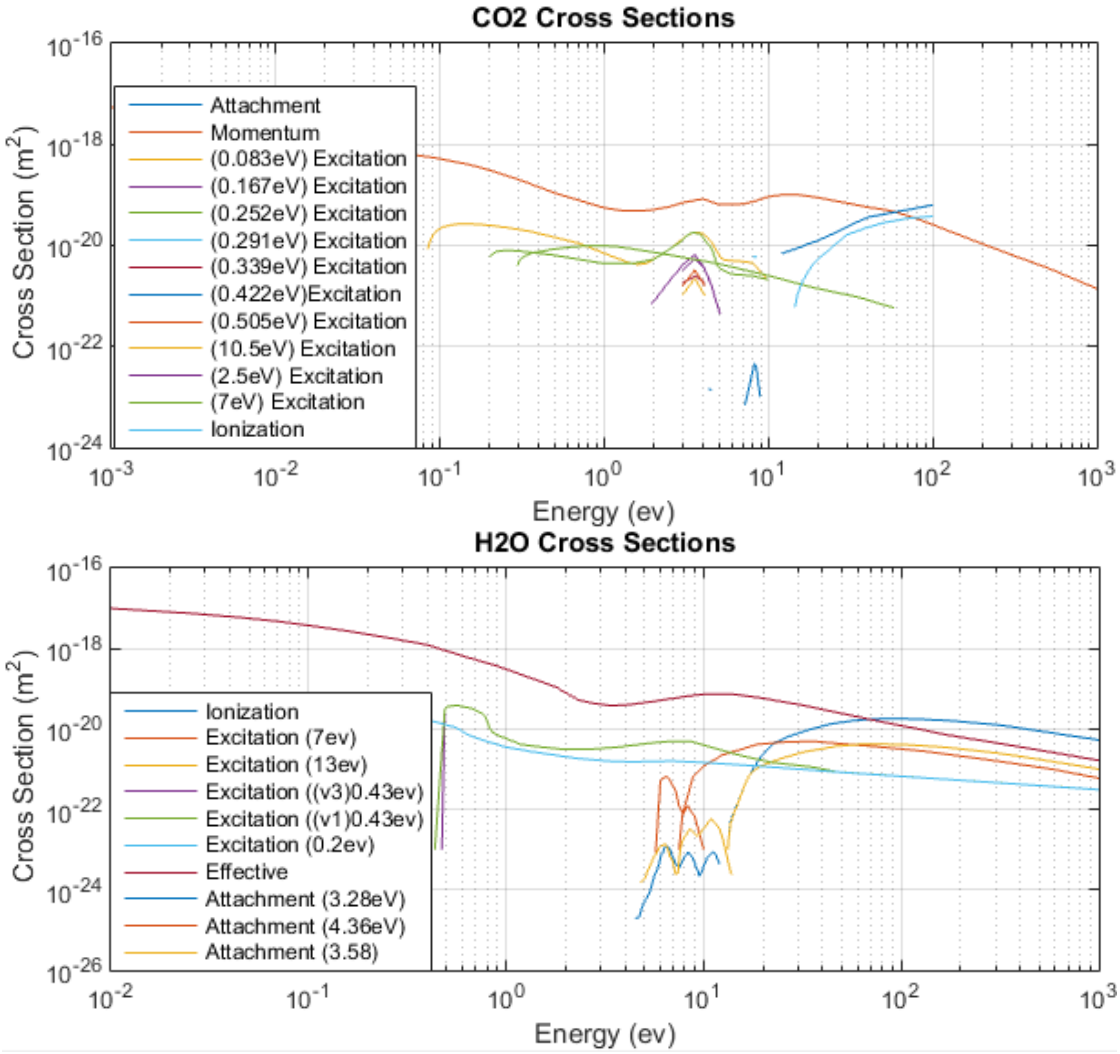

FIGURE 5.5: CO_2 and H_2O Collisional Cross Sections for the various possible reactions depending on the energy of the electrons colliding with the molecules.

Transport and Townsend Coefficients

The swamp parameters of interest are Townsend ionization and attachment coefficients, electron mobility and diffusion for both normal air and flue conditions. They feed in the transport algorithm used to describe how electrons and ions travel in space within an electric field over time. In this research, the transport and Townsend coefficients are computed by using the gas molecule's collisional cross sections described in the previous section. The cross sections are used in an algorithm that solves the

Boltzmann expression in equation 5.5; the algorithm is called Bolsig+ and it was developed by Hagelaar [39] for low temperature plasma.

$$\frac{\partial f}{\partial t} + \vec{v}.\nabla f - \frac{q}{m}\vec{E}.\nabla_v f = \left(\frac{\partial f}{\partial t}\right) \tag{5.5}$$

Where:

$$f = \text{Boltzmann Probability Distribution}$$

$$\vec{v} = \text{Electron velocity}[m.s^{-1}]$$

$$q = \text{Electron charge}[C]$$

$$m = \text{Electron mass}[g]$$

$$\vec{E} = \text{Electric Field}[V.m^{-1}]$$

The Bolsig+ algorithm is designed to compute the swamp parameters for standard pressure and temperature. This imposes a limitation on the temperature one can use to calculate the swamp parameters. The computed transport and Townsend coefficients are shown in Figure 5.6, comparing the swamp parameters of air and engine flue. When comparing the results for air and engine flue polluted air, it is evident that the reduced Townsend coefficient $(\alpha - \eta)/N$ for engine flue gas composition is less than that of normal air composed of 78% nitrogen and 22% oxygen. The difference is not significant but implies the possibility that at standard temperature and pressure, more voltage might be needed to breakdown a gap in flue gases than in air. The following sections detail the other aspects of the model algorithm.

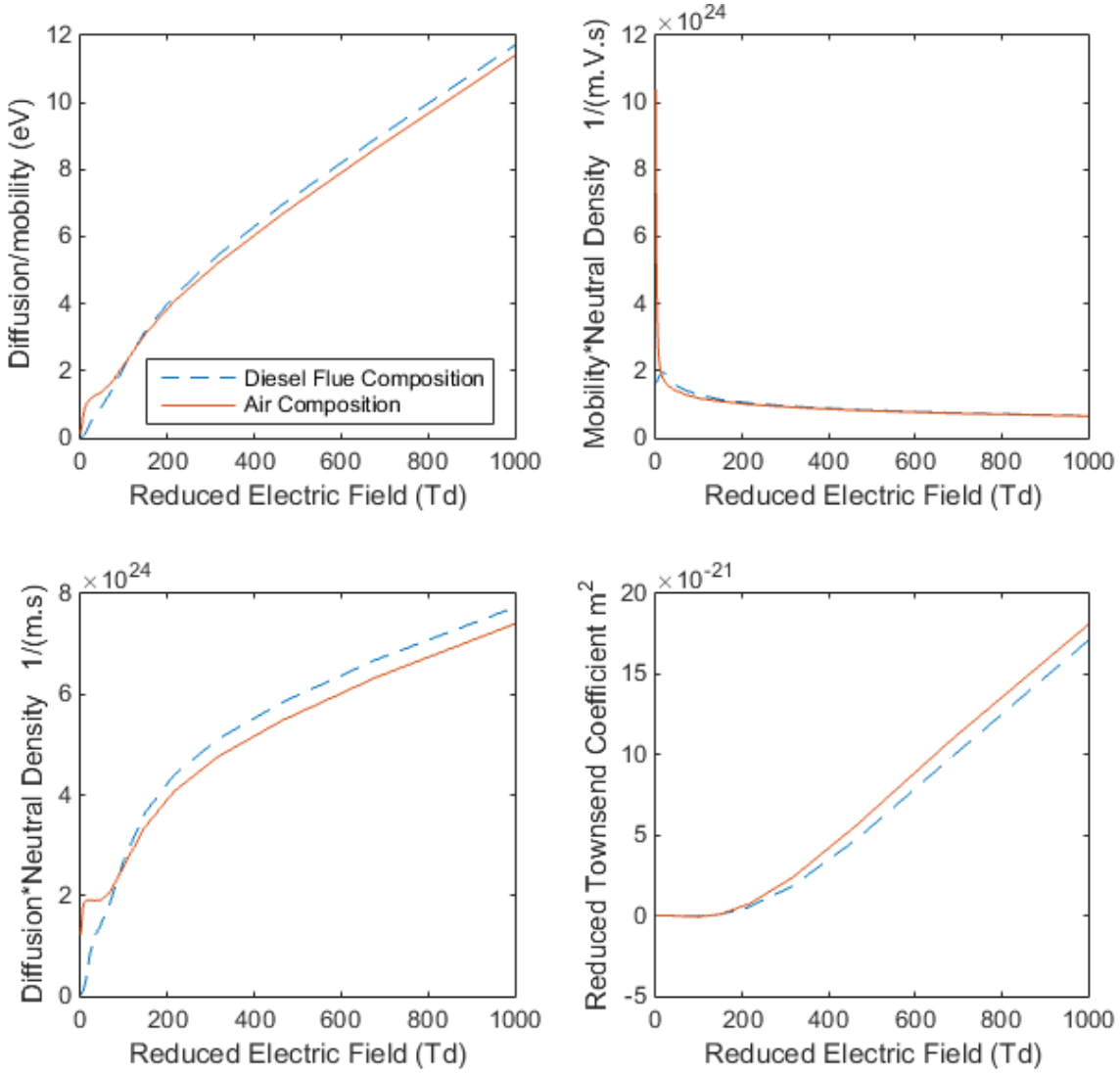

FIGURE 5.6: A comparison of transport parameters and townsend's coefficients for air and diesel flue gas compositions.

Photoionisation

The photoionisation term seen in the drift-diffusion equations was primarily developed by Kulikosvsky [41] based on a model that was developed to partially follow the photoionisation data by Penny and Hummert [42] who derived a relationship between the number of photoionisation events and photo-electrons produced in a specific volume. The photoionisation term describes the number of electron-ion pairs formed per second in a volume dV_1 due to photoionisation events in another volume dV_2 seperated by a distance r as described by equation 5.6 [41].

$$S\left(dV_1, dV_2\right) = \frac{I\left(dV_2\right) f\left(r\right)}{4\pi r^2} dV_2 \tag{5.6}$$

Electric Field

The net electric field is a found by computing the Laplacian and Poissonian electric fields and taking their summation as seen in equation 5.7.

$$E_T = E_L + E_P \tag{5.7}$$

Where the Laplacian electric field is defined as the electric field due to the applied voltage. It is determined from solving Poisson's equation 5.8 with zero particle number densities [35, 18].

$$\nabla^2 \phi = -\frac{q_e}{\epsilon_0} \left(N_p + N_n + N_e\right) \tag{5.8}$$

Such that:

$$E_L = -\nabla \phi \tag{5.9}$$

The Possionian electric field is the electric field due to the space charge density ρ. It is given at position x within a channel of radius r in a gap of length d showed by equation 5.10 [18].

$$E(x) = \frac{1}{2\epsilon_0} \int_{-x}^{0} \rho(x+x') \left[-1 - \frac{x'}{\sqrt{x'^2 + r^2}} \right] dx' + \int_{0}^{d-x} \rho(x+x') \left[1 - \frac{x'}{\sqrt{x'^2 + r^2}} \right] dx' \tag{5.10}$$

Circuit Current

The circuit current was derived by Morrow in [35] and is given by:

$$I(t) = \pi r^2 \frac{q_e}{V_{applied}} \int_{0}^{d} \left(N_p v_p - N_n v_n - N_e v_e + \frac{\partial^2 D N_e}{\partial^2 x} \right) E_L dx \tag{5.11}$$

Swanson then accounted for the circuit current's effect of a voltage drop through equation 5.12. Where the test circuit wiring is simplified and represented by a capacitance C and resistance R.

$$V_{applied} = I(t) R - \frac{1}{C} \int I(t) dt \tag{5.12}$$

Boundary Conditions

The model is required to take into account that in the space of charge flow, electrons are absorbed and released from the electrodes. As such, boundary conditions are defined to represent this and allow continous flow of electrons; Table 5.1 gives the respective boundary conditions [18].

TABLE 5.1: Model Boundary Conditions

Type	Boundary	Condition
Convective and diffusive N_p	Anode/Cathode	0
Convective and diffusive N_n	Anode/Cathode	0
Convective and diffusive N_e	Anode	0
Convective and diffusive N_e	Cathode	$\gamma \frac{v_p N_p}{v_e}$
Outer Boundary ϕ_d	Anode/Cathode	0
Inner Boundary ϕ_0	Anode/Cathode	$V_{applied}$

Accuracy, Stability and Noise

When solving the model algorithm, the accuracy, stability and noise is controlled by fulfilling the Courant-Friedrichs-Lewy and von Neuman criterions in equations 5.13 and 5.14 [18].

$$\triangle t < \frac{\triangle x}{v_e} \tag{5.13}$$

$$\triangle t \leq \frac{\triangle x^2}{2D} \tag{5.14}$$

Which ensures that during electron propagation in the gap D, electrons do not move outside the bounds of the gap space D due to irregular speeds in v_e. The Debye length λ_D is included in the modelling to represent the plasma characteristics and equation 5.15 gives the respective criterion.

$$\triangle x < \pi\lambda_D \tag{5.15}$$

5.2 Breakdown Simulation and Results

This section details how the model described above is implimented and executed in MATLAB^{TM}to simulate a complete discharge event. The simulation results are given and discussed along with any shortfalls of the model simulation.

5.2.1 Simulation Procedure

The simulation is an implementation of all the equations described in the modelling section, in which the outputs of interest are the breakdown voltages for the tested gap size range. The simulation is implemented through a series of loops that run in time to use the model formulation to propagate electrons and ions through the gap. In the process of doing so, the number densities, electric field and circuit current are observed to show the growth of avalanches in the gap. Furthermore, since breakdown

is of interest, the streamer criterion is used to define breakdown, in which equation 5.16 must be satisfied [2].

$$N_e \geq 10^8 \tag{5.16}$$

Where N_e is the electron number density of the avalanche electrons. The output of the simulation is a breakdown voltage versus gap size curve, and electron density evolution in time. The simulation flow chart is shown in Figure 5.7 and executes for the gap size range of 1 cm to 30 cm.

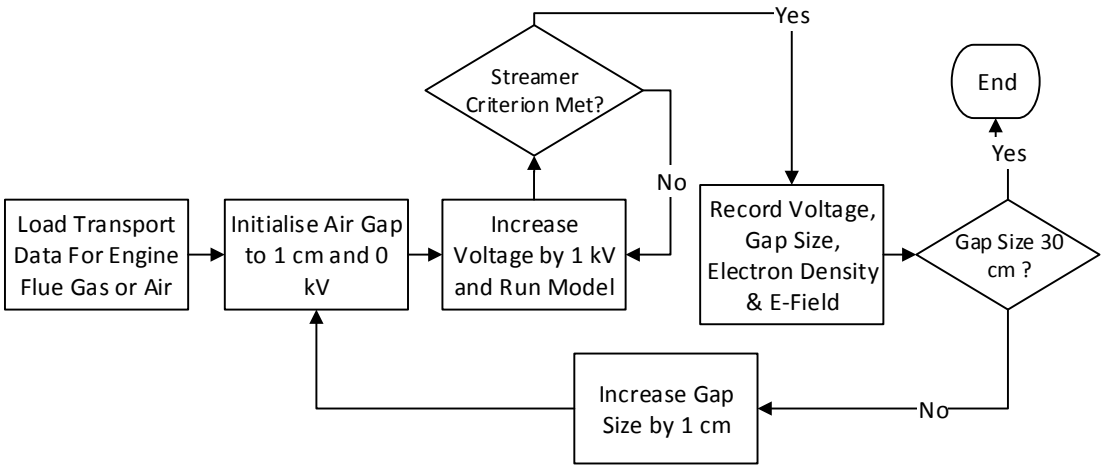

FIGURE 5.7: Simulation flow chart, the simulated gap sizes are increased in 1 cm steps to 30 cm and the result is a plot of the breakdown characteristic.

As mentioned before, the model uses swamp parameters calculated using Bolsig+ to represent air and flue chemical conditions under standard environmental conditions; the rest of the common parameters the simulation employs are given in Table 5.2.

TABLE 5.2: Input Parameters for Positive breakdown Simulations in Air and in Flue

Parameter	Symbol	Value
Pressure	P	1.304 kPa
Temperature	T	20 ^oC
Anode radius	r	7.5 mm
Grid size	N_g	800
Grid spacing	dx	0.3 mm
Time step	dt	10^{-12}
Recombination coefficient	β	$2{\times}10^{-7}$
Secondary ionization coefficient	γ	0.01
Positive ion mobility	μ_p	2.34 $cm^2.V^{-1}.s^{-1}$
Negative ion mobility	μ_n	2.7 $cm^2.V^{-1}.s^{-1}$
Positive ion diffusion	D_p	0.05 $cm^2.s^{-1}$
Negative ion diffusion	D_n	0.05 $cm^2.s^{-1}$

5.2.2 Simulation Results

This section gives and discusses the breakdown simulation results for both air and flue conditions. The breakdown characteristics produced by the simulation are shown in Figure 5.8. The results show a similar behaviour to the experimental data in Figure 4.11; an increasing linear trend with increase in gap size is observed. Furthermore, the simulations confirm that the breakdown voltages of flue gas are higher than the breakdown voltages of air in standard conditions.

The simulation shows two breakdown regions as opposed to three regions observed in the experiment results. These two regions are the breakdown voltages below 30 mm and above 30 mm gap size, these are classified by A and B, region C for gap sizes greater than 250 mm in the experiment results is not observed in the simulation results. In region A, the flue breakdown voltages are slightly lower than the air breakdown voltages in both experimental and simulation results. In region B, the presence of flue gas then enhances the dielectric strength of air and this is again seen in both experimental and simulation results. The simulation results however do not show region C, where it was experimentally observed that the flue gas decreases the

strength of air by as much as 20 %. The inability of the simulation to predict corona mechanism changes is a limitation of the modelling.

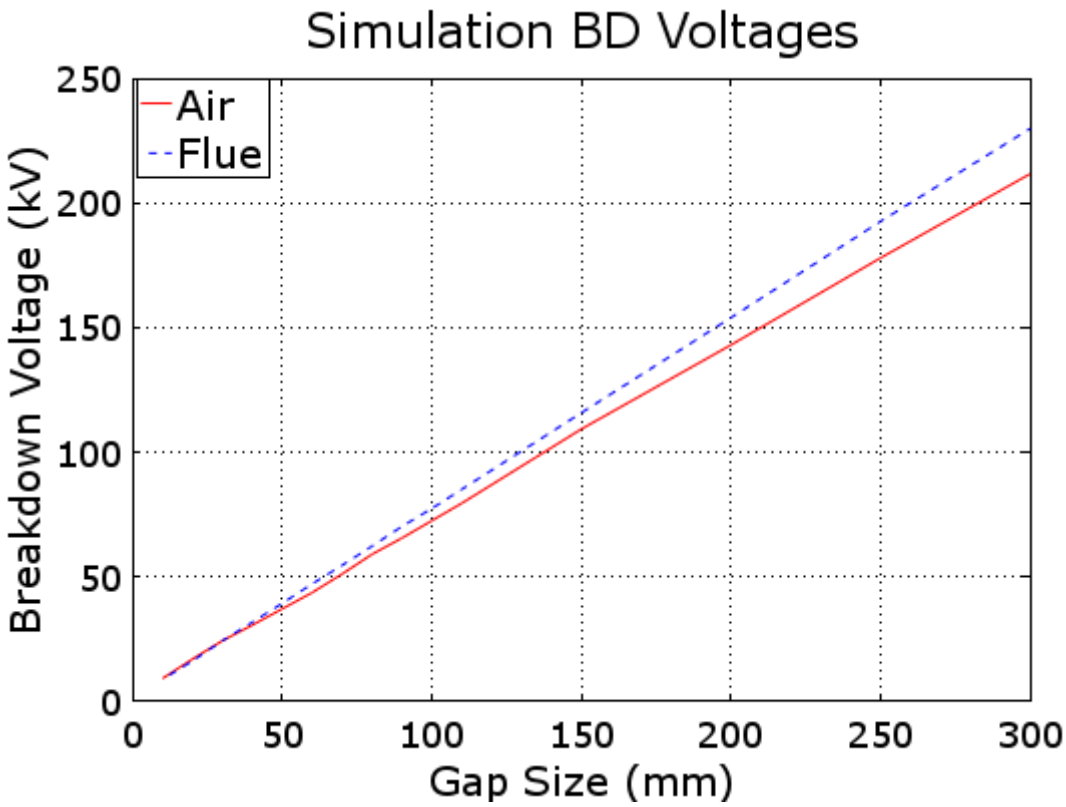

FIGURE 5.8: Simulation Results: breakdown characteristics of air and flue under standard conditions.

The simulations proved to be in good correlation with the experimental results but it could not predict certain characteristics. The good correlation is in regions A and B, but fails to reproduce region C where it is has been speculated that region C is caused by a change of breakdown mechanism in air and it results in the breakdown voltages of air being higher than that of flue. It is then apparent that the simulation is valid in small gap sizes less than 250 cm, where it was able to give results that are in correlation with experiment results. Furthermore, since it is thought that the change of breakdown mechanism in flue may happen at higher gap sizes, the flue simulation can be trusted for gap sizes of up to 250 mm since it is still in good correlation with flue experimental results. The observed charge dynamics in the simulation are discussed next.

Positive Corona

The simulation shows the growth of space charge in both space and time. The analyses of the space charge and how it affects the electric field and current is carried out for the two observed cases; region A where the breakdown strength of air is marginally higher than of flue and region B where flue exhibits higher breakdown strength.

Region A

Region A represents gap sizes less than 30 mm, and the initial current pulse in air and in flue is shown in Figure 5.9. The same voltage is applied in both cases so that the only difference are the gas composition. The initial pulse occurs at 60 ns for both air and flue, but the magnitudes differ.

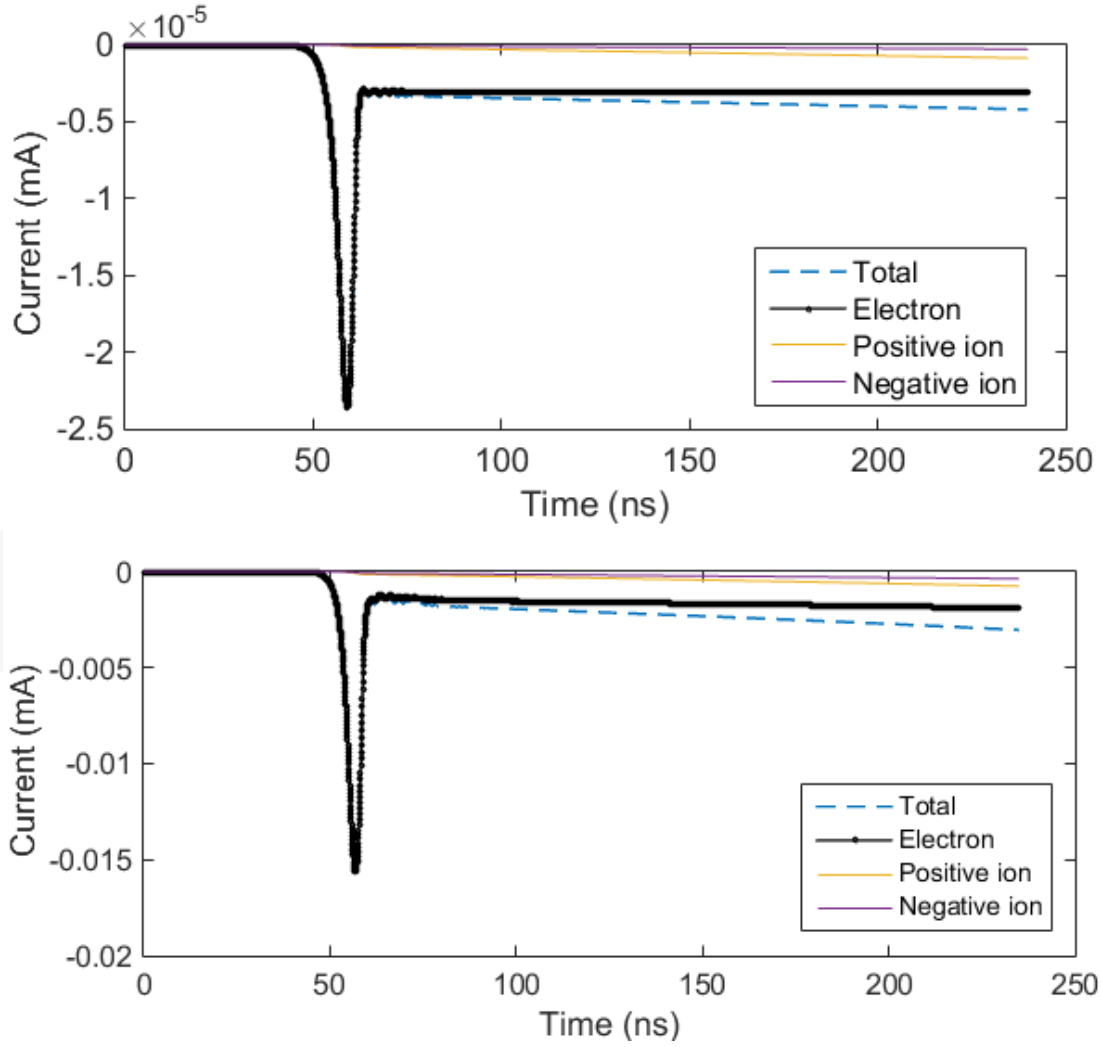

FIGURE 5.9: Current pulse in air (top) and in flue (bottom) for a 1 cm gap size.

The current pulse in flue has a higher magnitude than that in air; this is caused by the ease of electron and space charge generation in flue as is evident in Figure 5.10 showing the charge densities in flue and in air. It can be seen that the avalanche electrons of 10^9 cm^{-3} in flue generated twice as fast as that in air reaching the streamer criterion within 250 ns, while the avalanche in air still has roughly 10^4 cm^{-3}. It can be further seen that the number density of positive ions is greater than that of negative ions and electrons in both air and flue conditions, which is due to the low mobility of positive ions to escape the gap.

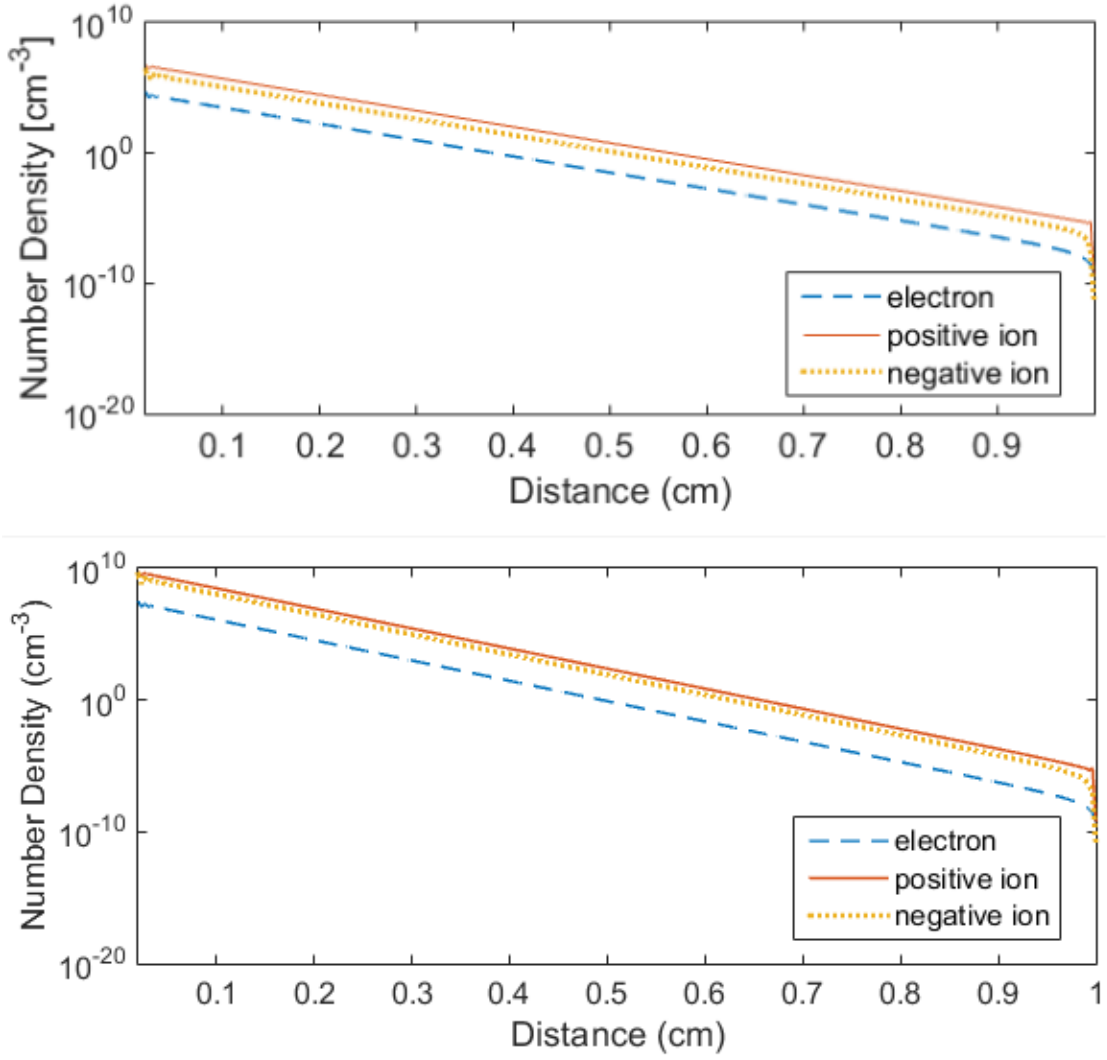

FIGURE 5.10: Space charge in air (top) and in flue (bottom) for a 1 cm gap size.

The electric field across the gap is shown in Figure 5.11, where the laplacian field is the electric field due to the applied voltage and the total field is a combination of the applied voltage and the generated space charge field. In both cases, it can be seen that the space charge deforms the electric field by increasing it, in turn, this allows the electron avalanches to self propagate through the air gap. The electric field is highest closer to the electrode where electrons are attracted. More importantly, the electric field is seen to have collapsed very close to the electrode, moving the peak a 1 mm distance away from the electrode. This is due to the positive space charge that caused the first corona pulse; the electric field restores after the pulse and continues the propagation of the electrons. For the same applied voltage, The electric field enhancement is seen to be slightly higher in flue by 80 $V.cm^{-1}$ compared to that in air. This shows that for this gap range, flue supports more ionization and hence why it breaks down at a lower voltage as seen in Figure 5.8

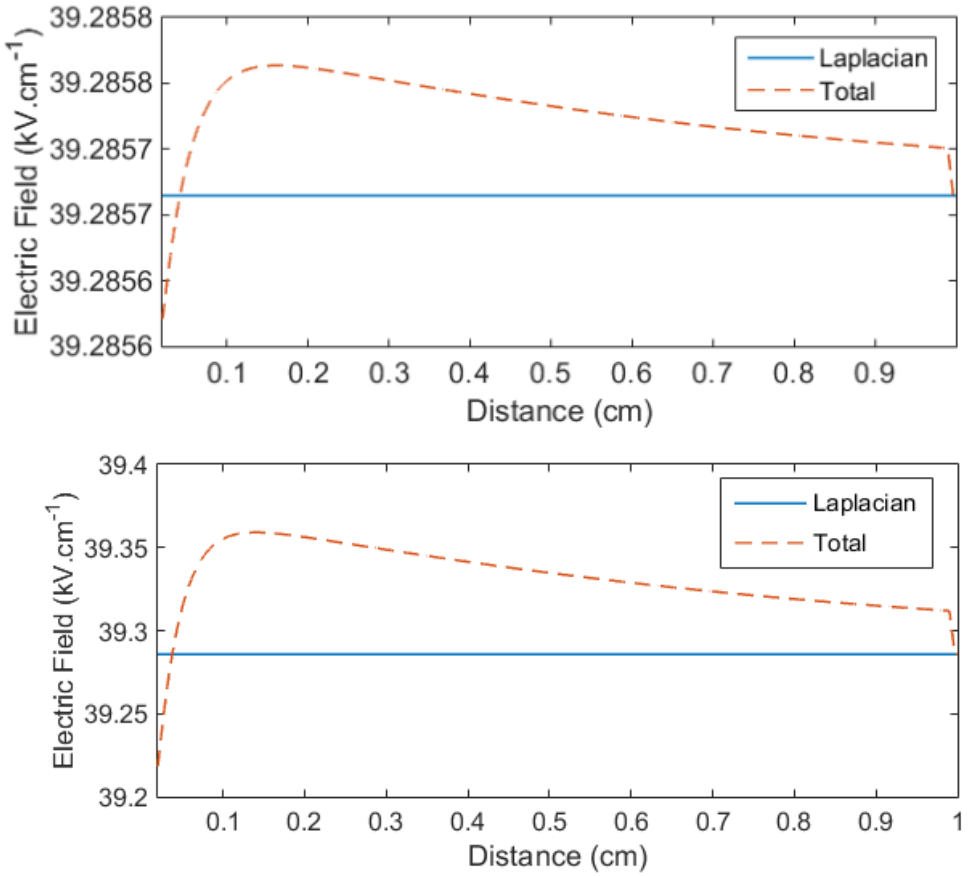

FIGURE 5.11: Electric field in air (top) and in flue (bottom) for a 1 cm gap size.

Cross Over

The 30 mm gap size point was found to have the same breakdown voltages for air and flue. This point is termed the cross over point in this study and it was of interest to check the charge dynamics and how they affect the electric field and current in air and in flue since they have the same observed breakdown voltage. Figure 5.12 shows the first current pulse in air and in flue for the cross over point.

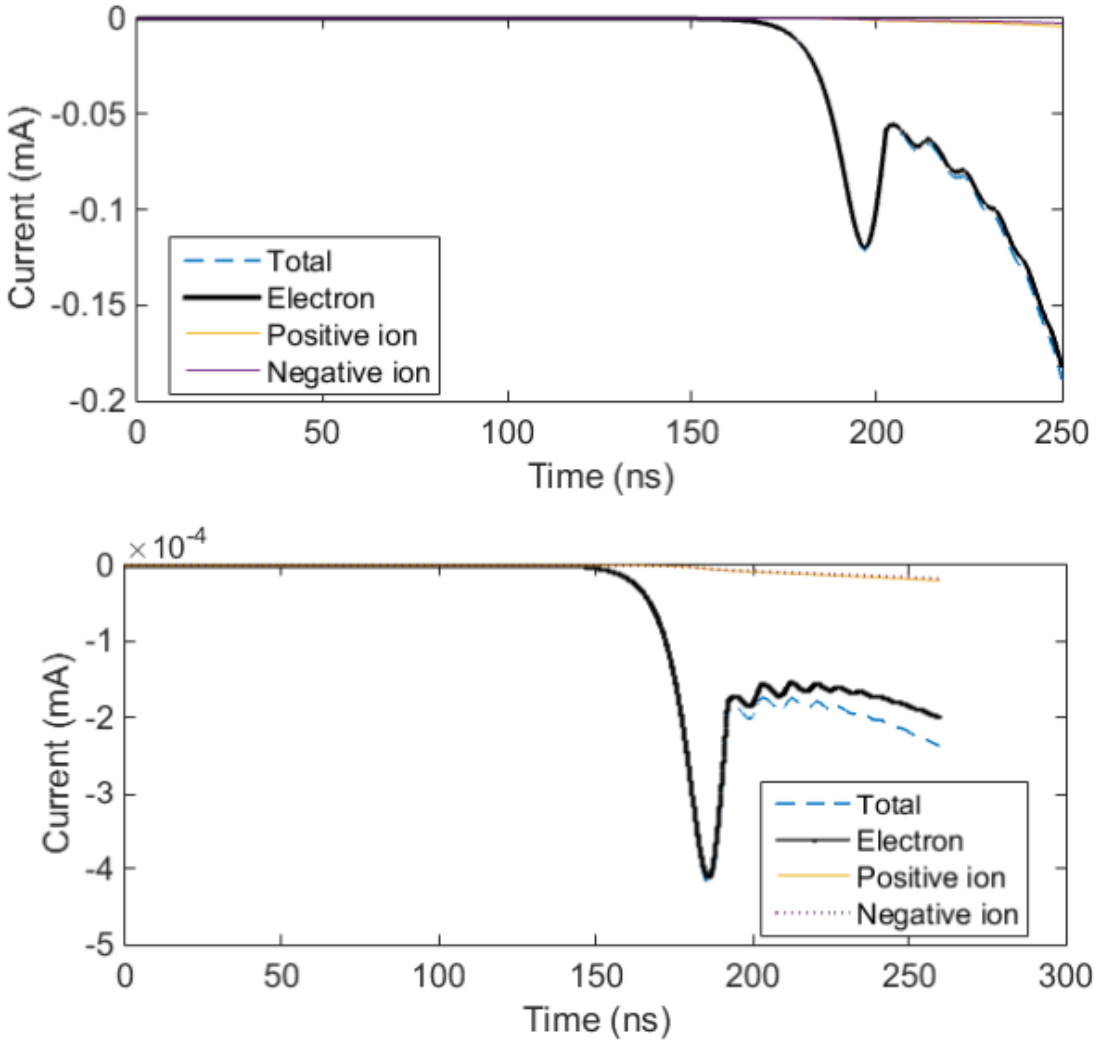

FIGURE 5.12: Current pulse in air (top) and in flue (bottom) for a 3 cm gap size (the cross over).

It is evident that at this point, the current magnitude in air has now increased beyond that in flue. The current pulses still occur around the same time at 180 ns to 190 ns, but the current in air is seen to grow faster after the pulse, while that in flue is very slow. Furthermore, the current in air is seen to be more electron driven. The

total current in flue is seen to have a sizable contribution of positive and negative ion current, which is known to prohibit electron flow and in this case signifies that flue is now gaining dielectric strength when compared to air. The space charge developed to form the current pulses at the cross over is shown in 5.13 for both air and flue conditions.

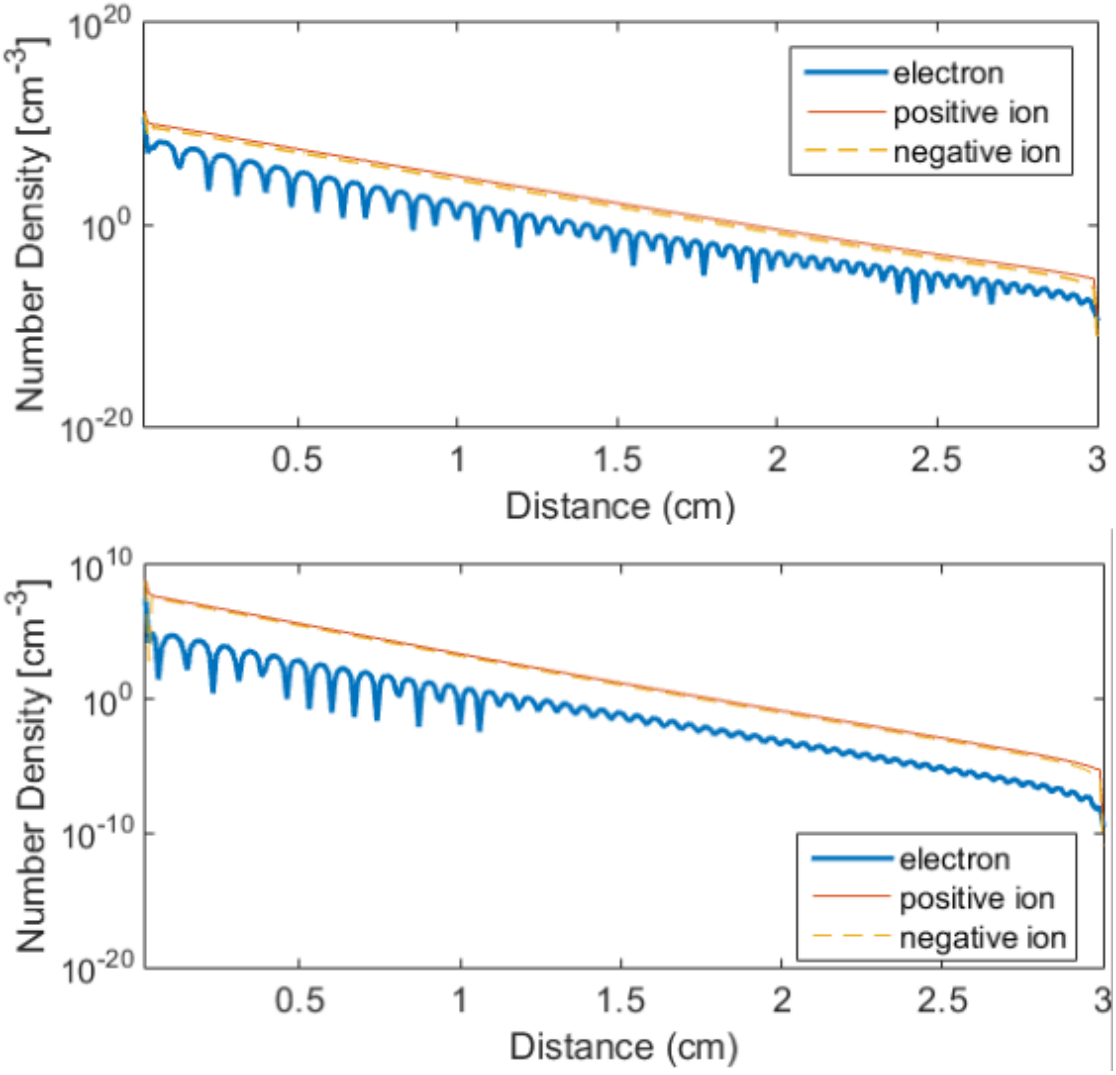

FIGURE 5.13: Space charge in air (top) and in flue (bottom) for a 3 cm gap size (the cross over).

The number of avalanche electrons in air is already seen to be almost 10^9, which explains the rapid growth of current in air. The avalanche electrons in flue are still at 10^5 at this point. The repeated dips in the electron number density graph is a representation of the absorption of electrons at the HV electrode and depletion due

to attachment; and it can be seen that these dips in flue are just a bit deeper than that in air. The attachment in air happens across the entire gap, while attachment only occurs within 1.2 cm from the electrode in flue where it is also evident that the ion number density is pronounced implying high electron absorption activity at this region. This is consistent with the cross sections; in air, attachment is across a large range of electron energies, while flue has a small range but many possible attachment processes. Figure 5.14 shows the electric field profiles for air and flue.

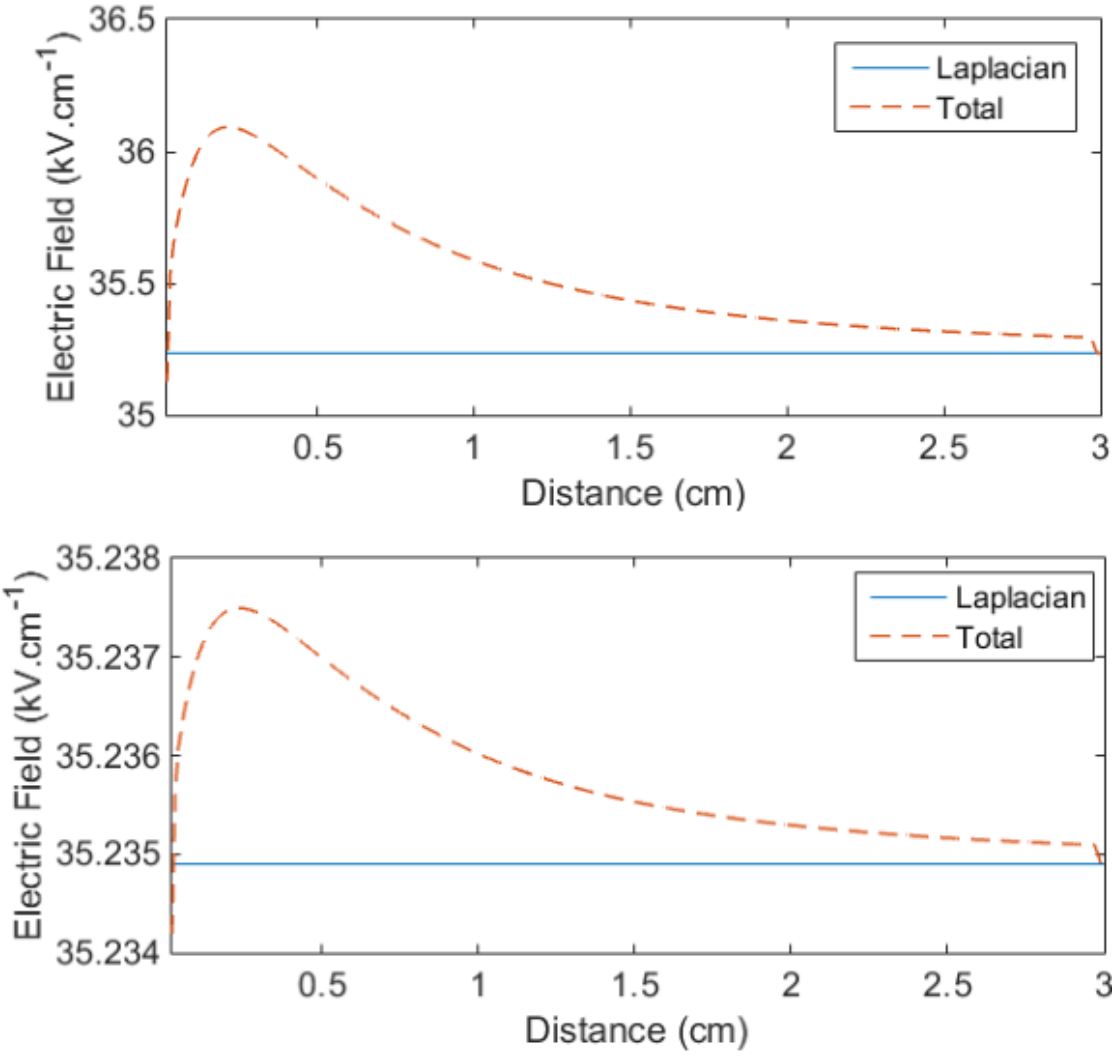

FIGURE 5.14: Electric field in air (top) and in flue (bottom) for a 3 cm gap size (the cross over).

The effects of the growth of the space charge in air is seen to increase the electric field more than that of the avalanches in flue. As expected, the field magnitude in air is higher due to the observed rapid avalanche growth. While the field in flue is

much lower due to the low electron density near the electrode. It can be further seen that the collapse of the field near the electrode is not apparent in both air and flue conditions at the cross over gap size.

Region B

Region B is defined as gap sizes from 40 mm to 300 mm. No corona pulse could be observed in both air and flue simulations for this region. This is because the simulation time step has been increased to fast track the simulation to breakdown since more run time was needed to breakdown the bigger gap sizes under a time step that allows corona pulse observation. Therefore the breakdown characteristics are shown for this region instead of the corona characteristics. This tradeoff between simulation run time and time step resolution is an inherent limitation of iterative gas discharge modelling. The breakdown current, space charge and electric field characteristics for a gap size of 200 mm in region B are shown in Figures 5.15 and 5.16 for an applied DC voltage of 136 kV. Only air results are shown to illustrate the overall breakdown profile, the flue results were observed to be similar. During breakdown, it can be seen that the current increases to tens of milli-amps which signifies a short circuit in the gap.

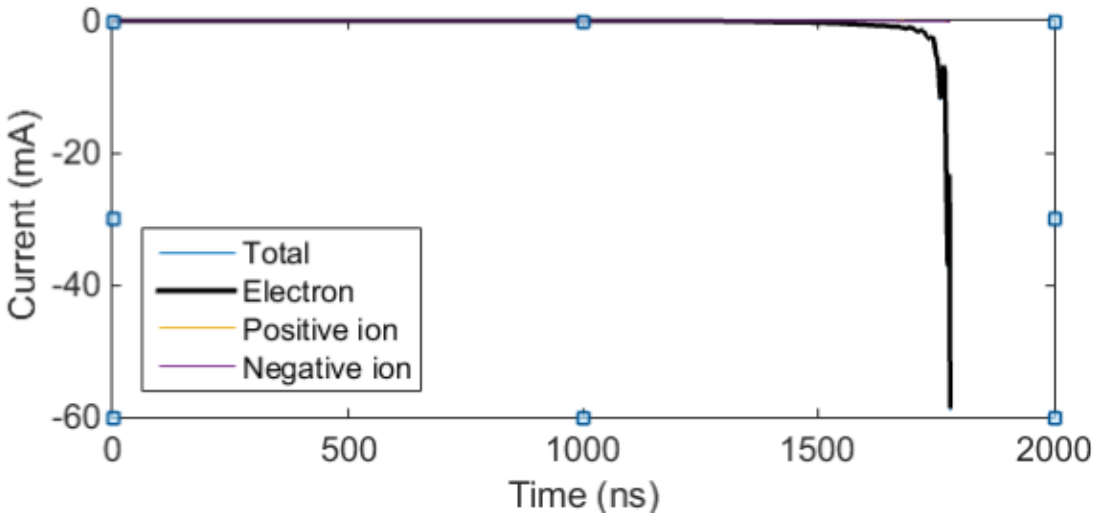

FIGURE 5.15: Current profile during breakdown of a 200 mm gap in air

The space charge distribution and the corresponding electric field during the breakdown are showed in Figure 5.16.

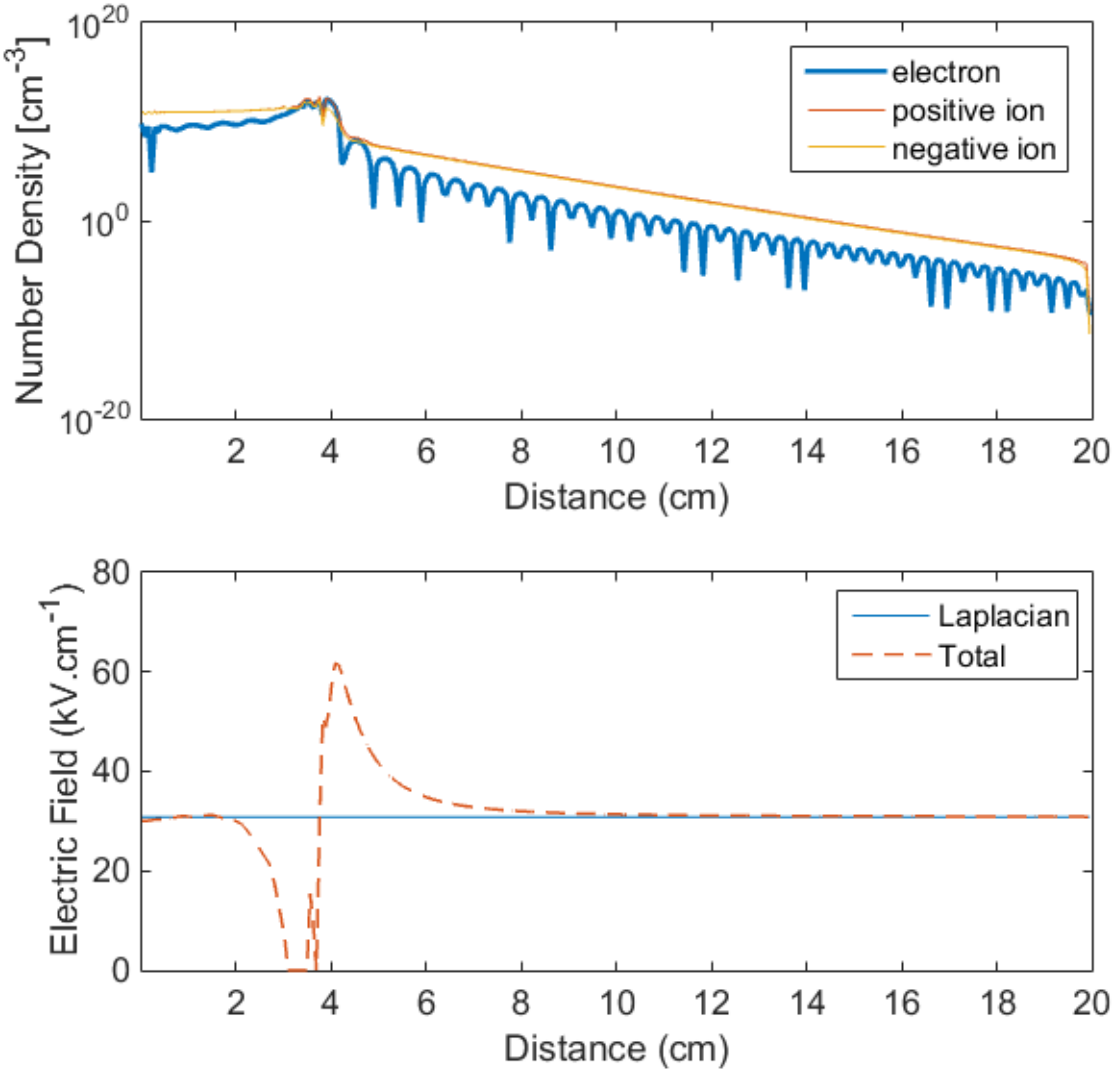

FIGURE 5.16: Space charge (top) and electric field (bottom) profile during breakdown of a 20 cm gap in air

Firstly, the total electron density is seen to be about 10^8 to 10^{10} in the gap size range 0 cm to 4 cm. Where it can be said that the avalanche head is at 4 cm where most of the ionization occurs and is seen by the peak of the space charge curve. The positive and negative ions are seen to be the same for the enteir gap length and they are still higher than electrons. The effects of this avalanche and space charge distribution is clearly seen on the electric field curve. The space charge does not affect the electric field (the laplacian) before 2 cm, after this length, the electric field collapses to 0 and

begins rising close to 4 cm, where it reaches a peak value at 4 cm before falling to the laplacian field again. This electric field profile confirms the discussion of how space charge deforms electric field. Where in this case the total electric field falls to zero since the avalanche and space charge are at the their maximum during breakdown. Furthermore, it can be seen that the space charge and avalanche electrons are present from the electrode to 8 cm into the gap, which was sufficient to allow a bridge of the 20 cm gap for breakdown to occur.

This chapter presented the gas discharge model used to simulate a gas breakdown event. The model treats gas particles as fluid and propagates the particles through a gap by simultaneously solving drift-diffusion equations under the influence of an electric field. The model simulation proved the results observed in the physical experiments by exhibiting the same trends and fairly replicating the actual data. Furthermore, the charge dynamics obtained from the simulation showed how the gas electrons and ions interact to explain the observed voltage breakdown characteristics. The next chapter concludes the research by outlining the main findings and giving recommendations for possible future work.

Chapter 6

Conclusion and Recommendations

6.1 Conclusions

This dissertation has presented the work carried out to determine the effects of engine flue gas on the dielectric strength of air gaps. The problem addressed by the study arises from the situation wherein diesel locomotives travel under electric railway lines in South Africa. The research was executed through a scaled down model of the problem for laboratory air breakdown experiments and computer simulations under normal air conditions and in flue polluted air conditions. The experimental procedure was in accordance with the IEC standards and the simulations were based on modelling gas discharge through fluid dynamics techniques. The following are the important findings of the research.

6.1.1 DC and Impulse Experiments

- The DC breakdown voltages of flue were measured to be higher than that of air in the gap range 30 mm to 250 mm. It was found that outside this range, the flue breakdown voltages were less than that of air.

- The maximum recorded increase in breakdown voltage was 26 % occuring at 50 mm in the petrol flue tests, while the maximum decrease was measured to be 21 % and 36 % for petrol and diesel flue respectively at 300 mm . The observed

decrease is similiar to results reported in literature, where the reported decrease was 20 % for AC tests in petrol and diesel flue.

- The observed breakdown results in both air and flue suggest that in a real world scenario, under the worst case of the air gap being at 110 mm, the supply voltage of 3 kV DC would not be enough to breakdown the gap. A voltage of 70 kV to 80 kV DC would be needed to breakdown this gap in both air and flue.

- The measured pre-breakdown corona activity in flue was observed to have increased in the tested gap range. It was postulated that flue enhanced the corona stabilization effect due to the increased humidity of the flue gas, which increased the rate of electron attachment and hence decreasing the effective Towndsend ionization coefficient of flue gas.

- The corona stabilization was then measured, and it was found to have a steady increase in flue while in air it had a higher rate of increase. Which lead to the case were the breakdown voltages measured in air after 250 mm being greater than that of flue.

- It is thought that the steady growth of the corona stabilization in flue shifts the point at which flue breakdown voltages are greater than that of air again to a range outside the tested range

- The impulse tests carried out confirmed that the corona stabilization effect was affected by the space charge, in which flue affected it by increasing the attachment of electrons. The overall decrease in the mean weighted percentage increase of the breakdown voltages from air to flue conditions was 10 % in DC tests and only 6 % in impulse tests.

6.1.2 Simulations

- The simulation showed a good correlation with the experimental results. It showed that indeed flue enhances the breakdown strength of air for gaps greater

than 30 mm. It also showed that flue compromises the dielectric of air for gaps lower than 30 mm.

- The simulation was limited in the modelling, where the effects of corona stabilization had not been included. This resulted in the simulation failing to predict the observed results for gaps greater than 250 mm where flue compromises the strength of air.

- Results of corona observation from simulations revealed that the space charge deformed the electric field and played a major role on when the breakdown will occur.

- The avalanche head could be observed through the simulations and it was found that prior breakdown, the density of positive and negative ions was almost the same as that of electrons. Where else they would be greater than that of electrons if no breakdown was to occur.

6.2 Recommendations for future work

The following are the recommendations for future work.

- The flue temperatures in the experiments was less than 100 ^oC. As such, for practical considerations in locomotives, it is recommended that the laboratory experiments are performed with temperatures around 200 ^oC to match real life scenarios.

- It is recommended that more research is carried out to study the observed phenomena of cross overs. The initial direction of research may be to investigate the differences between the nature of DC and impulse voltages and attempt to attribute the effects of space charge to the phenomena of crossover and stabilization.

- It is also recommended that the effects of the observed corona stabilization effect be included in the simulation model for an improved simulation output.

- Overall, the simulation run time needs to be greatly reduced to allow faster results output during research, the efficiency of the software implementation needs to be looked into.

Bibliography

[1] A.R. Timm,"Continuous Gauging of Electric Traction Contact Wire", Masters Thesis, University of Cape Town, December 1975.

[2] Kuffel, W.S. Zaengl, J. Kuffel, High Voltage Engineering: Fundamentals, Second Edition, Newnes, 2006

[3] P.J. Lambeth D.H. Nguyen, "Air clearances for electric railways: A study of the breakdown voltage of rode-plane gaps in variety of atmospheric conditions". IEEE Transactions on Power Apparatus and Systems, Vol. PAS-104, No. 10, October 1985

[4] IEC 60913- 2013: Railway applications - Fixed installations - Electric traction overhead contact lines

[5] Transnet, "Requirements to be adhered to when temporarily reducing the contact wire height above rail to less than the minimum on 3 kV DC", BBC1898 Version 2, February 2011

[6] N.L. Aleksandrov, E. M. Bazelyan, “Ionization processes in spark discharge plasmas”, Plasma Source Sci. Technol. 8 (1999) 285-294, UK

[7] M.K. Khair, W.A. Majewski, Diesel emissions and their control. SAE Inernational. 2006, ISBN: 978-0-7680-0674-2

[8] H. Jaaskelainen, “Diesel Exhaust Gas”, DieselNet Technology Guide. Online: https://www.dieselnet.com/tech/diesel_exh.php, Last accessed June 2016

[9] International Union of Railways - UIC, "Diesel locomotive emissions regulations". Online: https://www.dieselnet.com/standards/inter/uic_loco.php#emstd, Last accessed June 2016

[10] C. Filippone, "Diesel-Electric Locomotive Energy Recovery and Conversion", Transportation Research Board of the National Academies, Final Report for Transit IDEA Project 67, October 2014

[11] D. Yujian, L. Weiming, F. Jianbin, L. Quingfeng, Z. Jun, S. Zhiyi, “Altitude correction of switching impulse flashover voltage of rod-plane air gaps”, 18 International Symposium of High Voltage Engineering, Seoul, Korea, pp. 287-291 August 2013

[12] T. Harada, Y. Aoshima, Y. Ishida, Y. Ichihara, K. Anjo, N. Nimura, “Influence of Air Density on Flashover Voltages of Air Gaps and Insulators”, IEEE Trans. Power Appar. Syst., 1970, 89, pp. 1192-1202

[13] T.A. Phillips, L.M. Robertson, A.F. Rohlfs, R.L. Thompson, “Influence of air density on electric strength of transmission line insulation”, IEEE Trans. Power Appar. Syst., 1967, 86, pp. 948-961

[14] S.Y. Chu, “Some aspects of researches on the influence of atmospheric pressure on external insulation of H.V. electrical apparatus”, CIGRE 84-33 (WG- 03), IWD 1984

[15] Z. Zhijin , J. Xinliang, C. Yafeng , S. Caixin , H. Jianlin, “Influence of low atmospheric pressure on AC pollution flashoverperformance of various types of insulators”, IEEE Transactions on Dielectrics and Electrical Insulation, Volume 17, Issue 2, 2010

[16] R. Gou, “The influence of air pressure on the insulation strength of insulators”, Journal of High Voltage Engineering, Vol.16, No.2, pp. 30-32, 1990

[17] X. Lu, G.V. Naidis, M. Laroussi, K. Ostrikov, "Guided ionization waves: Theory and experiments", Physics Reports 540, pp. 123-166, 2014

[18] A.G. Swanson, I.R. Jandrell, "Investigation into the role of singlet oxygen in positive corona in air", SAIEE African Reaserch Journal, Vol. 106(4), pp. 182-194, December 2015

[19] "IEEE Guide for the Measurement of DC Electric-Field Strength and Ion Related Quantities", IEEE 1227-1990 (R2001).

[20] N. Mahatho, G.C. Sibilant, A.C Britten, "The influence of artificial floating metal objects on the breakdown of air gaps under dc voltage", HVDC 2006 Congress, July 2006

[21] N.L Allen, D.S.K Lam, D.A Greaves, "Test on the breakdown of air at elevated temperatures in non-uniform fields", IEE Proc.-Sci. Meas. Technol., Vol. 147, No 6, pp. 291-295, November 2000

[22] N.L allen, A Ghaffar, "The variation with temperature of positive streamer properties in air", J. Phys. D. Appl. Phys., Vol. 28, pp. 338-343, 1995

[23] P.M Cowan, J.A Dunn, P. Naidoo, J. Masters, "Sugar cane fire induced transmission line flashovers", Elektron, pp. 12-15, January 1991

[24] N.L Aleksandrov, E.M Bazelyan, "Temperature and density effects on the properties of a long positive streamer in air", J. Phys. D: Appl. Phys. 29, pp. 2873-2880, 1996

[25] B.S Aleksandrov, E.M Bazelyan, B.I Bekzhanov, Izv. Akad. Nauk SSSR Energ. Transp. N2 120, 1984

[26] N. L. Aleksandrov, E. M. Bazelyan, "Ionization processes in spark discharge plasmas", Plasma Source Sci. Technol. 8 (1999), 285-294, UK

[27] J.J Lowke, "Toward a new theory of electrical breakdown in air", Intern. Conf. Gas Discharges and their applications, Beijing, 2012

[28] J.J Lowke, "New Directions of Predictive Capability for Properties of Gas Discharges", CSIRO Materials Science and Engineering, 2012

[29] F. Llewellyn-Jones, "Ioninzation and breakdown in Gases", Methuen, 1966

[30] Pico Technology, "PicLog 1000 Series", online: https://www.picotech.com/data-logger/picolog-1000-series/multi-channel-daq , Last accessed: Octobeer 2016

[31] M.L. El-Sayed, E.M. El-Refaie, M.M. Awad,"Effects of pollution on the breakdown voltage of air", Correspondence of Proc.IEE, Vol. 125, No. 7, pp. 714, July 1978

[32] P. Naidoo, D.A Swift, "Large particle initiated breakdown of an atmospheric air gap: Relating to AC power lines faults caused by sugar-cane fires", 8th Int. Symp. on High Voltage Engineering. Yokohama, Japan, pp. 81-84, August 1993.

[33] SANS 60060-1:2011, High Voltage test techniques, Part1 : General definitions and test requirements. Ed. 3

[34] J. Boris and D. Book, “Flux-corrected transport. I. SHASTA, a fluid transport algorithm that works,” Journal of Computational Physics, vol. 11, pp. 38-69, 1973.

[35] R. Morrow and L. Crem, “Flux-corrected transport and diffusion on a non-uniform mesh,” Journal of Computational Physics, 1985.

[36] R. Morrow and J. Lowke, “Streamer propagation in air,” Journal of Physics D: Applied Physics, vol. 30, 1997

[37] N. Kim, S. Lee, G. Georghiou, D. Kim, and D. Kim, “Accurate prediction method of breakdown voltage in air at atmospheric pressure,” Journal of Electrical Engineering and Technology, vol. 7, 2012

[38] Plasma Data Exchange Project, “Lxcat,” http://fr.lxcat.net/home/, last accessed June 12, 2016

[39] G. J. M. Hagelaar and L. C. Pitchford, "Solving the Boltzmann equation to obtain electron transport coefficients and rate coefficients for fluid models", Plasma Sources Sci. Technol. 14, pp. 722-733, 2005

[40] Morgan Database, "Lxcat", http://fr.lxcat.net/home/, Retrieved 13 June 2016

[41] A. Kuliskovsky, "The role of photoionization in positive streamer dynamics", Journal of Physics D: Appl. Physics, vol. 33, 2000

[42] G. Penney and G. Hummert, “Photoionization measurements in air, oxygen and nitrogen,” Journal of Applied Physics, vol. 41, no. 2, 1970.

[43] H. J. Mohammed,"Corona Stabilization and Electrical Breakdown of Gases in Nonuniform Fields", PhD, University of Baghdad College of Science of Science-Department of Physics, Republic of Iraq, April 2013

[44] B. Sanjeev,"An investigation into methods of modelling positive inhomogeneous-field breakdown and discharge processes in SF6 with emphasis on the corona stabilisation phenomenon", MSc(Eng) Thesis, University of the Witwatersrand, Johannesburg, June 1998

[45] T. Hinterholzer, W. Boeck,"Breakdown in SF6 influenced by corona-stabilization", IEEE 2000 Annual Report Conference on Electrical Insulation and Dielectric Phenomena, Volume: 1, February 2000

[46] N.L Allen, G. Berger, D. Dring and R. Hahn, “Effects of humidity on corona inception in a diverging electric field”, IEE Proc, Vol. 128, Pt. A, No. 8, pp. 565-570, November 1981

[47] F.A.M. Rizk and G.N. Trinh, “High Voltage Engineering”, Taylor & Francis, 2014, ISBN 97814665113761

Appendix A

ISH 2017 Paper

This appendix gives the paper presented in the 20th International Symposium of High Voltage (ISH) at Buenos Aires, Argentina on August 2017.

DC AND IMPULSE BREAKDOWN CHARACTERISTICS OF SMALL GAPS IN ENGINE FLUE GAS

N. Msimango*, C. Nyamupangedengu and N. West
University of the Witwatersrand, 1 Jan Smuts Ave. Braamfontein, Johannesburg, South Africa
*Email: <MrN.Msimango@gmail.com>

Abstract: This paper presents the DC and impulse voltage breakdown characteristics of small gaps in engine flue gas. Railway electrical clearances in South Africa are designed based on IEC 60913:2013 which does not take into account the unknown effects of engine exhaust flue pollution on electrical air breakdown. High voltage DC and impulse breakdown experiments were carried out for a rod-plane gap under normal air and petrol engine flue polluted conditions. The tested gap range is 10 mm to 300 mm. Gas discharge simulations implemented in MATLAB™ are used to evaluate the test results. The simulations run a fluid transport model solving simultaneous drift-diffusion equations affected by Townsend's ionization coefficients and transport parameters for air and for flue. The experimental results showed that the presence of engine exhaust flue marginally increased the dielectric strength of air in both DC and impulse tests. It was observed that for gap sizes less than 250 mm, the breakdown voltages in flue increased by a maximum of 26%. Beyond 250 mm, the flue gas compromised the breakdown strength of air by as much as 21% in DC. The enhancement of the dielectric strength is attributed to the flue increased humidity and observed corona stabilization. In the impulse tests and simulations, no decrease was observed after 250 mm; this is attributed to the absence of corona stabilization in impulse tests and simulations.

1 INTRODUCTION

The South African railway system has both electric and diesel powered locomotives to meet demand in the growing economy. The diesel locomotives are mainly used for moving mass goods and passengers to locations that have no electric railway systems infrastructure. Consequently, diesel locomotives often have to also travel under electrified railway systems. The railway catenary systems (RCS) are designed based on the IEC 60913:2013 [1] standard that does not take into account cases where diesel locomotives travel under the RCS. The locomotive exhaust outlets are on top of the locomotive releasing engine flue gas directly to the high voltage RCS. This becomes a problem since the design of the railway clearances may not have included flue pollution, which from a high voltage perspective may compromise the integrity of the air dielectric strength and equipment [2]. The air clearances defined as the gap between the top of a locomotive and the high voltage supply lines [3] are usually set to meet the minimum international standards to reduce costs. The presence of engine flue in the air clearances therefore may lead to catastrophic accidents resulting from high voltage air breakdown, causing damage to equipment and injuring passengers. The omission of engine flue gas from the IEC standard is presumably because the case of diesel locomotive travelling under electric RCS is unique to South Africa. As such, there is a need to generate knowledge to address the possible issues from this situation. This study conducts laboratory air breakdown experiments using a rod-plane and sphere-sphere electrode configurations for normal air conditions and for flue polluted air conditions. Computer simulations are then used to evaluate the test results.

2 THE BACKGROUND

In the literature the only study that attempted to address the effects of engine flue pollution on breakdown voltage levels of air was conducted in 1985 by Lamberth and Nguyen [4]. They observed that the introduction of diesel and gasoline engine flue gases in a rod-plane gap geometry at a standard temperature of 20 °C reduced the AC breakdown voltages of air by 20% for gaps greater than 250 mm. The decrease was observed with engine flue as opposed to other tested pollution factors such as wheat flour, water droplets and salt fog. The results may suggest that the chemical composition of engine flue is the major contributor to the breakdown of air. This section explores further literature on how the presence of flue may affect the processes involved in gas discharge.

2.1 Engine Flue Gases

The by-products of an ideal and typical diesel combustion process are presented in Table 1 [5], where they are given as a range with variations depending on the quality, size and loading of the engine. It can be seen that compared to air, in flue there are less concentrations of oxygen and nitrogen to accommodate increases in water vapour and carbon dioxide. In the experiments and simulations, the worst case is considered. Among these gas components in flue, there are additional pollutants from the non-ideal processes in the

Table 1: Comparison of engine exhaust flue gas composition to air gas composition

Gas	Ideal Flue Volumetric %	Typical Flue Volumetric %	Ideal Air Volumetric %
CO_2	2 - 12	12	x
H_2O	2 - 12	11	x
O_2	3 - 17	9	22
N_2	59 - 92	67	78

combustion. These are hydrocarbons (HC), nitrous oxides (NOx), carbon monoxide (CO) and particulate matter (PM_{10}, PM_{25}). The combined volumetric concentration of the compounds is less than 0.1% [5]. Jasskelainen [6] argues that these pollutants can be ignored due their small concentrations. In this study, the pollutants considered are those in Table 1.

2.2 Effects of Atmospheric Conditions

Atmospheric air pressure is a function of altitude. Pressure in turn affects the voltage breakdown of an air gap [7, 8]. In the present work, the locomotive's exhaust flue is directed to the open atmosphere and therefore it is assumed that this has very little effect on the pressure in the electrode gap. Allen et al [9, 10] performed tests to determine the effect of elevated temperatures on breakdown of non-uniform fields. The results show that the breakdown voltage of a rod-plane air gap exponentially decreases with increased temperature. From their test results, it is found that temperature decreases the breakdown voltage more in larger gaps (200 mm) than in smaller gaps (100 mm) [9]. This result agrees with other researchers in the literature that investigated the effect of temperature on the dielectric strength of air. Aleksandrov et al [12] used a 1.5D simulation to show the effects of temperature and density on properties of a long positive streamer in air. The simulation results showed that temperature had a relatively bigger effect than air density. It is therefore expected that the increased temperature of the exhaust flue degrades the dielectric strength of the air. The effect of water particles on streamer breakdown processes can be explained in terms of charge dynamics in the streamer channel. It is understood that the loss of electrons in the channel in air is dominated by the three-body attachment process given in equation 1.

$$e + O_2 + M \rightarrow O_2 + M \qquad (1)$$

Where $M = O_2$ in dry air and $M = O_2$ & H_2O in humid air. The loss of electrons through the dissociative recombination with simple molecular ions (O_2^+, N_2^+) is given by equation 2 [13]:

$$e + AB^+ \rightarrow A + B \qquad (2)$$

Aleksandrov et al [12, 13] used simulations to conclude that an increase in humidity leads to an increase in the breakdown voltage of air. This result is in agreement with experiments performed by Lambeth and Nguyen's [4]. The presence of both humidity and temperature variables in the present study may imply that the major contributor will have prominent effects since these quantities have opposing effects on the dielectric strength of air. With regard to particulates, tests conducted by Loft et al in [14] on 0.2 mm to 0.63 mm diameter particles, along with tests conducted by Naidoo [15] and Lambeth [4] on large particles showed a small decrease in the breakdown voltage of polluted air. In the context of the present study, it is therefore assumed that the particulates have minimal effects due to their smaller sizes (μm) and concentrations that are less than 0.1%.

2.3 Gas Discharge and Ionization

The fundamental processes in gas discharge is the ionization phenomena that occur throughout the gas discharge duration. The ionization process is affected by all the environmental conditions discussed above and the gas system's dynamic characteristics such as reaction types during collisions. The overall effects can be approximated by Townsend's and Transport coefficients describing a particular gaseous system. Using Table 1 and gas collisional cross sections published in the LXcat database [16, 17] the Townsend coefficients for air and flue shown in Figure 1 were calculated using the Bolsig+ algorithm described by Hagelaar and Pitchford [18]. It can be seen that the reduced (normalised to unit volume) effective Townsend coefficient (defined as (α − η)/N) for engine flue gas composition is less than that of air composition. Where N is the density of neutral particles given in m^{-3}. The reduced electric field (defined as E/N) is used to interpret the results independent of the neutral particle density. Where $1\,Td = 10^{-21}\,V.m^2$. Figure 1 implies that under standard environmental conditions (temperature and pressure), the ionization process in flue will be slower and hence more voltage may be required to breakdown the gas. These coefficients are used later in the simulation section of this paper.

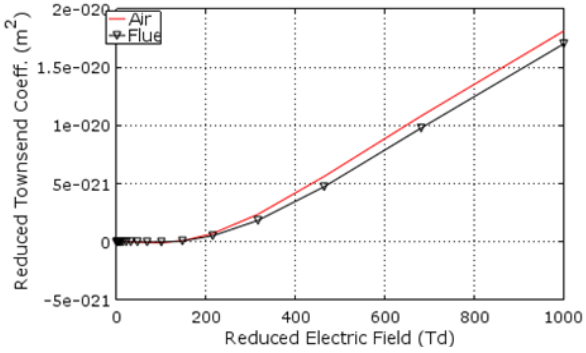

Figure 1: A comparison of Townsend's coefficients for air and engine exhaust flue gas compositions.

3 PHYSICAL EXPERIMENTAL TESTS

3.1 Setup and Procedure

The physical experimental tests were conducted at the Wits High Voltage Laboratory in Johannesburg South Africa which is located at an altitude of about 1740 meters above sea level. The experiment setup is shown in Figure 2, which is used to conduct DC and impulse breakdown in air and flue pollution.

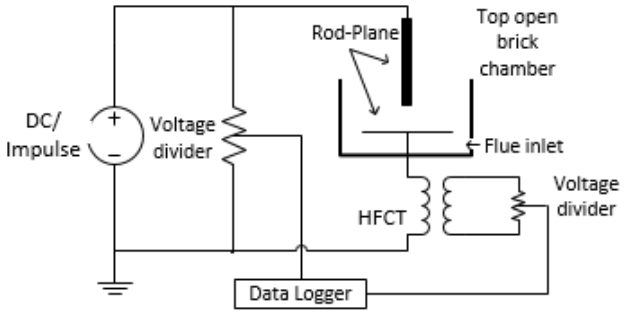

Figure 2: Experimental setup: Testing DC and impulse breakdown of engine flue and air.

The DC source is a 250 kV rated 3 stage Cockroft-Walton DC generator. For the case of impulse tests, the DC source is replace by a 1 MV Marx impulse voltage generator. The setup consists of a top open brick chamber to simulate a case in which a locomotive travels in a tunnel and the flue cannot easily escape. The flue source is a gasoline electric engine and the data acquisition is accomplished through a high frequency current transformer (HFCT) that connects to a PicoLog1012 data logger with a 1% accuracy. The applied voltage and leakage current are continuously measured using the data logger. A rod-plane gap geometry is used for testing since it approximates the practical situation of interest and also represents the worst case scenario. A sphere-sphere gap geometry is used for calibrating the test setup since it has been extensively studied in the literature and its breakdown voltages can be easily read off from tables. The rod has a flat bottom of 15 mm in diameter with edge radius of 1 mm, emulating a RCS feed cable of 16 mm, while the ground plane is 3 m by 3 m. The spheres are chosen to be 100 mm in diameter. The tests are conducted according to the IEC 60060-1:2011 standard [19] and the tested gap size range is 10 mm to 300 mm in increments of 10 mm with 10 breakdowns per gap size. The average chamber environmental conditions for air and flue are given in Table 2.

Table 2: Average chamber conditions

Parameter	Air	Flue
Temperature [*°C*]	23.4	48
Pressure [*mBar*]	832.8	833.5
Relative Humidity [%]	36.8	65

3.2 Test Results and Discussion

The calibration test results are shown in Figure 3, where it can be seen that the measured sphere-sphere breakdown voltages match published data. Since these results were corrected for environmental conditions, it implies that the measured conditions were accurate and that the validity of the experiments can be verified.

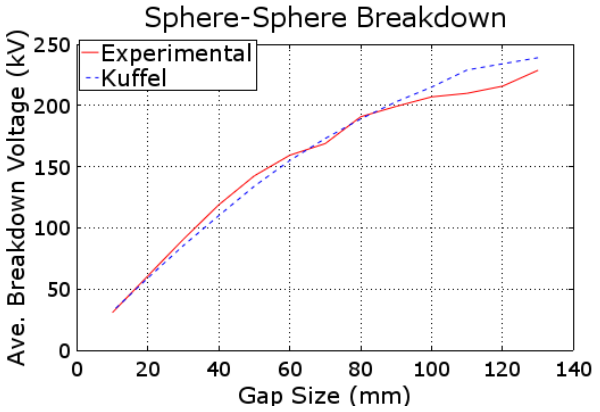

Figure 3: Sphere-Sphere average DC breakdown calibration results compared to published data in Kuffel [2].

The rod-plane breakdown results for the tested gap size range of 10 mm to 300 mm are shown in Figure 4 along with corona inception measurements. A maximum standard deviation of the data was computed to be 9 kV at 300 mm in air.

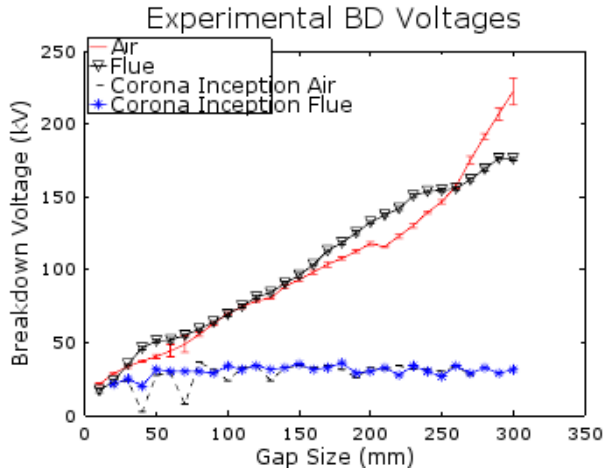

Figure 4: Corrected average DC breakdown and inception voltage curves for the rod-plane tests in air and flue.

The trend is as expected, where voltage increases with gap size. However it can be seen that the breakdown voltages for flue are higher than that of air in the gap range from 30 mm to 250 mm. Beyond this range, the flue decreased the dielectric strength of air. The highest increase is seen to be at 50 mm where breakdown voltage of flue is 26% higher than of air. After 250 mm the breakdown voltages in air become higher than that of flue by up to 21%. Although these results are for DC, Lambeth [4] obtained the same trend but for AC.

The invariance of corona inception voltages with gap sizes is explained by the fact that corona inception occurs within a critical region (δz) near the HV electrode. As such, once a critical applied field that results in equation 3 being met, inception occurs. In this study, it was observed that for reduced electric fields less than 200 Td, the ionization in flue and air are the same as seen in Figure 1 above. It therefore means that the corona inception occurs at this field and the applied voltages in every gap meet this field criteria at 30 kV in the 10 mm critical region, resulting in inception being independent of any gap sizes greater than 10 mm.

$$\exp[\int_0^{\partial z}(\alpha-\eta)dz] > N_{crit} \qquad (3)$$

Figure 5 shows the observed corona pulses at a smaller gap and a bigger gap size in flue and air. It was observed that in flue, corona pulsation was apparent while it was not so in air. The phenomenon implies that the corona activity in flue had more effects of collapsing the applied electric field which resulted in more voltage needed to breakdown the gap. This type of breakdown is termed corona stabilized breakdown [20] and it was found that the enhancement of corona stabilization phenomena in flue is due to the increased humidity in flue which resulted in the electron attachment reaction in equation 1 being dominant in the ionization. This leads to a positive ion space charge forming around the HV electrode which causes the electric field to collapse. It is postulated that after 250 mm, the breakdown mechanism changes and leads to flue compromising the dielectric strength of air. The changes in the breakdown voltages at 250 mm could also be attributed to the differences in the effect of temperature on breakdown mechanisms as the gap size increases [9].

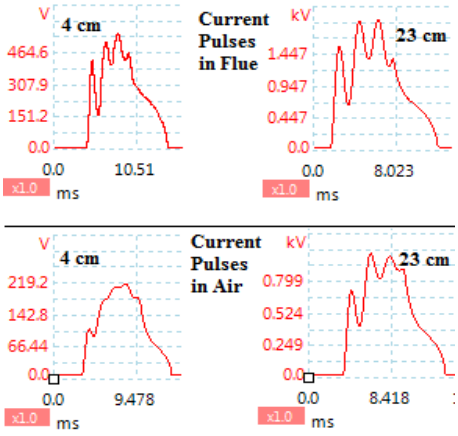

Figure 5: Comparison of pre-breakdown leakage current (represented as voltage output of the HFCT) showing discharge activity in air and flue at 4 cm and at 23 cm.

To confirm the effects of space charge on corona stabilization, impulse tests were conducted since there is limited space charge in impulse voltages due to the short statistical and formation time allowed by the impulse waveform. Figure 6 shows the 1.2/50 μs standard impulse test results, where the flue still had marginally higher breakdown voltages. The maximum standard deviation of the data was 1.38 kV. It was calculated that the differences between the flue and air breakdown voltages in impulse were less by 8% when compared to the DC difference. The concept of the influence of space charge on stabilized breakdown and that flue primarily affects the space charge is further substantiated by these results.

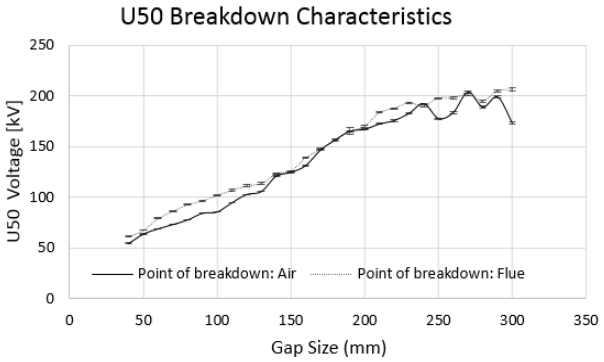

Figure 6: Experimental 1.2/50μs impulse U50 breakdown characteristics for flue and air

4 SIMULATIONS

The simulations are used to validate the DC experimental results by running a discharge model in MATLAB™. The simulation is ran under standard environmental conditions for both air and flue gaseous systems. An advantage of the simulation model is its ability to accept the gas composition of the two gas conditions as inputs to compare them and also contrast the theoretical results with the experiment results discussed above.

4.1 The gas discharge model

The gas discharge is modelled as a fluid of charged particles under the influence of an electric field. This fluid dynamic model is known as the flux corrected transport (FCT) algorithm by Boris and Book [21], which was then proposed by Morrow [22] to be used in numerically describing the flow of charged gas particles in air. Morrow and Lowke [23] used the model to successfully describe streamer development and propagation in standard air conditions. Swanson [24] also used the same model to study the effect of singlet oxygen on corona. In a similar manner, it is used in the present work to study the effects of the engine exhaust gas with composition as given in Table 1.

4.1.1 The flux Corrected Transport Algorithm

The flux corrected transport algorithm is a method of solving continuity equations for gas species and correct for errors introduced by out of bounds cases. Figure 7 shows the algorithm. Where a seed plasma

of electrons is given, then based on the applied voltage, a Laplacian electric field is computed. . The oissonian electric field is due to the charge distribution in the gap.

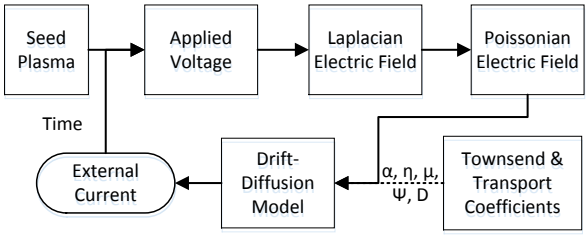

Figure 7: Flux Corrected Algorithm flow chart [24]

Simultaneous drift-diffusion equations then accept Townsend and transport data to propagate the charges through the gap. Then lastly, the developed current due to flow of charge is used to calculate the voltage drop in the system where this model runs in time iterations. The electron density N_e is monitored and breakdown occurs when N_e reaches 10^8, being the streamer breakdown criterion. The model component of the algorithm is briefly described below.

4.1.2 Drift-Diffusion Model

The movements of the electrons and ions in the gap space "*z*" are accomplished by a set of drift-diffusion equations that treat these species as fluid. Equations 4, 5 and 6 give the drift-diffusion equations for electrons, positive and negative ions [21, 22, 23, 24].

$$\frac{\partial N_e}{\partial t} = S + N_e\alpha|v_e| - N_e\eta|v_e| - N_e\,N_p\,\beta - \frac{\partial(N_e v_e)}{\partial z} + \frac{\partial}{\partial z}(D_e\,\partial^2\frac{N_e}{\partial z^2}) \quad (4)$$

$$\frac{\partial N_p}{\partial t} = S + N_e\alpha|v_e| - N_n N_p\beta - N_e\,N_p\,\beta - \frac{\partial(N_p v_p)}{\partial z} + \frac{\partial}{\partial z}(D_p\,\partial^2\frac{N_p}{\partial z^2}) \quad (5)$$

$$\frac{\partial N_n}{\partial t} = N_e\eta|v_e| - N_n\,N_p\,\beta - \frac{\partial(N_n v_n)}{\partial z} + \frac{\partial}{\partial z}(D_n\,\partial^2\frac{N_n}{\partial z^2}) \quad (6)$$

Where:

$_x$ = Electrons *e*, negative ions *n* & positive ions *p*
N_x = Number density for electrons and ions [cm^{-3}]
v_x = Electron and ion velocities [$cm.s^{-1}$]
α, η = Ionization and attachment coefficients [cm^{-1}]
S = Photoionization term [$cm^{-3}.s^{-1}$]
β = Recombination coefficient [$cm^3.s^{-1}$]
D_x = Diffusion coefficient [$cm^2.s^{-1}$]

4.2 Simulation Results

The breakdown voltage characteristics produced by the simulation are shown in Figure 8. The simulation give trends generally similar to those obtained through physical experiments which verifies that the main contributors in flue are the chemical composition used to compute the Townsend and transport parameters. It can been seen that the simulation fails to predict the change of breakdown mechanism at 250 mm seen in the experiments as this change has not been built in the model. This is an area of possible further development for the model where temperature effects and corona stabilization mechanisms could be incorporated in the model.

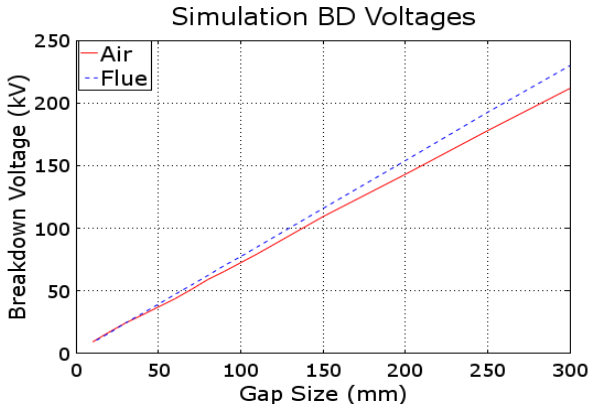

Figure 8: Simulation results: Breakdown characteristics of air and flue under standard conditions.

5 CONCLUSION

The DC and impulse voltage breakdown characteristics of small air gaps in engine exhaust flue have been presented. The aim was to find out the effects of engine flue gas on the breakdown strength of air gaps in the context of the effect of locomotive engine flue on overhead high voltage railway catenary system. Gas discharge experiments and simulations have shown that flue enhances the dielectric strength of air in the gap size range of 30 mm to 250 mm. Beyond 250 mm however, the presence of flue in the gap compromises the dielectric strength of the air gap. The enhancement is attributed to increased corona stabilization that in turn is affected by the increased humidity of the flue gas. The simulation model reproduced the general trend of the experimental data but could be refined by incorporating the corona stabilization and temperature effects.

ACKNOWLEDGMENTS

The authors would like to thank Eskom for their support of the High Voltage Engineering Research Group through the Tertiary Education Support Programme (TESP). They would also like to thank the Department of Trade and Industry (DTI) for THRIP funding and to thank the National Research

Foundation (NRF) for direct funding of the research group. Appreciations are also extended to the Passenger Rail Agency of South Africa (PRASA) for funding this research.

REFERENCES

[1] IEC 60913- 2013: Railway applications - Fixed installations - Electric traction overhead contact lines

[2] Kuffel, W.S. Zaengl, J. Kuffel, High Voltage Engineering: Fundamentals, Second Edition, Newnes, 2006

[3] A.R. Timm,"Continuous Gauging of Electric Traction Contact Wire", Masters Thesis, University of Cape Town, December 1975.

[4] P.J. Lambeth D.H. Nguyen, "Air clearances for electric railways: A study of the breakdown voltage of rode-plane gaps in variety of atmospheric conditions". IEEE Transactions on Power Apparatus and Systems, Vol. PAS-104, No. 10, October 1985

[5] M.K. Khair, W.A. Majewski, Diesel emissions and their control. SAE Inernational. 2006, ISBN: 978-0-7680-0674-2

[6] H. Jaaskelainen, "Diesel Exhaust Gas", DieselNet Technology Guide. Online: https://www.dieselnet.com/tech/diesel_exh.php, Last accessed June 2016

[7] D. Yujian, L. Weiming, F. Jianbin, L. Quingfeng, Z. Jun, S. Zhiyi, "Altitude correction of switching impulse flashover voltage of rod-plane air gaps", 18 International Symposium of High Voltage Engineering, Seoul, Korea, pp. 287-291 August 2013

[8] T. Harada, Y. Aoshima, Y. Ishida, Y. Ichihara, K. Anjo, N. Nimura, "Influence of Air Density on Flashover Voltages of Air Gaps and Insulators", IEEE Trans. Power Appar. Syst., 1970, 89, pp. 1192-1202

[9] N.L Allen, D.S.K Lam, D.A Greaves, "Test on the breakdown of air at elevated temperatures in non-uniform fields", IEE Proc.-Sci. Meas. Technol., Vol. 147, No 6, pp. 291-295, November 2000

[10] N.L allen, A Ghaffar, "The variation with temperature of positive streamer properties in air", J. Phys. D. Appl. Phys., Vol. 28, pp. 338-343, 1995

[12] N.L Aleksandrov, E.M Bazelyan, "Temperature and density effects on the properties of a long positive streamer in air", J. Phys. D: Appl. Phys. 29, pp. 2873-2880, 1996

[13] N. L. Aleksandrov, E. M. Bazelyan, "Ionization processes in spark discharge plasmas", Plasma Source Sci. Technol. 8 (1999), 285-294, UK

[14] M.L. El-Sayed, E.M. El-Refaie, M.M. Awad, "Effects of pollution on the breakdown voltage of air", Correspondence of Proc.IEE, Vol. 125, No. 7, pp. 714, July 1978

[15] P. Naidoo, D.A Swift, "Large particle initiated breakdown of an atmospheric air gap: Relatingto AC power lines faults caused by sugar-cane fires", 8th Int. Symp. on High Voltage Engineering. Yokohama, Japan, pp. 81-84, August 1993.

[16] Plasma Data Exchange Project, "Lxcat," http://fr.lxcat.net/home/, last accessed June 12, 2016

[17] Morgan Database, "Lxcat", http://fr.lxcat.net/home/, Retrieved 13 June 2016

[18] G. J. M. Hagelaar and L. C. Pitchford, "Solving the Boltzmann equation to obtain electron transport coefficients and rate coefficients for fluid models", Plasma Sources Sci. Technol. 14, pp. 722-733, 2005

[19] SANS 60060-1:2011, High Voltage test techniques, Part1 : General definitions and test requirements. Ed. 3

[20] B. Sanjeev,"An investigation into methods of modelling positive inhomogeneous-field breakdown and discharge processes in SF6 with emphasis on the corona stabilisation phenomenon", MSc(Eng) Thesis, University of the Witwatersrand, Johannesburg, June 1998

[21] J. Boris and D. Book, "Flux-corrected transport. A fluid transport algorithm that works," Journal of Computational Physics, vol. 11, pp. 38-69, 1973.

[22] R. Morrow and L. Crem, "Flux-corrected transport and diffusion on a non-uniform mesh," Journal of Computational Physics, 1985.

[23] R. Morrow and J. Lowke, "Streamer propagation in air," Journal of Physics D: Applied Physics, vol. 30, 1997

[24] A.G. Swanson, I.R. Jandrell, "Investigation into the role of singlet oxygen in positive corona in air", SAIEE African Research Journal, Vol. 106(4), pp. 182-194, December 2015

Appendix B

SAUPEC 2017 Paper

This appendix gives the paper presented in the South African Universities Power Engineering Conference (SAUPEC) at Stellenbosch University in January 2017.

INVESTIGATING THE EFFECTS OF ENGINE FLUE GAS ON DIELECTRIC STRENGTH OF AIR GAPS

N. Msimango and C. Nyamupangedengu *

* *School of Electrical & Information Engineering, University of the Witwatersrand, Private Bag 3, 2050, Johannesburg, South Africa E-mail: MrN.Msimango@gmail.com, Cuthbert.Nyamupangedengu@wits.co.za*

Abstract: The effects of engine flue gas pollution on the dielectric strength of air gaps in railway electrical clearances were investigated. In South Africa, diesel locomotives sometimes have to use electrified railway lines. There exists very little knowledge on the effects of a diesel locomotive's flue gas in railway high voltage systems. As such, this research aims to find the effects if any, of engine flue gas on the dielectric strength of air gaps. In order to reliably investigate the present question, the research method included a combination of rod-plane and sphere-sphere gas discharge gap configurations to draw conclusions on findings. Initial experiments have revealed that for a gap size less than 25 cm, the introduction of flue gas enhanced the dielectric strength of air, the increase in breakdown voltage is as much as 19%. For gap sizes greater than 25 cm, the flue gas decreased the dielectric strength of air whereby the maximum recorded decrease of the breakdown voltage is 30% from that of air. It is speculated that the enhancement of the dielectric strength is due to the increased humidity through corona stabilization. For gaps greater than 25 cm the corona stabilisation phenomena cease to be influencial and hence the degradation of the air dielectric strength. The study intends to contribute to the improvement of current pollution and clearance standards for locomotives in South Africa.

Key words: Corona stabilization, Engine flue gas, HV Breakdown, Humidity, Railway Electrical clearances

1. INTRODUCTION

Since the inception of railway systems in South Africa, British standards have always been used for guidance on technical requirements such as determination of electrical clearances; the air gap between the locomotive electric supply lines and the ground and the top of a locomotive [1]. As the economy grows, there is increased reliance on locomotives to transport mass goods and passengers. There are many regions in the country where there are unelectrified railway systems and this entails the use of diesel powered locomotives. Consequently the South African railway systems are operated with a fleet comprising of both electrical and diesel powered locomotives. Diesel locomotives often have to use the electrified railway lines. This poses a problem as the exhaust on top of the locomotives release flue gas directly onto the electrical railway catenary system (RCS). From a high voltage perspective, pollution of the air and of high voltage equipment may greatly compromise the integrity of the dielectric strength of the air and equipment [2]. In the case of a RCS this affects the air gap that would have been set to meet minimum international standards and this may lead to catastrophic accidents causing damage to equipment and injurying passengers. This becomes a major problem more so when the locomotives pass under a bridge or a tunnel because the clearances under these structures are already set at their minimum mostly due to costs [3]. The flue gases cannot easily escape a tunnel which might have major unknown electrical safety implications.

The current standard used to design an electric RCS in South Africa is IEC 60913:2013 [4]. This standard unfortunately does not cater for diesel flue gas pollution of electric railway systems. The omission is presumably because the case of diesel locomotives travelling under electrified railway lines is unique to South Africa and this poses a unique problem as there is no knowledge of how the flue gases interact with electric systems. Additionally, it would be imperitive to see how they can cause danger to people and equipment. It is therefore important to understand how engine flue gases affect the dielectric strength of air in order to generate knowledge for mitigating this problem. The study is carried out through laboratory high voltage breakdown experiments using rod-plane and sphere-sphere electrode configurations for normal air conditions and flue polluted air conditions.

2. THE BACKGROUND

There exists limited literature directly addressing the effects of engine flue pollution on breakdown voltage levels of air or any equipment. An experimental study conducted in 1985 by Lambeth and Nguyen [3] showed that the introduction of diesel and gasoline flue gases in a rod-plane gap greater than 25 cm resulted in a 20 % reduction in the AC breakdown voltage of such a gap. This decrease was only observed with diesel flue gas as compared to other pollution experiments which included water droplets, wheat flour and salt fog pollution. These results may suggest that the chemical compositions of the flue gases are the major contributors to these results since this is the only difference between these pollution

types. All the experiments were conducted under the same standard pressure and temperature. The following sections explore relevant literature to relate how the presence of engine flue gas might affect the processes involved in gas discharge phenomena.

2.1 Diesel Flue Gases

A major by-product of the engine combustion process is heat and in an ideal process, the other byproducts are vapour, carbon dioxide and nitrogen, which according to Majewski [9], the volumetric concentrations are usually in the ranges stipulated in Table 1.

Table 1: Ideal diesel flue gas composition in a diesel engine exhaust

Gas Molecule	Volumentric % Range
CO_2	2 - 12
H_2O	2 -12
O_2	3-17
N_2	59 - 92

Among these gases, the combustion process further results in pollutants that come from various non-ideal processes in the combustion. The pollutants are hydrocarbons (HC), carbon monoxide (CO), nitrous oxides (NO_x) and particulate matter (PM_{10}, PM_{25} for particulate diameters of 10 and 25 microns respectively). The combined volumetric concentration has been experimentally found to be approximately 0.1 % [9]. Due to the small amounts of these pollutants, Jasskelainen [10] claims that they can be ignored and the diesel exhaust gas properties may be approximated to that of air. It is stated that this method brings errors and requires results to be corrected for the increased vapour, carbon dioxide and decreased oxygen. As such these pollution byproducts can be viewed important for this study's accuracy of findings.

2.2 Effects Of Atmospheric Conditions

Atmospheric air pressure is normally a function of altitude. Pressure in turn affects the voltage breakdown of an air gap [12] - [18]. In the case of this study, the locomotive's exhaust flue is directed to the open atmosphere and thus it is assumed that this has very little effect on the pressure in the electrode gap.

Allen *et al* [19, 20] performed tests to determine the effect of elevated temperatures on breakdown of non-uniform fields. The results show that the breakdown voltage of a rod-plane air gap exponentially decrease with increased temperature. From their test results, it is found that temperature decreases the breakdown voltage more in larger gaps (20 cm) than in small gaps (10 cm) [19]. This result agrees with other publications that investigated the effect of temperature on the dielectric strength of air [23]. Aleksandrov *et al* [22] used a 1.5D simulation to show the effects of temperature and density on properties of a long positive streamer in air. The calculated results show that temperature has a pronounced effect than air density. It is therefore expected that the increased temperature of the exhaust flue degrades the dielectric strength of the air.

The effect of water particles on streamer breakdown can be explained in terms of charge dynamics in the streamer channel. It is believed that the loss of electrons in the channel in air is dominated by the three-body attachment process given in equation 1 [24]:

$$e + O_2 + M \rightarrow O_2^- + M \tag{1}$$

Where $M = O_2$ in dry air and $M = O_2$ & H_2O in humid air. The loss of electrons through the dissociative recombination with simple molecular ions (O_2^+ ,N_2^+) is given by equation 2:

$$e + AB^+ \rightarrow A + B \tag{2}$$

Aleksandrov *et al* [8, 22] used simulations to conclude that an increase in humidity leads to an increase in the breakdown voltage of air. This result is in agreement with experiments performed by Lambeth and Nguyen's [3]. The presence of humidity and temperature in this study implies that the major contributor will have prominent effects since these quantities have opposing effects on the dielectric strength of air.

Tests conducted by Loft *et al* in [25] on 0.2 mm to 0.63 mm diameter particles, along with tests conducted by Naidoo [26] and Lambeth [3] on large particles showed a small decrease in the breakdown voltage of polluted air. Since the changes were very small, in the context of this study, it is expected that the particulates have minimal effects due to their smaller sizes (microns) and volumetric concentrations being less than 0.1%.

2.3 Gas Discharge Fundamentals

The process of electrical breakdown involves a number of important stages that have been covered in literature. Additionally, ongoing research looks to come with new theories of the possible processes and conditions involved in air breakdowns [5, 6]. The most established and long used theories for electrical breakdown in gases is "Townsend's Discharge Mechanism" [2] stating that in order to establish a continous discharge in an electronegative gas, free electrons must be accelerated by an electric field and as they ionize other molecules they create an avalanche of free electrons and thus forming a conducting plasma in the air gap [7]. The "Streamer Breakdown Criterion" [2] then maintains that for electrical breakdown to occur, the space charge must be suffiecient to influence the local electric field and thus ionization. These avalanche electrons due to ionization can influence the local fields when they reach a value of 10^8 such that streamers become self propagating and bridge the air gap, forming an arc between electrodes. The number of avalanche electrons in a gap is given by equation 3.

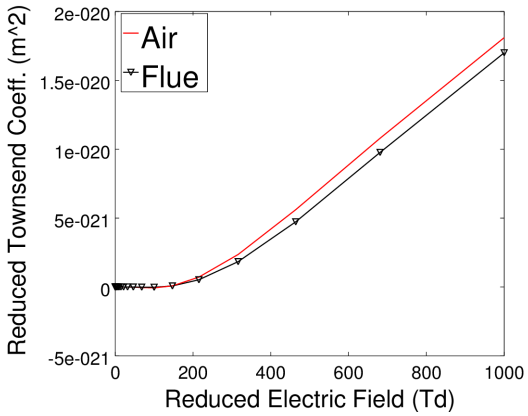

Figure 1: A comparison of Townsend's coefficients for air and engine exhaust flue gas compositions.

$$N = e^{\int(\alpha-\eta)d} \tag{3}$$

Where:

N = Number of avalanche electrons in gap d
α = Townsend's first ionization coefficient
η = Townsend's attachment coefficient

It is crucial to understand gas discharge collisional dynamics in order to combine the atmospheric effects described above into a single meaningful result. Transport and townsend coefficients representing a particular gaseous system can give an approximate prediction of this result. The coefficients depend on the many types of collisional reactions that could occur in the gaseous system. Where the reactions are based on a probabilistic phenomena related to the energy of an electron and the collisional cross sections of a type of reaction that may occur depending on the molecule the electron collides with [27]. The coefficients will be different for distinct gaseous systems. Using Table 1 and the known air oxygen and nitrogen concentrations for air, cross sections for these gaseous systems were obtained from the data published in the LXcat database [28, 30]. The cross sections have been used in calculating the net Townsend coeffients shown in Figure 1 for air and engine flue using Bolsig+, an algorimthm developed by Hagelaar [29]. It is evident that the reduced Townsend coefficient $(\alpha-\eta)/N$ for diesel flue gas composition is less than that of normal air composed of 78% nitrogen and 22% oxygen. The difference is not significant but implies the possibility that at standard temperature and pressure, more voltage might be needed to breakdown a gap in flue gases than in air. These Townsend parameters are used together with transport coeffiecients in a fluid gas discharge model for computer simulations, which are not within the scope of this paper.

3. EXPERIMENTAL SETUP AND PROCEDURE

Experiments are conducted in a laboratory setup in which the main purpose is to evaluate whether the presence of engine flue gas in air affects the breakdown strength of the air. A preliminary investigation is conducted with a petrol engine instead of diesel to provide a scalable methodology since it has been difficult to aquire a diesel engine. The parameters of interest to be monitored are the temperature and humidity of the flue. It is important to note that these parameters along with gas composition and particulate matter are all simultaneously present. Therefore this poses a problem to running a controlled experiment since the parameters cannot be seperated, which contributes to the uniqueness of this study. The experimental setup is shown in Figure 2 in which there is a high voltage source (250 kV DC rated Cockroft-Walton generator in this study), a breathing gas chamber made of bricks which represents a case where a locomotive travels under a tunnel and exhaust flue cannot easily escape, an engine flue source (a petrol generator is used) and a data acquisition system. The data acquisition system is composed of a high frequency current transformer (CT) and a data logger that connects to the HV source and CT through potential dividers. Two electrode setups are tested, a sphere-sphere and a rod-plane configuration; the sphere-sphere is used to calibrate the tests because it provides a uniform electric field. Additionally it is known that for uniform fields, 1 cm is likely to breakdown at 25-30 kV at standard conditions [2]. The vertical rod-plane has been considered the worst case scenario in literature and most geometries in practical applications approximate to it [3].

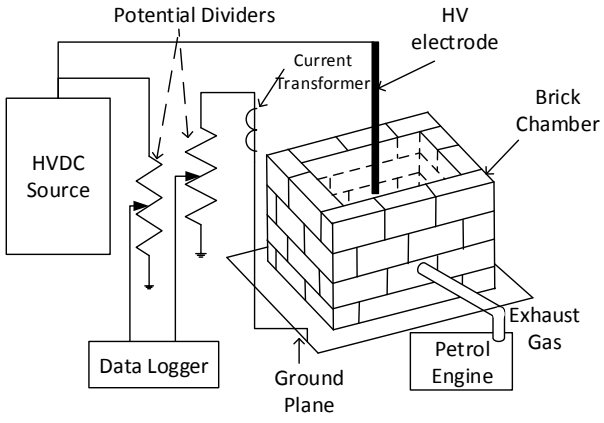

Figure 2: Experimental setup: testing breakdown of engine flue inside a brick chamber.

The diameters of the spheres are 10 cm, chosen such that their curvature is large enough and does not represent a point-to-point gap. The rod diameter is 1.5 cm to attempt to emulate the railway feed cable of 1.6 cm diameter and the ground plane is 3m by 3m.

The breakdown tests are performed in accordance with the SANS 60060-1:2011 testing techniques. Gap sizes from 10 mm to 300 mm are tested in 10 mm increments for

breakdown in both normal air conditions and in engine flue gas conditions. For each electrode setup, a gap size of 10 mm is fixed, then the high voltage is increased at a rate of 1 kV/sec until the gap breaks down as detected through the data acquisition system. The input source voltage and the leakage current are measured and logged by a data logger throughout this process. The air gap is given 5 minutes to de-energise and displace the formed space charge then the process is repeated 10 times before the gap size is increased by 10 mm. This process is repeated until a gap size of 300 mm is reached. Table 2 gives the average recorded environmental conditions during the tests.

Table 2: Chamber air conditions for the two test conditions

Parameter	Sphere Sphere	Rod-Plane Air	Rod-Plane Flue
Temperature [^oC]	21	23.4	48
Pressure [$mBar$]	833.7	832.8	833.5
Relative Humidity [%]	35.2	36.8	65

4. RESULTS AND DISCUSSION

It can be seen in Figure 3 that the use of a sphere-sphere gap in air to calibrate the setup proved to be in good correlation with the published data in Kuffel [2] which validates the setup. The SANS60060-1:2011 standard is used to correct the data, and the fact that the corrected test data replicates published data shows that the recorded environmental conditions are valid.

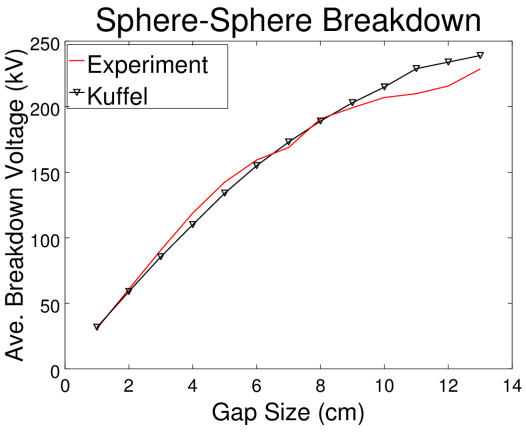

Figure 3: Breakdown characteristic for sphere-sphere electrode setup in air.

The corrected breakdown and corona inception voltages for both air and engine flue conditions are shown in Figure 4 and as expected the breakdown voltages are lower than that of the sphere-sphere configuration. The breakdown results show that the introduction of engine flue gases in the air enhances the breakdown strength of air for gap sizes in the range of 3 cm to 25 cm. The maximum enhancement observed in this range is a 30% increase in the breakdown voltage of air when there's flue gases. The introduction of the engine flue gas for gap sizes outside this range resulted in a compromise of the dielectric strength of air, in which for the small gaps tested the decrease is not detrimental. For the gap sizes higher than 26 cm, a maximum decrease of 19% in the breakdown voltage of the air was recorded. The results agree with the 20% decrease reported by Lambeth [3].

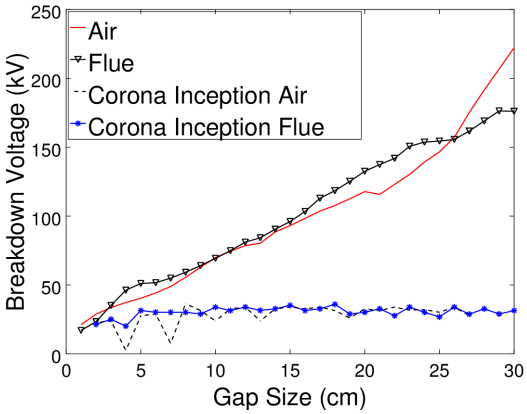

Figure 4: Breakdown and corona inception voltage comparison for air and flue.

In order to find the cause of these observations, corona needed to be investigated since it preceeds arc formation in a gap breakdown. The pre-breakdown corona mechanisms involved determine the breakdown voltages and behaviour [2,33]. Three corona parameters are investigated as per the norm in the field of corona studies; these are the corona inception voltage, the shape and frequency of the corona pulses if present, and lastly the magnitude of these pulses. It can be seen from Figure 4 that the corona inception voltage averaging at 30 kV does not change with gap size for both normal air and flue polluted conditions. This is consistent with the results reported by Hassan in [33] who experimentally studied corona inception and breakdown in small gaps within 5 mm with a needle-plane setup. The invariance of the corona inception voltage is an interesting phenomenon that warrants further investigations. It can be further seen that the corona inception voltage for the gaps less than 5 cm is very close to the breakdown voltage of these gaps. It is important to note that corona inception could not be detected at 1 to 2 cm in both air and flue conditions, this is thought to be due to the fact that the diameter (1.5 cm) of the high voltage electrode was bigger than the gap spacing and so created a quasi-parallel plate gap configuration. The breakdown mechanism in uniform feilds is essentially Townsend type and therefore no precursed by corona activity.

Corona pulses were recorded and as expected, their magnitude increased with increasing gap spacing. The pulsations of the corona at lower gap sizes and higher gap sizes are shown in Figure 5. It is remarkable to note that in flue gas, the corona pulsations are sginificantly higher than in air. The maximum recorded differences in the pulse

magnitudes for flue are 95% at 4 cm and 94% at 23 cm higher than the pulsations in air respectively.

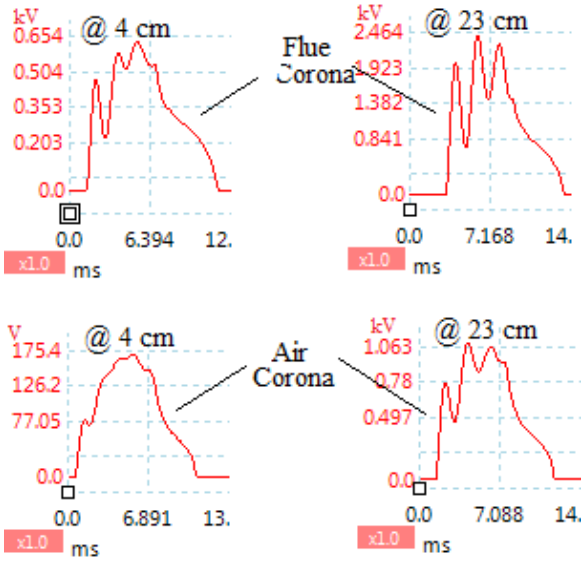

Figure 5: Comparison of corona pulsation and magnitude from small gap spacing to large gap spacing for flue and air.

It is known that in positive corona, pulsation is due to the collapse of the electric field as the electrons near the high voltage electrode get absorbed into the electrode and the positive space charge shields the electrode by forming a space charge cloud. Consiquently, the space charge modified resultant electric field strength decreases resulting in the ceasation of electron avalanches. The positive ion cloud then drifts away and the process repeats [2, 33]. This phenomenon is what is refered to as corona stabilization, it results in more voltage needed to initiate leader breakdown [34]. Although the concept of stabilization is not fully understood, research has established that corona stabilization decreases with increasing gap spacing in air. This is consistent with the results found in this study, the corona pulses dimished as the gap spacing was increased to 25 cm. It can therefore be concluded that below 25 cm, the presence of flue gases enhanced corona stabilization which in turn caused the breakdown voltage to be higher than that of air. However beyond 25 cm, the processes change and the reasons for this are still being explored. It is speculated that the reason flue gas can enhance corona stabilization is because of the increased humidity. Both the humidity and temperature double in flue compared to air as shown in Table 2. In small gaps it has been found that the electron recombination process given by equation 1 dominates. The effect of 48^oC is relatively insignificant compared to the effect of the 65% relative humidity. In this case it is thought that this process enhances the corona stabilization by removing electrons from the channel near the HV electrode.

Future experiments with impulse voltages will be conducted to evaluate how the lack of space charge build up will affect these observations. Furthermore, computer simulations will be used to analyse the extent of the recombination processes.

5. CONCLUSION

This paper has presented an experimental investigation of how engine exhaust flue gases affect the dielectric strength of air. The experiments are conducted with a high voltage DC Cockcroft-Walton generator on a rod-plane gap for normal air and flue gas pollution conditions. Investigating the pre-breakdown corona gave more insights into the breakdown mechanism in flue gas. The results showed that the presence of flue gas pollution increased the breakdown voltage of air by up to 30% for gap spacings less than 25 cm. However beyond 25 cm, the breakdown voltage in flue gas became lower than that in air by 19%. The increase of breakdown voltage for gap spacings less than 25 cm is attributed to the observed enhanced corona stabilization due to the higher relative humidity of flue gas.

6. ACKNOWLEDGEMENTS

The authors would like to thank Eskom for their support of the High Voltage Engineering Research Group through the Tertiary Education Support Programme (TESP). They would also like to thank the Department of Trade and Industry (DTI) for THRIP funding and to thank the National Research Foundation (NRF) for direct funding of the research group. Appreciations are also extended to the Passenger Rail Agency of South Africa (PRASA) for funding this research. Lastly, the authors would also like to thank Mr Sfiso, Mr Mark and Mr Muzi from the Wits HV and Gemnin Labs for their guidance and assistance on building the test chamber.

REFERENCES

[1] A.R. Timm,"Continuous Gauging of Electric Traction Contact Wire", Masters Thesis, University of Cape Town, December 1975.

[2] Kuffel, W.S. Zaengl, J. Kuffel, High Voltage Engineering: Fundamentals, Second Edition, Newnes, 2006

[3] P.J. Lambeth, D.H. Nguyen, "Air clearances for electric railways: A study of the breakdown voltage of rode-plane gaps in variety of atmospheric conditions". IEEE Transactions on Power Apparatus and Systems, Vol. PAS-104, No. 10, October 1985

[4] IEC 60913- 2013: Railway applications - Fixed installations - Electric traction overhead contact lines

[5] J.J Lowke, "Toward a new theory of electrical breakdown in air", Intern. Conf. Gas Discharges and their applications, Beijing, 2012

[6] J.J Lowke, "New Directions of Predictive Capability for Properties of Gas Discharges", CSIRO Materials Science and Engineering, 2012

[7] F. Llewellyn-Jones, ”Ioninzation and breakdown in Gases”, Methuen, 1966

[8] N. L. Aleksandrov, E. M. Bazelyan, Ionization processes in spark discharge plasmas, Plasma Source Sci. Technol. 8 (1999) 285-294, UK

[9] W. A. Majewski, What are diesel Emissions, in: DieselNet Technology Guide. https://www.dieselnet.com/tech/emi_intro.php, last accessed: 10/2016

[10] H. Jaaskelainen, Diesel Exhaust Gas, in: DieselNet Technology Guide. https://www.dieselnet.com/tech/diesel_exh.php. Last accessed: 10/2016

[11] International Union of Railways - UIC, ”Diesel locomotive emissions regulations”.

[12] D. Yujian, L. Weiming, F. Jianbin, L. Quingfeng, Z. Jun, S. Zhiyi, Altitude correction of switching impulse flashover voltage of rod-plane air gaps, 18 International Symposium of High Voltage Engineering, Seoul, Korea, pp. 287-291 August 2013

[13] T. Harada, Y. Aoshima, Y. Ishida, Y. Ichihara, K. Anjo, N. Nimura, Influence of Air Density on Flashover Voltages of Air Gaps and Insulators, IEEE Trans. Power Appar. Syst., 1970, 89, pp. 1192-1202

[14] T.A. Phillips, L.M. Robertson, A.F. Rohlfs, R.L. Thompson, Influence of air density on electric strength of transmission line insulation, IEEE Trans. Power Appar. Syst., 1967, 86, pp. 948-961

[15] S.-Y. Chu, Some aspects of researches on the influence of atmospheric pressure on external insulation of H.V. electrical apparatus, CIGRE 84-33 (WG- 03), IWD 1984

[16] Z. Zhijin , J. Xinliang, C. Yafeng , S. Caixin , H. Jianlin, Influence of low atmospheric pressure on AC pollution flashoverperformance of various types of insulators, IEEE Transactions on Dielectrics and Electrical Insulation, Vol.17, pp. 425-433, 2010

[17] R. Gou, The influence of air pressure on the insulation strength of insulators, J. of High Voltage Engineering, Vol.16, No.2, pp. 30-32, 1990

[18] X. Lu, G.V. Naidis, M. Laroussi, K. Ostrikov, ”Guided ionization waves: Theory and experiments”, Physics Reports 540, pp. 123-166, 2014

[19] N.L Allen, D.S.K Lam, D.A Greaves, ”Test on the breakdown of air at elevated temperatures in non-uniform fields”, IEE Proc.-Sci. Meas. Technol., Vol. 147, No 6, pp. 291-295, November 2000

[20] N.L allen, A Ghaffar, ”The variation with temperature of positive streamer properties in air”, J. Phys. D. Appl. Phys., Vol. 28, pp. 338-343, 1995

[21] P.M Cowan, J.A Dunn, P. Naidoo, J. Masters, ”Sugar cane fire induced transmission line flashovers”, Elektron, pp. 12-15, January 1991

[22] N.L Aleksandrov, E.M Bazelyan, ”Temperature and density effects on the properties of a long positive streamer in air”, J. Phys. D: Appl. Phys. 29, pp. 2873-2880, 1996

[23] B.S Aleksandrov, E.M Bazelyan, B.I Bekzhanov, Izv. Akad. Nauk SSSR Energ. Transp. N2 120, 1984

[24] N. L. Aleksandrov, E. M. Bazelyan, Ionization processes in spark discharge plasmas, Plasma Source Sci. Technol. 8 (1999), 285-294, UK

[25] M.L. El-Sayed, E.M. El-Refaie, M.M. Awad,”Effects of pollution on the breakdown voltage of air”, Correspondence of Proc.IEE, Vol. 125, No. 7, pp. 714, July 1978

[26] P. Naidoo, D.A Swift, ”Large particle initiated breakdown of an atmospheric air gap: Relating to AC power lines faults caused by sugar-cane fires”, 8th Int. Symp. on High Voltage Engineering. Yokohama, Japan, pp. 81-84, August 1993.

[27] A.G. Swanson, I.R. Jandrell, ”Investigation into the role of singlet oxygen in positive corona in air”, SAIEE African Reaserch Journal, Vol. 106(4), pp. 182-194, December 2015

[28] Plasma Data Exchange Project, Lxcat, http://fr.lxcat.net/home/, last accessed June 12, 2016

[29] G. J. M. Hagelaar and L. C. Pitchford, ”Solving the Boltzmann equation to obtain electron transport coefficients and rate coefficients for fluid models”, Plasma Sources Sci. Technol. 14, pp. 722-733, 2005

[30] Morgan Database, ”Lxcat”, http://fr.lxcat.net/home/, Retrieved 13 June 2016

[31] A. Kuliskovsky, ”The role of photoionization in positive streamer dynamics”, Journal of Physics D: Appl. Physics, vol. 33, pp. 1514-1524, 2000

[32] SANS 60060-1:2011, High Voltage test techniques, Part1 : General definitions and test requirements. Ed. 3

[33] H. J. Mohammed,”Corona Stabilization and Electrical Breakdown of Gases in Nonuniform Fields”, PhD, University of Baghdad College of Science of Science-Department of Physics, Republic of Iraq, April 2013

[34] T. Hinterholzer, W. Boeck,”Breakdown in SF6 influenced by corona-stabilization”, Electrical Insulation and Dielectric Phenomena, 2000 Annual Report Conference on, Volume: 1, February 2000